44886

NAME OF AUTHOR/*NOM DE L'AUTEUR* _____ Henri Pierre-Emile DAUTET

TITLE OF THESIS/*TITRE DE LA THÈSE* _____ "Yield of Deep Spallation Products of Medium to Heavy

_____ Mass Targets Bombarded with 480-MEV Protons"

UNIVERSITY/*UNIVERSITÉ* _____ Simon Fraser University

DEGREE FOR WHICH THESIS WAS PRESENTED/
   GRADE POUR LEQUEL CETTE THÈSE FUT PRÉSENTÉE _____ Ph.D.

YEAR THIS DEGREE CONFERRED/*ANNÉE D'OBTENTION DE CE GRADE* _____ 1980

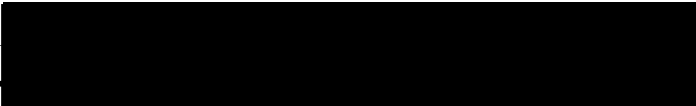NAME OF SUPERVISOR/*NOM DU DIRECTEUR DE THÈSE* _____ Dr. B.D. Pate, Professor

DATED/*DATÉ* _____ August 22, 1979 _____ SIGNED/*SIGNÉ* _____

PERMANENT ADDRESS/*RÉSIDENCE FIXE* _____

NL-91 (3-74)

NOTICE

AVIS

The quality of this microfiche is heavily dependent upon the quality of the original thesis submitted for microfilming. Every effort has been made to ensure the highest quality of reproduction possible.

If pages are missing, contact the university which granted the degree.

Some pages may have indistinct print especially if the original pages were typed with a poor typewriter ribbon or if the university sent us a poor photocopy.

Previously copyrighted materials (journal articles, published tests, etc.) are not filmed.

Reproduction in full or in part of this film is governed by the Canadian Copyright Act, R.S.C. 1970, c. C-30. Please read the authorization forms which accompany this thesis.

La qualité de cette microfiche dépend grandement de la qualité de la thèse soumise au microfilmage. Nous avons tout fait pour assurer une qualité supérieure de reproduction.

S'il manque des pages, veuillez communiquer avec l'université qui a conféré le grade.

La qualité d'impression de certaines pages peut laisser à désirer, surtout si les pages originales ont été dactylographiées à l'aide d'un ruban usé ou si l'université nous a fait parvenir une photocopie de mauvaise qualité.

Les documents qui font déjà l'objet d'un droit d'auteur (articles de revue, examens publiés, etc.) ne sont pas microfilmés.

La reproduction, même partielle, de ce microfilm est soumise à la Loi canadienne sur le droit d'auteur, SRC 1970, c. C-30. Veuillez prendre connaissance des formules d'autorisation qui accompagnent cette thèse.

THIS DISSERTATION HAS BEEN MICROFILMED EXACTLY AS RECEIVED

LA THÈSE A ÉTÉ MICROFILMÉE TELLE QUE NOUS L'AVONS REÇUE

YIELD OF DEEP SPALLATION

PRODUCTS OF MEDIUM TO HEAVY MASS TARGETS

BOMBARDED WITH 480-MEV PROTONS

by

Henri Pierre-Emile Dautet

Maitrise es sciences, Universite de Paris, 1969

Doctorat de 3eme cycle, Universite de Paris, 1971

A THESIS SUBMITTED IN PARTIAL FULFILLMENT

OF THE REQUIREMENTS FOR THE DEGREE OF

DOCTOR OF PHILOSOPHY

in the Department

of

Chemistry

(C) Henri Pierre-Emile Dautet   1979

SIMON FRASER UNIVERSITY

June 1979

Title of Thesis/Project/Extended Essay

"Yield of Deep Spallation Products of Medium to Heavy

Mass Targets with 480-MEV Protons"

Author:

(signature)

Henri Pierre-Emile DAUTET

(name)

August 22, 1979

(date)

APPROVAL

Name: Henri Pierre-Emile Dautet

Degree: Doctor of Philosophy

Title of Thesis: Yield of deep spallation products of medium to
                 heavy mass targets bombarded with 480-MeV protons

Examining committee:

_____

Professor B.D.Pate
Research supervisor

_____

Professor L. Yaffe
External examiner
McGill University

_____

Professor J.M. D'Auria

_____

Professor E.J. Wells

_____

Doctor I.M. Thorson

Date approved : _26 June 1979_

ABSTRACT

Formation cross-sections for deep spallation products of the target nuclides Ho,Tm,Ta,Re,Ir,Au,Bi, bombarded with 480 MeV protons have been measured at the TRIUMF research facility in Vancouver, B.C. The products in question, which differ from the target mass by as much as 45 nucleons, are characterized by alpha emission and also by half-lives ranging down to the order of one second.

A gas-jet recoil transport system, using ethylene gas as the carrier, was developed to transport the nuclides to be studied from their point of production to a shielded detection location, in measured times of about 1.5 second.

The transport efficiency of the TRIUMF gas-jet system, for the elements to be studied, was calibrated by means of the comparison of the intensities of the characteristic X-ray radiations emitted by nuclides caught on a catcher foil placed immediately behind the target and the activity caught at the end of the gas-jet system. The overall transport efficiency was determined to be of the order of 7%.

The effective target thickness in the gas-jet system was determined as a function of dA (the change in mass

number between the target and the product). These data were
obtained using the thick target-thick catcher method.

The characteristic alpha decay of the subject nuclides
was employed to measure, absolutely, the decay rate in the
presence of a large gamma-radiation background from the
other spallation products. A typical experiment consisted
of a series of measurements taken as a function of delay
time in order to provide both alpha-energy and half-life
data to assist in radio-nuclide assignment.

The absolute intensity data, together with the other
information indicated earlier and monitoring of the incident
proton beam by means of a secondary emission monitor,
permitted calculation of absolute formation cross-sections.
In general, these are believed to be accurate within a factor 2.

These measured cross-sections have been compared with
calculated values obtained with two computer codes. The
agreement between the experimental data and results of the
semi-empirical calculations due to Silberberg and Tsao
(which are based on the cross-section systematics due to
Rudstam) was generally poor, the calculated values being too
low by one or two orders of magnitude. Agreement with
calculation obtained via the VEGAS code plus de-excitation

calculated following Dostrovsky, Fraenkel and Friedlander was better, although a single set of calculation parameters did not produce agreement over the complete range of target and product compositions.

The possible reasons for this disagreement are discussed.

DEDICATION

To my mother

REMERCIEMENTS

Le personnel des ateliers de mécanique et d'électronique à
S.F.U a construit les chambres du jet de gaz et l'électronique
associée. Je les en remercie vivement ainsi que le personnel
de TRIUMF qui a fourni les ~10^{19} protons utilisés pendant
cette thèse.

Une mention particulière doit être faite de la
contribution que ma femme Danielle a apportée. Son
assistance en de nombreuses occasions, y compris pendant la
correction de cette thèse m'a été précieuse. La patience
avec laquelle elle a supporté mes fréquentes absences
(spécialement en fin de semaine) a été remarquable. Pour
toutes ces raisons, je lui suis infiniment reconnaissant.

TABLE OF CONTENTS

LIST OF TABLES

LIST OF FIGURES

I - INTRODUCTION

Studies of the interaction between medium energy protons and medium to heavy mass targets are mainly performed, either by measuring the characteristics of the various particles emitted in the process (i.e.: Azh.59, Ber.63, Coc.72, Ber.73, Bla.76, Ber.78, Lux.78, Gre.78), or by determination of the production cross-sections of radioactive residual nuclides (i.e.: Fri.55, Bey.67, Cum.68, Sah.72, Hey.72, Gar.73, Sil.73, Eri.75). These approaches have led to a great deal of understanding of the phenomenon, and have resulted in the formulation of a two-step interaction model described in detail in section IV. The first (fast) step, the so-called prompt-cascade or pre-equilibrium phase, is thought of in terms of direct two body interactions between the projectile and nucleons in the target nucleus, and between target nucleons as the cascade develops. At the end of the cascade, some amount of residual energy is shared between the nucleons and de-excitation occurs during the second "evaporation" step through statistical emission of various particles.

One characteristic of this interaction is the large number of so-called spallation products, in contrast to heavy-ion induced reactions that lead to a relatively small number of products. During the evaporation step, the emission of neutrons is favoured compared to the emission of protons and, as a result, the resulting nuclides will be generally neutron deficient, in contrast to the products resulting from such reactions as fission (spontaneous or induced) and neutron capture.

The two step model has been very successful in reproducing most of the experimental data, particularly those events leading to low excitation energies, and hence to residual products close in composition to the target nucleus (Sah.72, Har.74, Ber.78).

Among the computer codes (described sect.IV) which reproduce the prompt intranuclear cascade phase, ISOBAR or VEGAS are frequently used. They offer the advantage of following closely the physics of the interaction as it is presently understood, and have the potential to yield more detailed information than other codes based on the pre-equilibrium model (Exciton and G.D.H. models).

Furthermore the information needed to perform the
computations are largely extracted from experimental data on
nucleon-nucleon interactions, thus leaving few degrees of
freedom for parameter adjustment. To a large extent they
have been tested by comparison of the particle spectra that
they predict with the experimental results. Other aspects
of the interaction between incident nucleons and complex
nuclides can be compared as well, such as production
cross-sections of residual nuclides, or recoil energies.
However, there are still some open questions; for example,
the more sophisticated versions sometimes yield poorer
agreement with experimental results than simpler versions do
(Che.68, Ber.74).

The yield pattern of the residual nuclides following
the intranuclear cascade can be addressed experimentally by
measuring the cross-sections for the production of nuclides
at various degrees of remoteness in composition from the
target. In the present work, nuclides produced by emission
of between 15 and 40 nucleons have been studied, and their
yields are expected to be strongly influenced by the
excitation energy distribution of the residual nuclei
following the intranuclear cascade step. One advantage of

the cross-sections measured in this work, is that they were

obtained for very neutron deficient nuclides; therefore the

measured cross-sections are probably for independent formation

rather than cumulative, and are thus more informative.

In addition to their theoretical importance, the data

obtained in this work have some practical utility. They

bring cross-section information in a region where there was

none thus far and, as a result, they will allow improvement

of the various recipes and computer codes for calculation of

nuclear reaction products yields (e.g. due to Rudstam

(Rud.66) and Silberberg and Tsao (Sil.73)) which are of

considerable importance in the design of accelerator

shielding and estimating residual activity generation

resulting from their operation. The correction of such

codes, by means of data for nuclear reaction products of

composition remote from stability, allow their calculation

of the more prominent products of composition closer to

stability with greater accuracy.

Such improvements may be even more critical, when

designing experiments where the production of low-yield

short-lived radioactive nuclides is intended. Such is the

case for production of radioactive samples for spectroscopic

purposes , as well as in the (rapidly expanding) field of
production of radio-isotopes for pharmaceutical use.

However, in the present work a number of experimental
difficulties needed to be surmounted, resulting from the
very short half-lives and low yields of the nuclides to be
examined. Thus much of this thesis is concerned with the
development of necessary techniques, including those of the
so-called gas-jet recoil transport system for radioactive
nuclides.

The work described in this thesis was performed at the
TRIUMF research facility in Vancouver B.C.. TRIUMF is with
SIN (Zurich-Switzerland) and LAMPF (Los-Alamos U.S.A.) one
of three high intensity medium-energy accelerators. The
facility was well suited to this study due to the high
intensity and energy range of the proton beam available.
TRIUMF had initially been intended to be mainly used as a
"meson factory", but, it has lately turned out to be
excellent for proton experiments, including production of
polarized protons, although these were not used in the
present studies.

II - EXPERIMENTAL TECHNIQUES

The nuclides of which the yield has been studied in the present work are short lived, typically from one second to several minutes in half-life, and produced with low cross-sections. Thus rapid and efficient transport to the detection set-up was needed, and a method of detection was required which would provide discrimination against a relatively intense beta and gamma radiation background from radionuclides produced in much greater yield.

The gas-jet recoil transport system was a satisfactory answer to the first point. One characteristic of the gas-jet transport system is its weak selectivity in "Z", which means that in principle it transports the hundreds or so spallation products to the counting station with similar (although not necessarily identical) efficiency. The necessary detection selectivity was achieved by taking advantage of the fact that deep spallation products from medium mass targets are characterised by their alpha decay. Alpha radiations can be measured with good sensitivity and resolution in the presence of a strong background of beta and gamma radiations.

As will be seen section II-B various other types of experiments were needed, some involving X- and γ-radiation measurements, in addition to the main measurements on α-radiations.

All the experiments were performed under computer control of the gas-jet and data acquisition apparatus.

II-A - Experimental set-up.

1) Irradiation facilities.

The work presented in this thesis has been performed almost entirely using the proton beam delivered by TRIUMF.

TRIUMF is an H^- relativistic isochronous cyclotron located on the campus of the University of British Columbia. It is operated jointly by the University of Alberta, Simon Fraser University, the University of Victoria, and the University of British Columbia.

Two or more proton beams can be extracted by interception of the H^- internal beam with stripping foils of low Z material. The proton beam energies are individually variable from 180 to 525 MeV by appropriately choosing the H^- orbit of interception. The extracted intensities can also be independently adjusted, since it depends upon the fraction of the H^- internal beam intercepted by the stripping foils.

There are, presently, two main beam lines (Fig.1)
- Beam line 1 (in the meson hall) is capable of carrying a

Figure 1

The TRIUMF facility.

BL1B (p)

MI3 (π/μ)

MII (π)

BL I (p)

CYCLOTRON VAULT

SERVICE ANNEX

BL 4A (p)

GAS JET CHAMBER

IRRADIATION CELL

BEAM MONITOR

PROTON HALL

BL 4B (p)

MRS SPECTROMETER
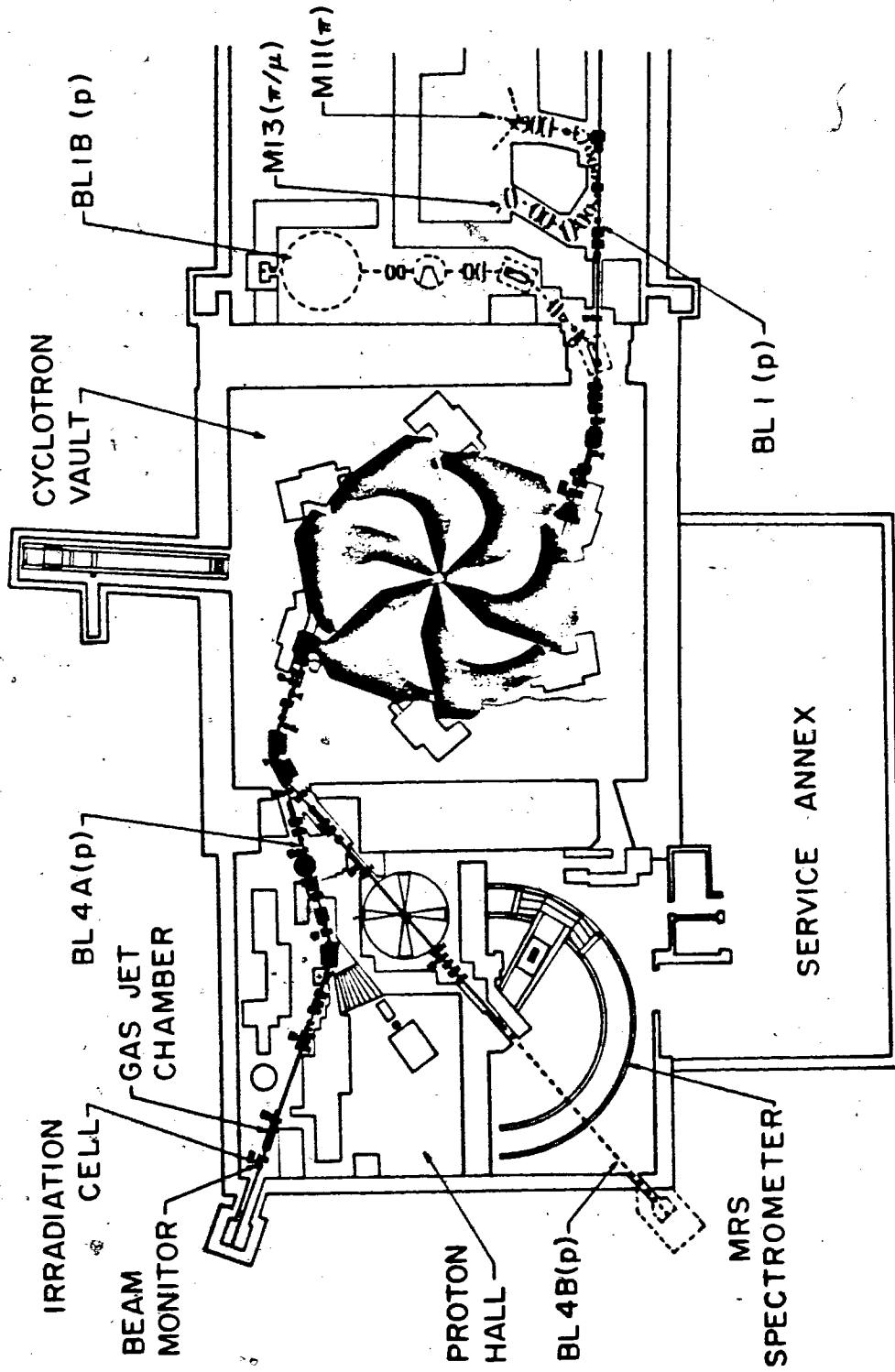
high intensity proton beam (up to 100 µa at 500 MeV). As suggested by the name given to its location, its main purpose is to produce mesons.

- On the other side, in the proton hall, beam line 4 (divided into A and B) is designed for low (few nanoamperes) to medium (up to 10 µamperes) proton beam intensities.

The irradiation facility used for these studies was located in beam line 4A, as indicated in Fig.1. After passage through upstream experiments, the beam was refocussed by three quadrupoles magnets, so that the beam size at the location of the gas-jet system targets was of the order of one square centimeter. A secondary emission detector located just downstream of the gas-jet system monitored the beam intensity through the electron emission from gold foil surfaces struck by the proton beam.

All the irradiations in the present work were performed at a 480 MeV bombarding energy, an energy close to the maximum available (525 MeV) and for which a good beam line tune was available, the proton-beam current was generally of the order of one micro-ampere.

2) The gas-jet transport system.

This section gives a general description of the gas-jet transport system and its components; a more detailed investigation of its characteristics can be found in section II-B.

When a target nucleus is struck by a projectile (Fig.2), it may undergo a nuclear reaction; if so either from the initial projectile-target interaction, or the subsequent evaporative de-excitation process, it will in general acquire some kinetic energy. Depending upon its range in the target material, and how far from the surface of the target the site of the nuclear reaction is located, this recoiling nucleus may or may not escape from the target material. Some fraction of all nuclear reaction products in a foil target will however do so.

In a gas-jet system, the escaping nuclear reaction products are then thermalised in a small ("production") chamber filled with a gas kept at a constant pressure (in the present system ~10 torr). Once thermalised, they attach themselves to carriers (clusters or droplets) that may be present in the gas, and are transported with the gas flow to

Figure 2

Schematic representation of the recoil of nuclides from a thick target and thermalization in a gas filled chamber.

R = average range of the reaction products A and B

The nuclides of type -A- will escape from the target material if their momentum vector is directed within the cone of angle α.

The nuclides of type -B- will be trapped inside the target.
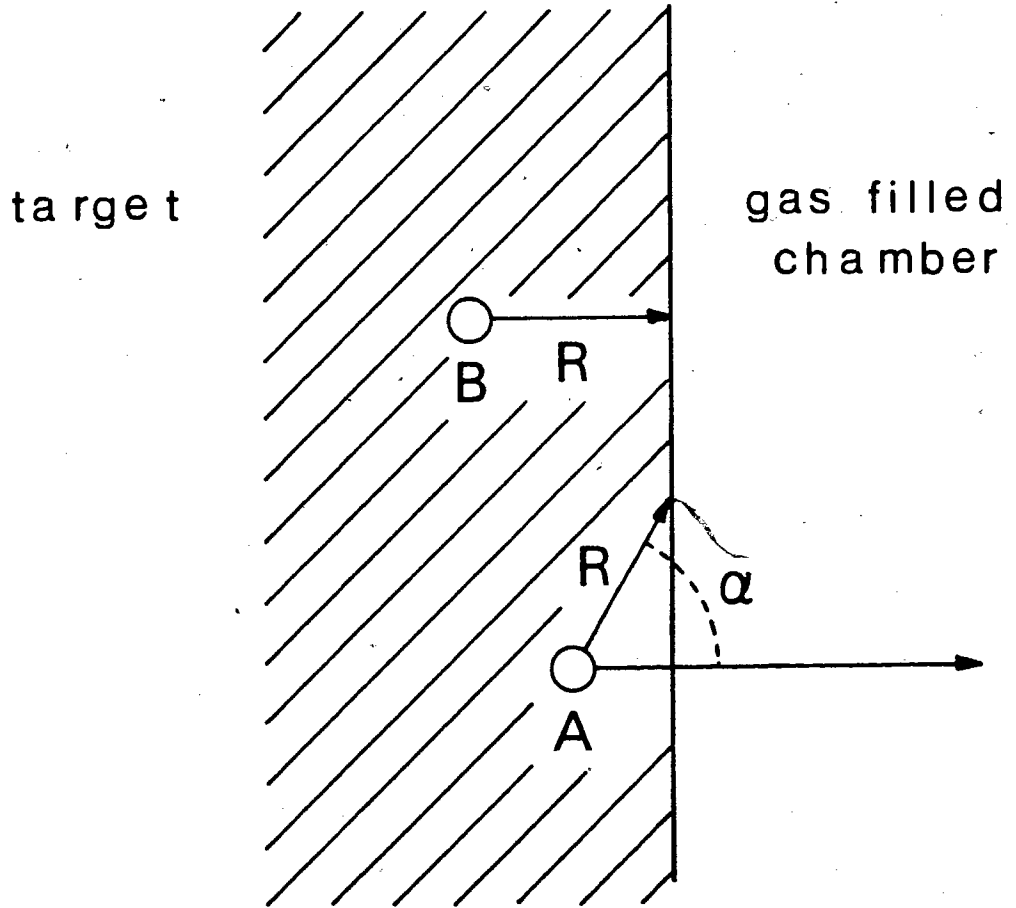
a remote "collection" chamber.

Thus the transport of radioactive nuclides by a jet of gas can be divided in three steps.

step 1 : production

"   2 : transport

"   3 : collection

2,1 - Production

A sketch of the irradiation cell can be found in Fig.3. A small target chamber was inserted inside a larger chamber permanently bolted to the beam line, allowing modification of the target chamber geometry without perturbing the beam line vacuum.

The reaction chamber was of cylindrical form, with 5 cm inner diameter and 4 cm in length. Such dimensions kept the time in which the radioactive nuclides were swept out of the chamber as short as possible, while assuring that most of the most energetic recoiling products would be stopped in the gas, and not become buried in the chamber walls.

Both chambers (inner and outer) under normal operating conditions were at a pressure of ~10 torr, and separated

Figure 3

Schematic representation of the irradiation cell:

- The larger chamber served as a housing to the
  small production chamber
- The target ladder could be raised or lowered to
  position the desired target in front of the
  production chamber
- The gas flowed through the system as indicated by
  the arrows at the top of the figure.

gas inlet → gas outlet

target ladder →

gas - filled thermalization
chamber p≃10 torr

beam window
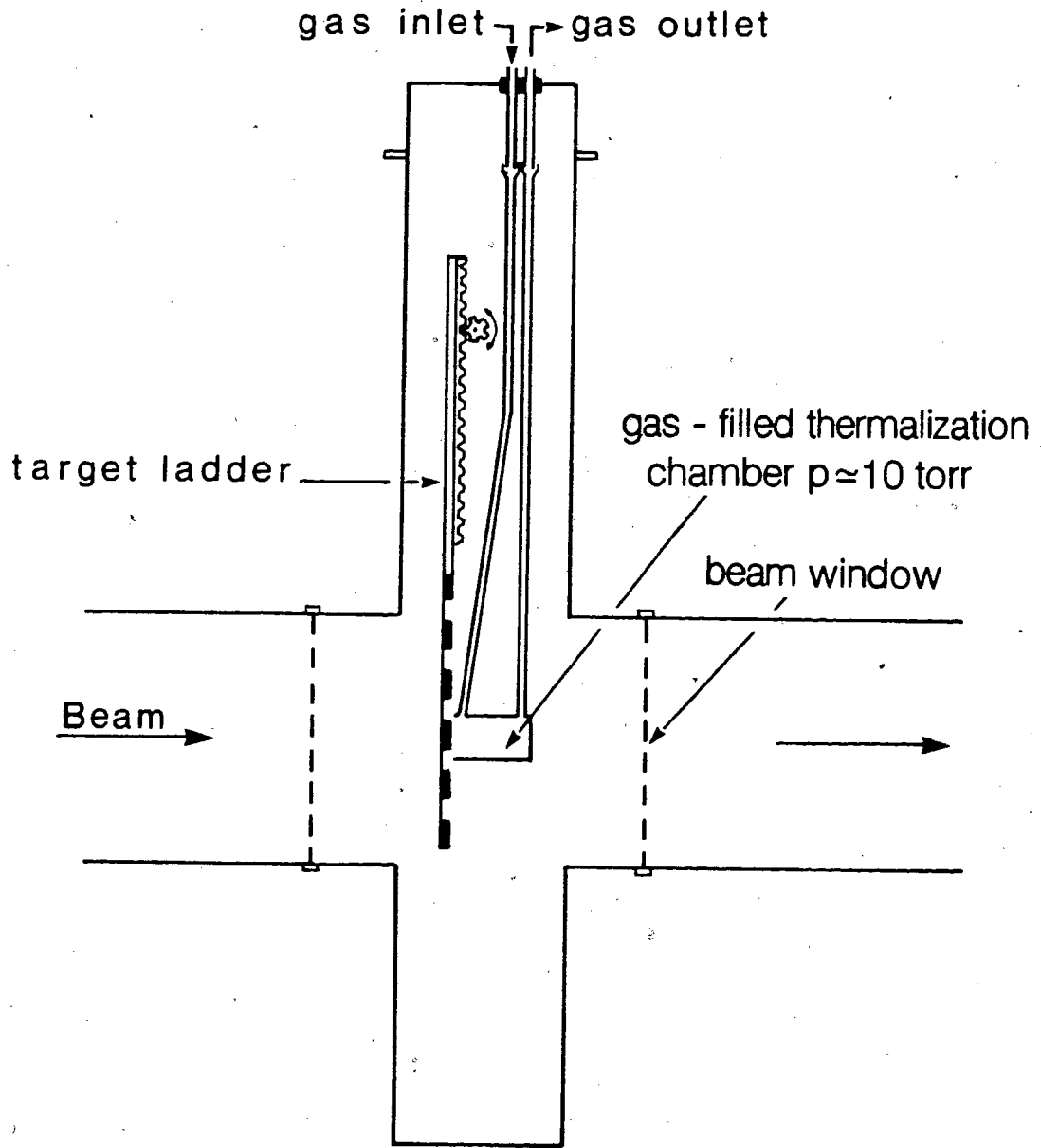
Beam →

from the rest of the beam line by stainless-steel windows
($\sim$20mg.cm^{-2}) on either side. A six-position remotely
controlled target ladder brought a chosen target foil into
position for irradiation (in front of the production
chamber).

The targets were metallic foils of which the details
are given in Table I. The effective target thickness of
these targets for the production of nuclides recoiling into
the reaction chamber gas, was of the order of few
hundreds µg.cm^{-2} (about 50% of the maximum recoil range).
Thus, since total foil thicknesses were typically 20 to
200 mg.cm^{-2}, all the foils were infinitely thick compared
with this range, and it was necessary to measure the
effective target thickness (from which the various products
to be studied were derived). The procedure used is
described later.

2,2 - Transport

The gas - under differential pumping - flowed
through the reaction chamber into a capillary tubing (4mm
inner diameter, 30m long) connecting the target chamber with
the collection chamber, which was located in an area with a

Table I

Target element	Thickness in mg/cm^2	Purity in %	Typical impurities* in ppm
Ho[a]	100.	99.9	Er(200),Eu(100),Tm(170)
Tm[a]	200.	99.9	Dy(100),Ho(100)
Ta[b]	12.5	99.96	W(10)
Re[a]	50.	99.99	W(10)
Ir[a]	112.	99.9	Pb(30)
Au[b]	24.	99.999	
Bi[b]	3.5	99.9	

* - Only those impurities which could have interfered with

the results of these studies are listed.

The target materials were obtained from :

a) - ALFA products, a division of Ventron corporation
16207 South Carmenita Road, Cerritos, California 90701

b) - Good-Fellow metals, Science Park, Milton Road
Cambridge. CB44DJ (UK)

radiation background low enough to permit radiation measurements. The thermalised products were swept out of the reaction chamber by the gas stream, and those that were not attached to clusters or other carriers were lost presumably through Brownian motion to the wall of the capillary (as described in Appendix I). Those attached to carriers of adequate size (as will be seen section II-B) were focussed into the center of the capillary (as explained in Appendix I), and, as a consequence, sustained little loss during transport even over long distances.

2,3 - Collection

At the output of the capillary tubing Fig.4, (inside the collection chamber), the gas impinged on a surface (the collector), and the nuclear reaction products adhered to it, forming a spot of radioactivity of a size (~4mm diameter) suitable for radiation measurement. In the present system, the collector was a used computer tape (material which was readily available and, due to its low "Z", would produce little alpha backscattering). It could be moved by a modified tape drive mechanism, at regular time intervals under computer control, to position the radioactive spot in front of a detector in an adjacent

Figure 4

Schematic representation of the collection chamber
at the end of the gas-jet system.

1) 30m capillary tubing carrying the ethylene gas
(and clusters) from the irradiation cell of Fig.3

2) Spot of collected radioactivity on a movable
computer tape (3)

4) Alpha detector assembly

a) surface barrier Si detector (200um thickness)

b) collimator (8mm diameter)

5) Thin lucite window ($\sim$70mg.cm^{-2}) to minimize
X-ray absorption when "on line" X-ray
measurements were performed

6) Distance between the collection tape and the alpha
detector, was $\sim$2mm in normal running conditions

7) Regulated air inlet maintained pressure $\sim$2 torr
around alpha detector assembly

p ≃ 2 torr

7

6

a b

4

5

X - ray

detector

p ≃ 0.2 torr

1

2

3
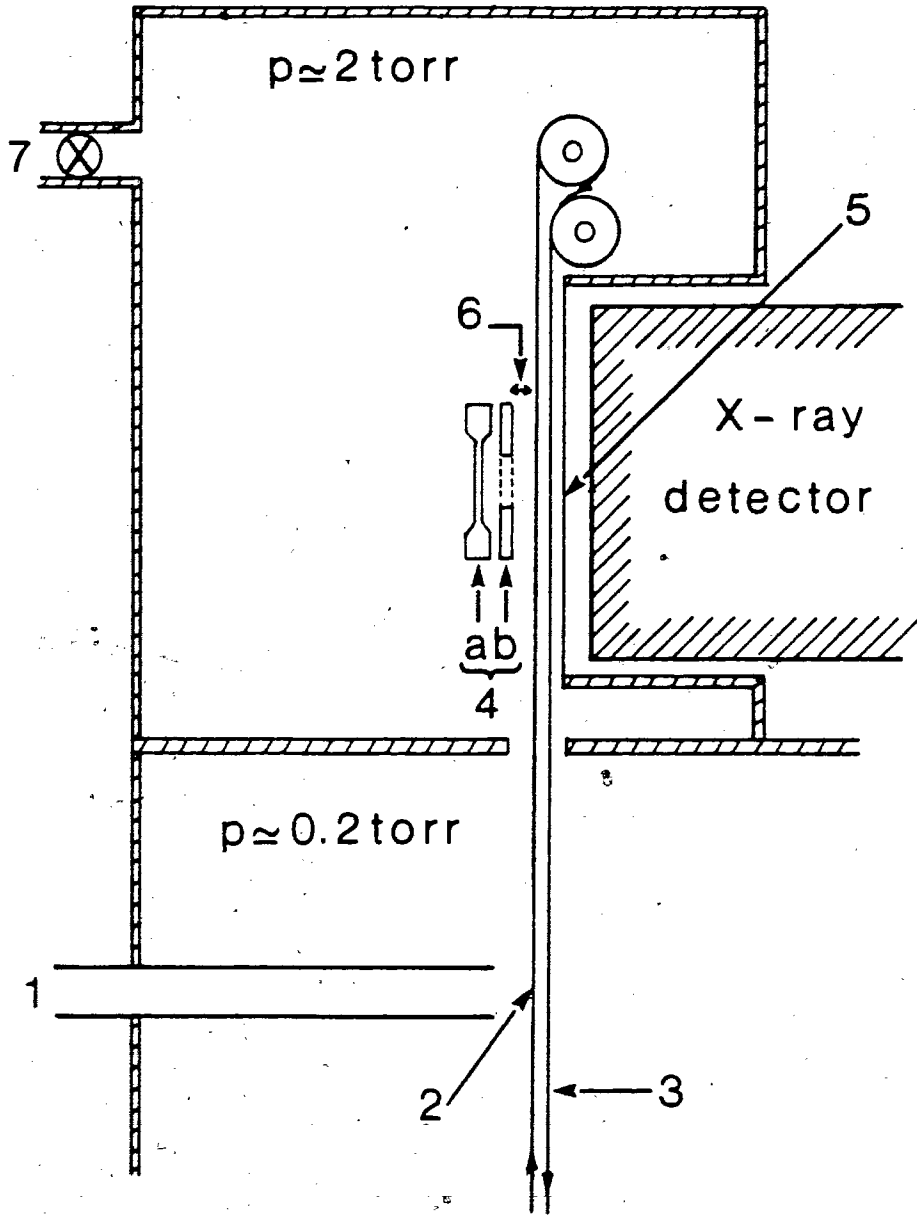
chamber (Fig.4).

3) Detectors and electronics.

Since the nuclides investigated were alpha emitters, the detector which was utilised for most of these studies was an alpha detector, while some of the supplementary experiments (described in section II-C) were performed using either a gamma or a X-ray detector.

3,1 - Alpha detector

This detector was a standard Ortec[*] 200 μm transmission surface barrier silicon detector model TB-17-100-250; its quoted energy resolution was 15 keV. Such a detector cannot operate in the gas-pressure range 1×10^{-2} torr to ~2 torr due to surface breakdown of the detector potential; since the collection chamber was at a pressure of 2×10^{-1} torr, the detector could not be operated in the collection chamber itself. A second chamber was therefore constructed (adjacent to the collection chamber) (Fig.4), which was kept at a constant pressure of 2 torr by differential pumping, and into which the collection tape could be transported. This pressure was sufficiently

---

*** Ortec Incorporated, 100 Midland Road- Oakridge TENN.37830

high that the detector would not be harmed, and

sufficiently low that the energy loss of the alpha particles

along the 2mm path separating the tape from the detector was

negligible. The measured energy resolution in this

environment was ~18 keV.

Under this arrangement there was always a flow of air

from the detector chamber to the gas-jet collection chamber

through the small tape-transport aperture between the two

chambers. This had two important advantages :

- It prevented the ethylene and the various organic

impurities mixed with it from reaching the detector. This

is an important point, since this type of detector is very

sensitive to organic contamination on its exposed front

surface.

- It prevented the (small) fraction of clusters carrying

the radioactive products which might not have been deposited

on the tape from contaminating the surface of the detector

and surrounding areas, which would have interfered with the

measurements.

A collimator (8mm diameter) was placed in front of the

detector to insure that it measured only the alpha particles

which came directly from the source (without scattering),
and not those from possible ambient contamination. It also
insured that the alpha particles were registered by the
central region of the silicon where charge collection was
more complete than at its periphery.

The energy calibration of the alpha spectra was
performed with the following radioactive sources (Nuc.73):

^{241}Am :	5.5443	MeV	(.35%)
	5.48574	"	(85%)
	5.44298	"	(13%)
^{212}Pb : ($^{212}Po-64\%$)	8.7848	"	(100%)
($^{212}Bi-36\%$)	6.09006	"	(27%)
	6.05077	"	(70%)
	5.7681	"	(1.7%)
	5.6071	"	(1.1%)

The ^{212}Pb sources were obtained by collecting on
aluminum strips the ^{220}Rn resulting from the decay of a
^{228}Th source.

3,2 - X-ray detector

X-ray measurements were needed (see section II-C)
when measuring the gas-jet transport efficiency. The
detector used was a .49 cm^3 Ge(Li) low energy photon
detector (Ortec model 8133-10200). The energy resolution

was ~400 eV for the 59-keV line of ^{241}Am. It was used for two different types of measurements:

- Off line measurements: the radioactive samples were placed at calibrated positions in front of the detector located away from the gas-jet system.

- On line measurements, that is measurements directly on the radioactive spot as it was collected with the gas-jet transport system. In this case the detector was positioned as indicated in Fig.4 and two correction factors had to be applied:

a) The absorption of the X-ray through the lucite window was estimated by measuring the absorption of the 59-keV gamma-ray from a ^{241}Am source. A value of 1.5% was measured. This value was assumed constant and applicable over the energy range of X-rays measured (~40-70 keV) since it introduced, in any case, only a minor correction.

b) The difference in geometrical efficiency between these two sets of measurements (on and off line) was measured by comparison of the counting-rate of the 59-kev line from a ^{241}Am source.

The reproducibility of the counting geometries was

found to be ~5% for the "on line" position, while that of
the "off line" geometry was ~3%.

3,3 - Gamma detector

An Ortec Ge(Li) detector (model number 8101-1521W)
was used when measuring the effective target thickness of
gold and tantalum foils. Its energy resolution was 1.5 keV
for the 1.33-MeV ^{60}Co line, and its quoted efficiency was
19% relative to a 3"x3" NaI detector.

3,4 - Electronics

Only single (rather than coincidence) events
needed to be detected, and as a result the electronic
apparatus needed was quite simple. A diagram of the set-up
is given at the lower part of Fig.5 in the case of the alpha
detector. The only difference when using X-ray or
gamma-radiation counting, was that the preamplifier assembly
was directly mounted on the cryostat (as is generally done
for a cooled Ge-Li detector). The Ortec, models 472 and 572,
spectroscopy amplifiers were the most significant item in
the electronic apparatus employed, in maintaining good
energy resolution over the range of counting rates
encountered in the experiments. These ranged up to 1000

Figure 5

Diagram of the electronic set-up including both alpha

detection and computer control of the gas-jet.
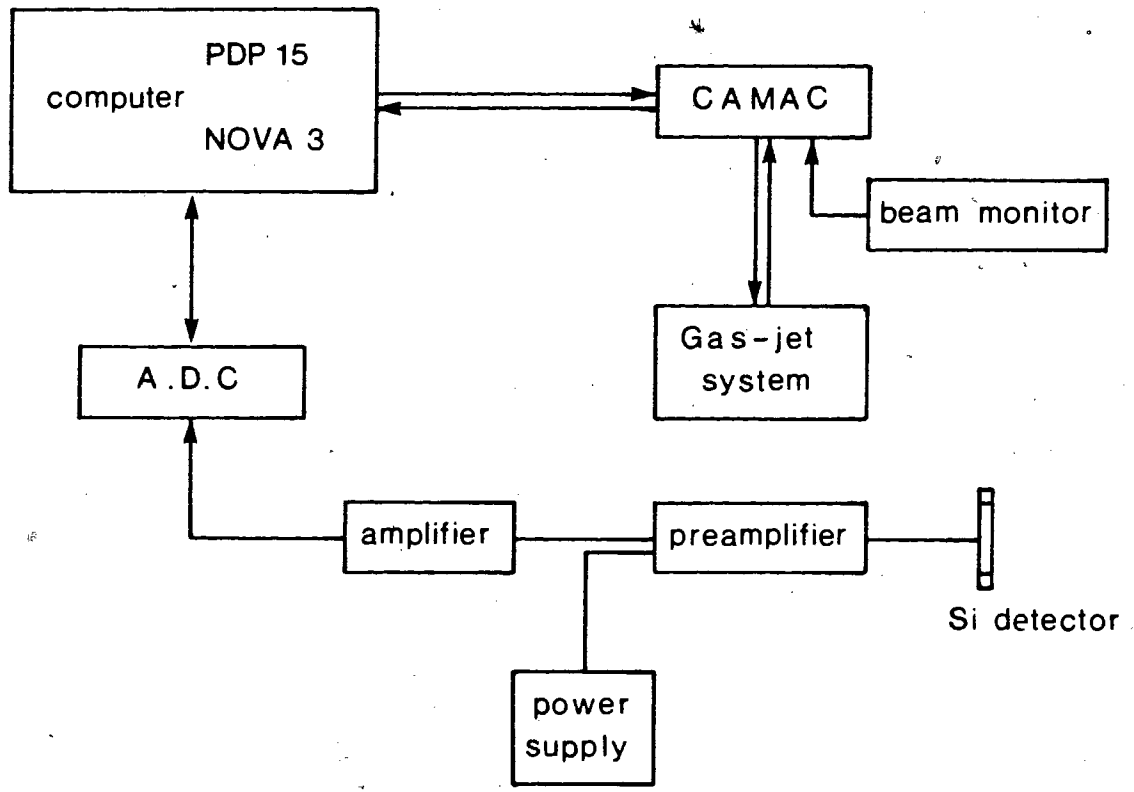
events per second when measuring the alpha activity, and
5000 events per second when measuring the X-ray
radioactivity.

The amplifier model 572 was found to be particularly
reliable with no appreciable shift in peak position or
degradation of the energy resolution for counting rate well
over 10000 counts per second. This is due to a combination
of several factors: a) an improved very symmetrical pulse
shaping, b) excellent baseline restoration, c) pulse pileup
rejection.

4) Computer control

The gas-jet transport system and the data
acquisition system were controlled by either a PDP-15 or a
NOVA-3 computer. A schematic of the most important features
of the apparatus is given Fig.5 and there was no fundamental
difference between the way the two computers functioned in
this respect.

The NOVA-3 was programmed using a temporary "home made"
language called "DUMB" (written by W.Bishop and A.Kurn). A
listing of one of the programs used to control the gas-jet
and data acquisition system is given in Appendix II

(Fig.34), and the corresponding flow chart is given Fig.6.

The PDP-15 programming was performed using the FOCAL
language modified by W.Bishop, A.Kurn and R.Torren to handle
the data acquisition system, and also to allow the user to
write and introduce machine language subroutines without
recompiling the entire program. A listing of the part of
the program dealing with the data acquisition is given in
Appendix II (Fig.33).

Depending upon the computer used, the data were either
written on tape (in an event by event fashion) or stored in
the computer memory. In both cases, the data could be
retrieved during off-line analysis as a function of the
elapsed time after the end of collection of the radioactive
sample at the end of the gas-jet (similar to the end of
bombardment in a classical radiochemical experiment).
Typically the time intervals into which the events or counts
were grouped ranged in length from .5 second for a
collection time of five seconds to several seconds in the
case of a collection time of several minutes.

Figure 6

Typical simplified flow chart of a program used to
collect the data.

- Initially various parameters are set such as
    number and length of time intervals into which
    the collection time will be divided or distance
    that tape will be moved.
- The tape is first moved to expose a fresh area
    in front of the exit of the capillary
- After the selected length of time the spot of
    radioactivity collected is moved in front of the
    detector and counting is started. At appropriate
    time intervals, either a special timing buffer is
    written on magnetic tape, or the data are placed
    in different parts of the computer memory
- When the last time interval has elapsed, a switch
    is interrogated and the run is either ended (with
    various housekeeping operations performed) or a
    new cycle initialized
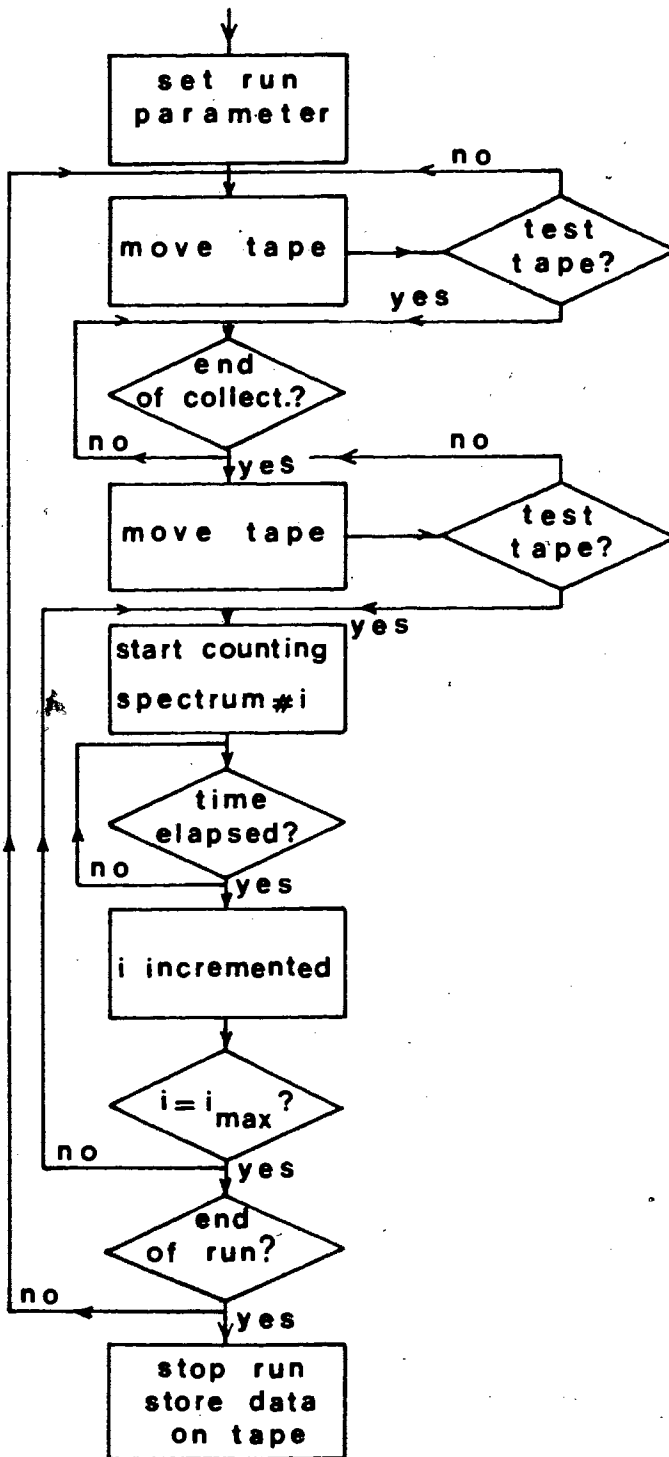
II-B – Operational characteristics of the gas-jet

recoil transport system

1) Previous studies

The transport of radioactive products from a production site to a low background measurement area is not new. Initially noble gases or volatile compounds emanating from a target were carried to a detector by molecular diffusion (All.59). The gas-jet transport system as it is presently used originated however with the accidental discovery in 1961 by Macfarlane and Griffioen that nuclides recoiling from a target and stopped in a chamber filled with helium were carried with the helium that leaked out when a pin hole developed in a silver foil window. The gas-jet system principle was then independently proposed by Friedman et all (Fri.62) and Macfarlane et all (Mcf.63).

Much of the initial work leading to the development of this method is due to the work of Macfarlane and coworkers, who indicated for example in 1962 (Mcf.62) that thermalised nuclear reaction products appeared to attach to impurities, although the importance of this phenomenon was not realised

until it was demonstrated that the use of ultra pure helium reduced considerably the efficiency of transport of the gas-jet system. The mass of the species in impure helium responsible for carrying the radioactivity was measured (Jun.71a) to be of the order of 10^6 amu with either positive or negative charges.

This essentially was the state of knowledge when the development of the S.F.U. gas-jet transport system started. Until that time the technique had been used mostly in the case of heavy-ion induced nuclear reactions where the intense ionisation field produced by the beam passing through the chamber led to the production of macromolecules from either oil vapours (always present) or impurities (such as benzene or water vapour) added to the helium.

2) Present work

The studies at S.F.U. by the writer in collaboration with W.Wiesehahn, J.M.D'Auria and B.D.Pate (Dau.73, Wie.73a, Wie.73b) were initially conducted with the usual helium as the carrier gas. The performance was disappointing at first, and even the addition of impurities such as benzene vapour failed to increase the transport

efficiency over 1% for the products of the fission of ^{238}U induced with 14 MeV neutrons.

Substantial progress was made however when a new impurity namely ethylene (selected amongst others for its potential for producing free radicals under irradiation), was introduced. Studies were performed on the transport efficiency it gave, both alone and in binary mixture with helium and nitrogen (Dau.73). Experiments on the system geometry (production-chamber size, capillary-tubing characteristics) and its effect on transit time and transport efficiency, the effect on collection of the distance between the exit nozzle and the collector, as well as a theoretical understanding of the system behaviour in terms of classical fluid dynamics, all led to a working system with a transport efficiency for fission products of the order of 70%. It soon became clear, however, that the role of ethylene was quite different from that initially thought, since consistently the efficiency of transport dropped to near zero when the pressure in the ethylene supply cylinder dropped to about 40-50 atmospheres. Investigations (Wie.73b) of this phenomenon led to the conclusion that cluster formation in the gas near the

critical pressure and temperature was responsible for the efficient transport of radioactive products by ethylene.

First the gas was checked for the presence of impurities by the use of a mass spectrometer. No impurities other than methane and water were observed (the limit of detection was ~0.01%). Further addition of these impurities to the ethylene gas did not produce any significant improvement in efficiency over that with pure ethylene alone. Also transport efficiency measurements performed with high-purity ethylene yielded identical results with those made when ethylene of lower quality was used.

Next, formation of liquid drops (resulting from partial liquefaction of the ethylene gas during expansion from the supply tank pressure to the gas delivery line pressure) was eliminated as a source of carriers by first varying the gas line pressure with no detectable effect, and by the insertion of a holding chamber as well as various kinds of traps in the supply line, which would have removed droplets had they been present: again the yield variations were minimal.

Finally, studies of the temperature and pressure in the

supply tank below which the transport efficiency dropped
abruptly led to the conclusion (Wie.73b) that these were
slightly above the critical temperature and pressure of
ethylene, where molecular cluster formation in the gas tank
might be expected to occur. Indeed such clusters, in
ethylene gas under conditions near the critical point, have
been studied by Cataldi and Drickamer (Cat.50) who measured
a cluster mass of 3×10^7 amu similar to the value which
Macfarlane et al (Jun.71a) had found for the molecular
clusters in helium carrying radioactivity.

Following the drop in pressure from the supply tank to
the gas-jet supply line, such clusters in ethylene would
then be unstable and would evaporate in a time which would
depend on many factors including whether or not they collide
with a heat source. Experimentally, it was found that the
insertion in the delivery line of Millipore* filters with
pore size of .5 and .8μm caused the transport efficiency to
drop to zero, while the flow rate changed only by about 5%.
This would be consistent with the fact that due to the
complex structure of the filters, the probability for the

*** Millipore Filter Corporation, Bedford, Mass. U.S.A.

ethylene clusters to collide with the filter material and
evaporate would be large, and thus lead to a zero
radioactivity transport yield.

Finally, further studies by W.Wiesehahn and J.D'Auria
via light scattering (Wie.74), confirmed the presence of
clusters in ethylene supplied from tanks with temperature
and pressure above the critical values (9.9°C, 50.5 atm),
and it was also shown (Wie.75) that aerosols of various
liquids (i.e. methanol in a N_2 carrier) also gave good
transport efficiency. The size of these clusters was
determined to be of the order of one micron in order to
achieve maximum transport efficiency. This has been
established both experimentally and theoretically (that is
analysis of losses that may occur due to sedimentation,
Brownian motion as well as coagulation and evaporation) in
agreement with results obtained by Wollnik and co-workers
(Wol.75).

All these studies had been performed for the transport
of fission products. When the gas-jet system was moved to
TRIUMF, further experiments were performed to test its
performances with spallation products. Three types of
targets were used:

- Gas targets - The gas studied flowed through an aerosol generator, where it was seeded with droplets of methanol (size ~1μm). The spallation products formed in the gas, were picked-up by neighbouring droplets and carried to the collection chamber by the gas. Alternatively, the target gas was mixed with ethylene gas which provided the necessary clusters.

- Liquid targets - A gas (N_2 or He) flowed through the aerosol generator filled with a liquid containing a compound of the element to be studied (i.e. when the spallation products of iodine were under investigation, the aerosol generator was filled with CH_2I_2

- Solid-foil targets - This is the type described previously, (near the beginning of this chapter), and used to obtain the cross-sections of spallation products reported in this thesis. Fig.7a displays the efficiency of the gas-jet (versus the flow-rate of ethylene) for the transport of alpha-active spallation/products recoiling from a solid foil target. Two types of alpha-activity were simultaneously measured: that arising from the spallation products of the target (in this case a Re target), and that

Figure 7

a) Gas-jet efficiency for the total alpha
   radioactivity produced with a Re target (1) and
   the radioactivity due to the production from the
   gas itself of alpha particles from ^{8}Li and ^{8}B
   decay (2) as a function of gas flow-rate.

b) Ratio of a(1) over a(2) as a function of the gas
   flow-rate. The arrow indicates the flow-rate of
   gas employed during collection of the spallation
   products.
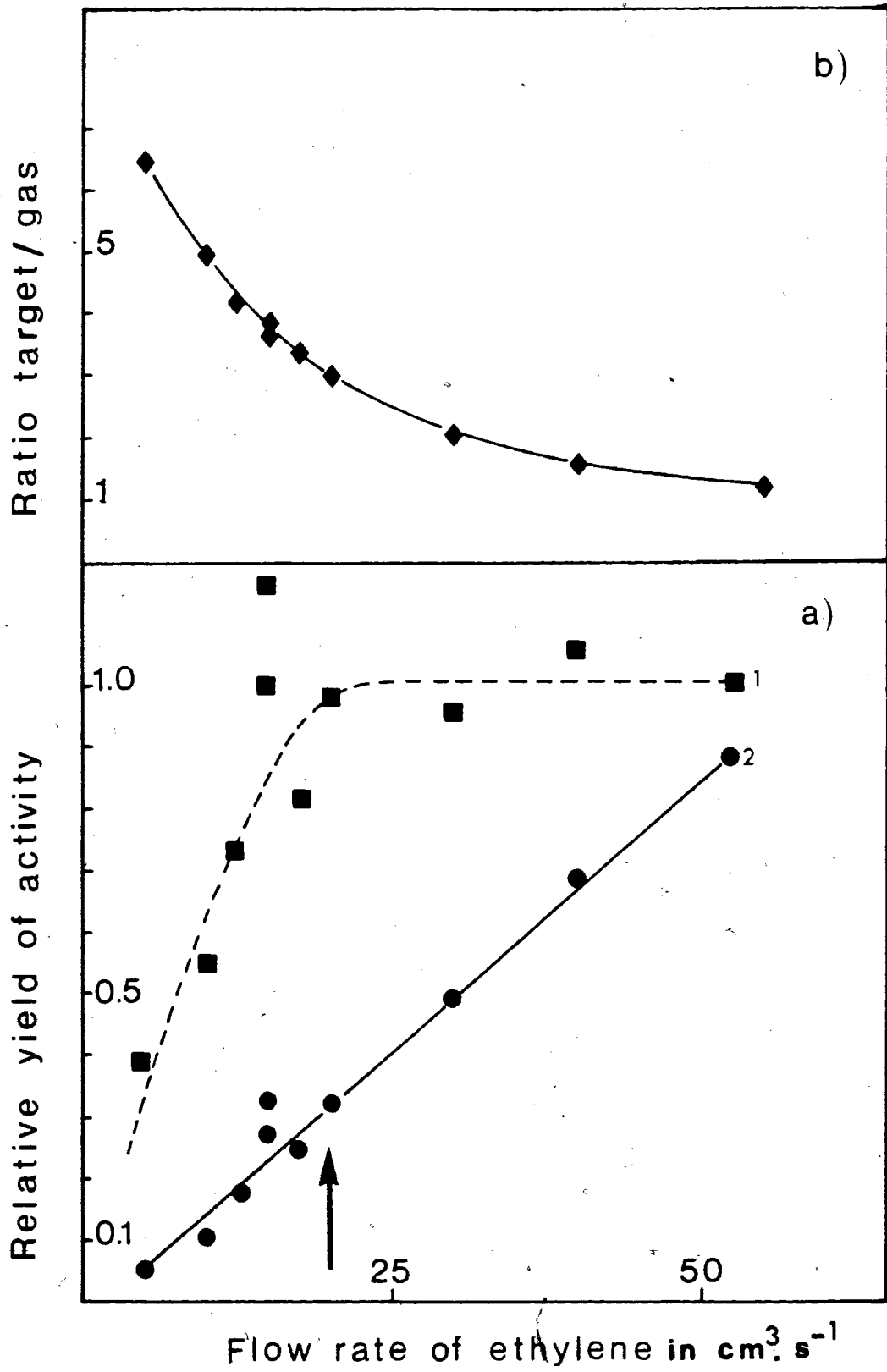
due to the decay of ^{8}Li and ^{8}Be (spallation products of
the ethylene gas). The corresponding curves present two
interesting aspects:

a) - While the data on each curve considered independently
fluctuate by a large amount, the ratio of corresponding
yields seems to fluctuate very little as seen in Fig.7b.
This indicates that fluctuations in the transport efficiency
of the gas-jet system influenced the yield of spallation
products from the solid target and from the gas in the same
way. As a result the latter could be used as a monitor of
the gas-jet system performance (i.e. when changing from one
target to another).

b) - It was desirable to utilise the lowest flow-rate of
ethylene compatible with a good transport yield in order to
minimise both, the build up of material on the collection
spot (to maintain good energy-resolution) and the proportion
of alpha radioactivity arising from the ethylene gas, since
it corresponds to a broad peak at 1.5 MeV with a high energy
tail extending up to 5 - 6MeV (region in which the
alpha-activities of interest are present). From the curves,
a flow-rate of 20 cm^3.s^{-1} was chosen, as indicated by
the arrow in Fig.7a.

In conclusion, the gas-jet recoil transport system, due to the studies performed by many groups in various countries, has in the last few years lost much of its aura of mystery (a description of some of this research can be found in Mcf.74). During this time, several techniques have been devised to couple the recoil gas-jet transport system with various devices in order to provide a mean of identification and/or separation of the radioactive products of interest. Such devices includes : SYSAK (Tra-75) (fast chemistry), RAMA (Nit-70) (hollow cathode mass separators), MAGGIE (Mcf-74) (time of flight).

However there are still aspects which are not fully understood, for example, although a chemical selectivity of the gas-jet has been observed by several author (Wil.74, Kos.75, Cab.75), as well as by the writer, in collaboration with the other members of the S.F.U. gas-jet research group (Bis.76), during studies of the spallation products of the gas target argon (it was then noticed that the halogen activities were collected when the argon was seeded with methanol droplets, while they were not when ethylene was the source of clusters), there is to date, no systematic understanding of this phenomenon. The experiment described

later is certainly the most comprehensive performed so far,
but shed little light on the mechanism responsible for such
a selectivity.

II-C - Ancillary data.

Since the alpha detector measured radioactivity at the end of the gas-jet transport system (rather than that in the target itself), the following data were needed if the absolute production cross-sections were to be calculated for the nuclear species in question from the measured alpha disintegration rates :   effective target thickness, gas-jet system transport efficiency, gas-jet transport time, and integrated beam current. These measurements will now be described in sequence.

1) Effective target thickness

Experiments were performed, using the thick target-thick catcher method (Har.60, Ale.68, Sch.76, Win.78). this technique pionered and developped by Sugarman allows to determine what fraction of the activity created in a target of known thickness recoils out of the target into a catcher (Fig.8) placed downstream. Provided that the variation of this fraction with composition of the reaction products was known, its value could be used to calculate the effective target thickness for the product nuclides observed.

Figure 8

Schematic representation of a thick target-thick catcher assembly:

1) Target foil

2) Catcher foil for forward recoiling nuclei
   ($\sim$12mg.cm^{-2} polyethylene)

3) Polyethylene bag

4) Catcher foil for backward recoiling nuclei
   ($\sim$12mg.cm^{-2} polyethylene)

5) Aluminum foils in sandwich to monitor the beam
   via the production of ^{24}Na in Al
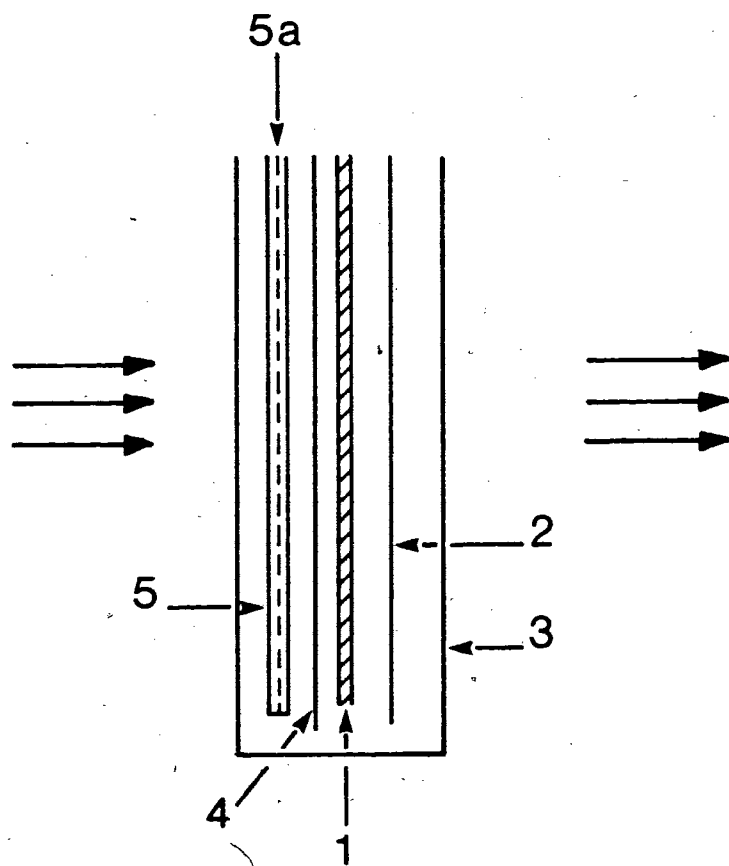
From the work of others (Nei.72, Lag.76, Kau.78) it was expected that a monotonic relationship would exist between -R-, the effective target thickness (proportional to the recoil range of a particular reaction product), and $-\Delta A-$, the mass difference between the product and the target species. Thus the present experiment was performed on Ta and Au, among the presently studied targets, with the expectation that data for products from other targets could be then obtained by assuming that the same -R- vs $-\Delta A-$ relationship applied in the target mass range of interest. The experiment involved irradiation times of the order of 30 minutes and the gamma-radioactivities were measured for several days.

The results are displayed Fig.9. Included in the figure are previous data (Pie.63, Sug.56) which as can be seen are not in disagreement with the present results. A straigth line relationship between R and A seemed to fit the data reasonably well, and the result of a least square fit (to the present measurements only) is displayed by the solid curve.

A further assumption was made in applying this relationship to the deep spallation products of this study:

Figure 9

Effective target thickness plotted as a function of the mass difference between the target and the product nuclides for various targets.

- The results obtained with the Ta and Au targets resulted from this work

- The data of Sugarman et al suffer from some spread but are not inconsistent with the results of this work

- The line corresponds to a linear fit to the data (of this work only). Although the gold and tantalum do not coincide perfectly, the difference was judged small enough so that the same linear relationship was used for both targets
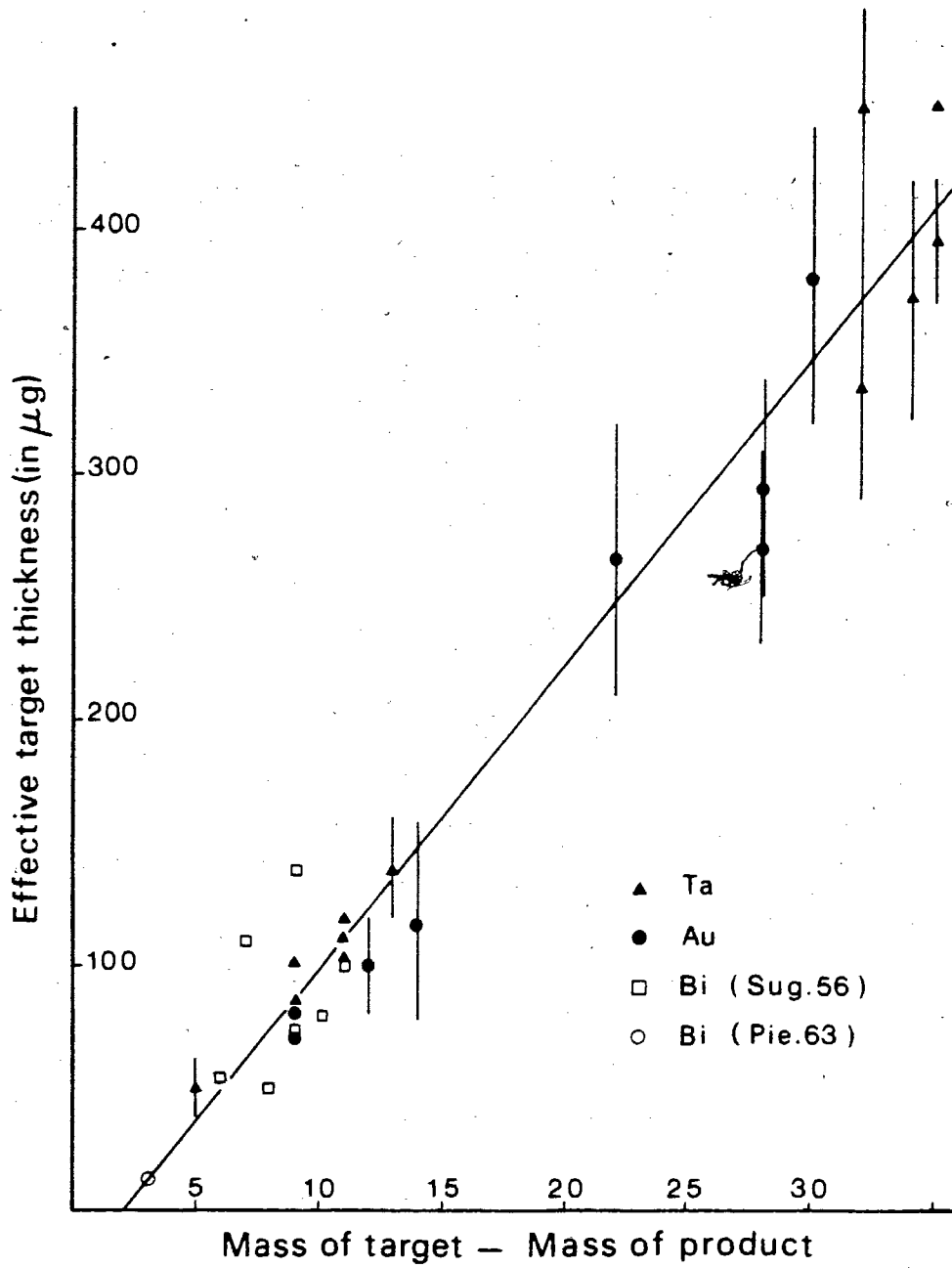
it was assumed that R depended only on ΔA, and not on other factors such as N/Z, etc...

2) Determination of absolute gas-jet efficiency

The gas-jet transport system is very useful to bring radioactive reaction products from their production site to a detection area with speed and efficiency. However its performance is influenced by many parameters which are difficult to control and even to appreciate properly. As a result, variations in collected activity of almost an order of magnitude have sometimes been noticed (with an apparently constant beam and other experimental conditions) both by previous workers and by the writer in the early stages of the present studies. Also no certain information existed as to whether or not every element studied during this work is carried with the same efficiency for a given gas mixture. Since the present purpose was to measure cross-sections, this aspect was critical for the present study. Thus the influence of all system parameters was carefully studied to stabilise yields as much as possible, and an absolute efficiency determination was attempted for products from the targets: Ho, Tm, Ta, Re, Au .

2,1 - Description of the experiment

An absolute transport efficiency determination should involve direct measurement of the products recoiling from the target (as for example was done for the determination of the effective target thickness) and comparison with the results obtained by measurement of the same products at the end of the gas-jet system.

Such measurements cannot unfortunately be done on the alpha-radioactive species of which the yield was being studied because of their short half-lives. These are generally less than, or of the order of, one minute, and it was not possible for practical reasons (opening of the irradiation area, dismantling of the irradiated target assembly and its transport to the counting station) to start counting a sample of activity recoiling directly from a target before 5 minutes after the end of irradiation. Furthermore, the activity generated in one irradiation was small, and this would have necessitated many irradiations for each target to gain statistical accuracy. In addition, measurements with good resolution were impossible on alpha activities buried in thick catcher foils, and subdivision

into a stack of thinner foils to reduce self absorption
would have increased counting times to an impossible extent.

As a result, transport efficiencies were measured for
more accessible nuclear species via a multistep approach
according to the diagram of Fig.10. The intermediate step
involved the measurement of X-ray radiations (trial
spectroscopy with gamma-radiations being unsuccessful due to
a combination of several factors, including the high Compton
background produced by the mixture of nuclides, and the high
level of radioactivity induced in the catcher foil).

In a first measurement (Fig.10a), a thick-target
thick-catcher package (Fig.8) was irradiated (in air at
ambient pressure) for 30 seconds with 300 nanoamperes of
protons. The catcher foil (polyethylene) was then assayed
via the X-ray detector described previously. The
X-radiations were counted for 5 minutes starting 5 minutes
after the end of irradiation. The data were recorded as a
function of the time, so that dead time corrections could be
made, and so that average half-life data for the nuclides
present were available (see below).

The second measurement was identical (i.e. same

Figure 10

Representation of the time sequence used in experiments performed to obtained the efficiency of the gas-jet system.

a) The proton beam was turned on for 30 seconds; a 5mn measurement of the X-ray radioactivity was started 5mn after the end of bombardment.

b) The gas in the gas-jet system was allowed to flow for 30s. (simulating the previous 30-second irradiation) X-ray measurements were performed immediately afterwards for 30s. and then for 5 minutes starting at 5 minutes after the end of collection

c) Collection of the radioactive species for 30s. followed by 30s. measurements of alpha as well as X-ray radiations.

a)

beam $\{^{on}_{off}$

X-ray $\{^{on}$ counting $\{_{off}$

b)

Gas-jet $\{^{on}_{off}$

X-ray $\{^{on}$ counting $\{_{off}$

c)

Gas-jet $\{^{on}_{off}$

α and X-ray $\{^{on}$ counting $\{_{off}$

time in minutes

0 1 2 3 4 5 6 7 8 9 10
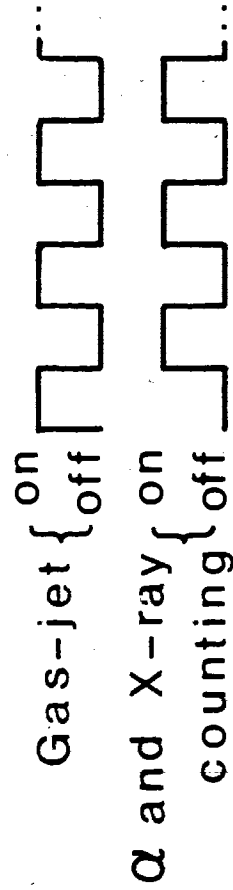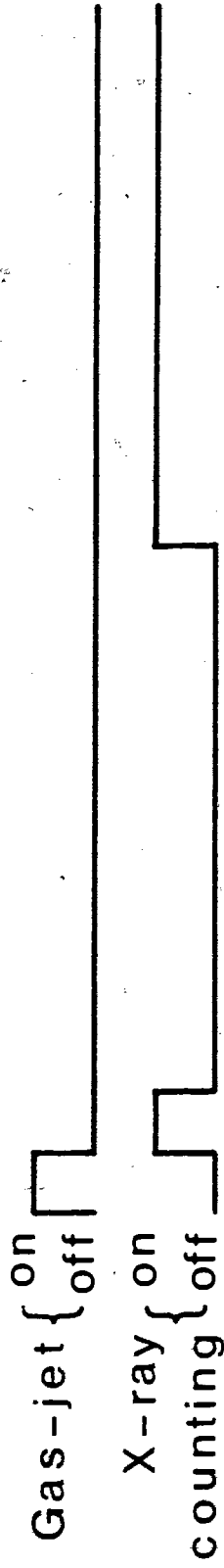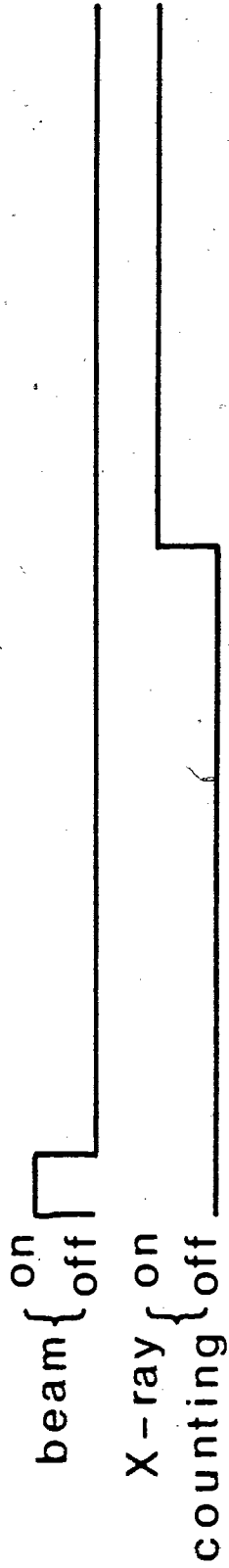
target, bombardment time and integrated beam current)
(Fig.10b), except that the radioactive sample was collected
at the end of the gas-jet, and counted twice: a first time
for 30 seconds immediately following the end of collection,
and a second time in a fashion identical to the first set of
measurements (for 5 min. after a delay time of 5 min.),
the decay of activity during this period also being
followed. A typical X-ray spectrum, corresponding to the
spallation products recoiling out of a Ta target and
measured during this last counting interval, is given
Fig.11. The cycle was then repeated to improve statistical
accuracy.

By direct comparison of the activities measured during
the 5 minute counting intervals (corrected for fluctuations
in the beam current), the efficiency of the gas-jet system
was obtained for the various elements of which the X-ray
were strong enough to be detected with a good statistics
(typically about several thousand counts in the k_1 lines
were obtained). An example of the results obtained with a
Re target is given Table II.

It can be noted on this table that the various
transport efficiencies were in most cases obtained from both

Figure 11

Typical X-ray spectrum. For reason of clarity, only the $k\alpha_1$ lines have been indicated on the figure.

The peaks with an energy of the order of 60-65 keV correspond to the $k\beta_1$ lines. The peaks at still higher energy are due to X-ray fluorescence of the surrounding lead shielding.

Ta TARGET
(30 sec. collection)

ENERGY IN KEV

COUNTS / CHANNEL
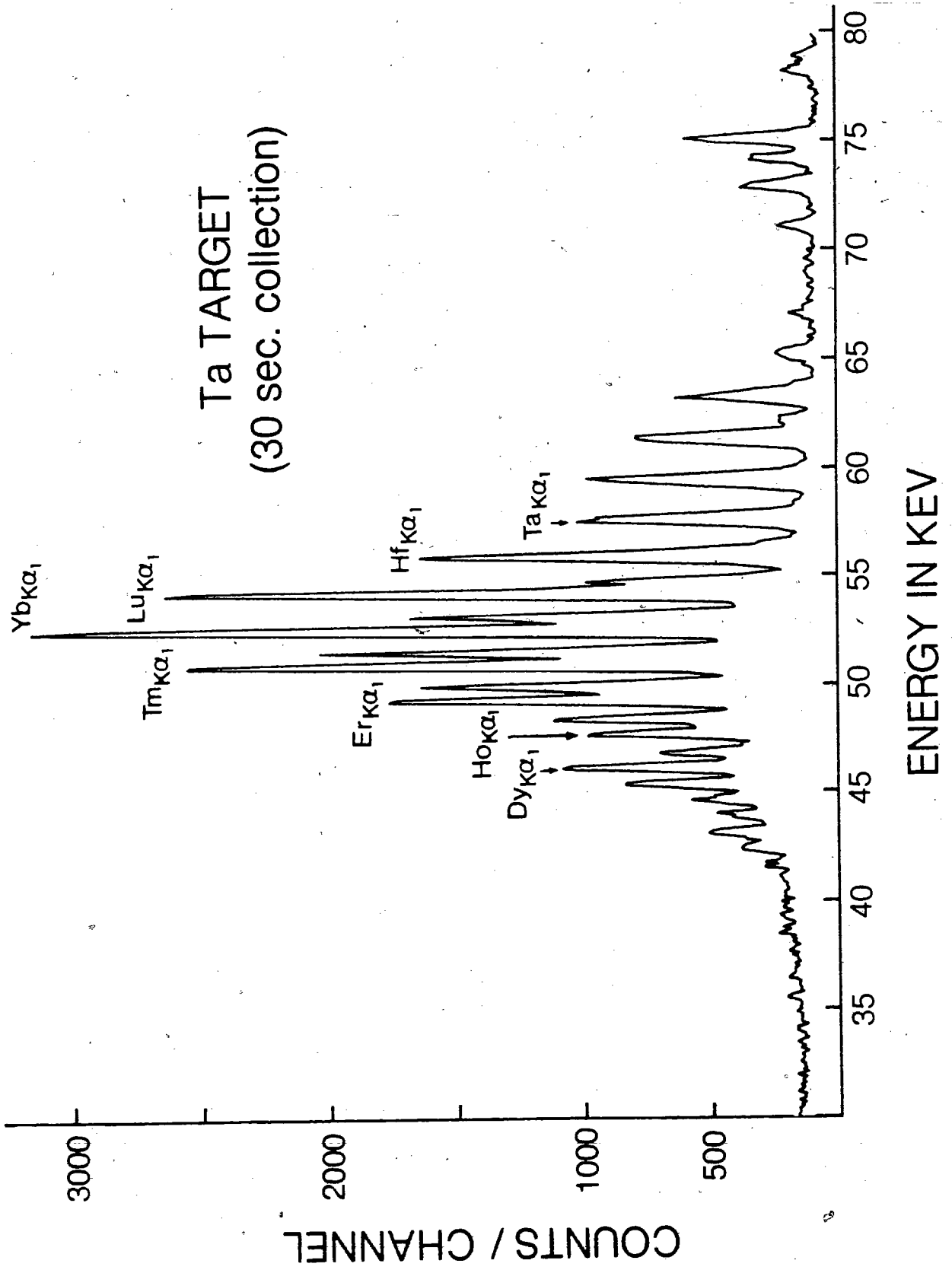
Table II

Efficiency of the gas-jet system (Re target)

Product element[o]	Activity* measured on the catcher foil		Activity* measured at the end of the gas-jet		Efficiency %		Average	
Dy $k\alpha_1$	35.6	± 2.5	4.92	± 0.20	14.	± 3.	14.	± 3.
Ho $k\alpha_1$	111.5	± 8.0	7.16	± 0.40	6.4	± 0.5	6.5	± .5
$k\alpha_2$	45.9	± 3.0	4.3	± 1.0	9.	± 3.		
α_2/α_1	0.41	± .06	0.60	± .05				
Er $k\alpha_1$	315.	± 7.	23.6	± 0.35	7.5	± 0.3	7.2	± 0.4
$k\alpha_2$	183.0	± 5.3	12.6	± 0.25	6.9	± 0.4		
α_2/α_1	0.58	± .03	0.53	± .02				
Tm $k\alpha_1$	455.0	± 8.3	36.4	± 0.4	8.0	± 0.5	7.6	± 0.4
$k\alpha_2$	262.	± 6.	19.2	± 0.3	7.3	± 0.3		
α_2/α_2	0.57	± .02	0.53	± .01				
Yb $k\alpha_1$	554.	± 9.	49.3	± 0.5	8.8	± 0.3	8.3	± 0.4
$k\alpha_2$	335.	± 20.	25.4	± 0.4	7.6	± 0.6		
α_2/α_1	0.60	± .02	0.52	± .01				
Lu $k\alpha_1$	378.	± 8.	38.0	± 0.5	10.0	± 0.3	9.8	± 0.3
$k\alpha_2$	223.	± 6.	21.4	± 0.4	9.6	± 0.4		
α_2/α_1	0.59	± .05	0.56	± .02				
Hf $k\alpha_1$	276.	± 15.	29.1	± 1.2	10.5	± 0.9	9.5	± 1.0
$k\alpha_2$	160.	± 8.	14.1	± 1.	8.8	± 1.0		
α_2/α_1	0.58	± .06	0.51	± .06				
Ta $k\alpha_1$	281.	± 12.	26.5	± 1.0	9.5	± .5	9.2	± 0.4
$k\alpha_2$	163.	± 7.	13.5	± .8	8.5	± .8		
α_2/α_1	0.58	± .05	0.51	± .05				
W $k\alpha_1$	224.	± 11.	11.7	± 1.0	5.2	± .7	5.4	± .5
$k\alpha_2$	116.	± 5.	6.4	± .7	5.5	± .8		
α_2/α_1	0.52	± .05	0.55	± .10				

* - activity in counts per second

the $k\alpha_1$ and $k\alpha_2$ X-ray transitions, a fact which allowed

cross-checking of the results. The results obtained via the

two transitions are generally within or close to the

statistical uncertainties. Also the intensity ratios

observed for $k\alpha_1/k\alpha_2$ are close to the theoretical

values, fact which indicates that the peak areas have been

adequately estimated.

In a third set of measurements, again with identical

targets, bombarding times etc, (Fig.10c) the radioactive

samples were again collected for 30 seconds at the end of

the gas-jet system. This time however alpha- as well as

X-radiations were measured for 30 seconds, corresponding to

the first counting interval of the previous set of

experiments. Such a short cycling time allowed for all this

process to be repeated many times to improve the statistical

precision of the alpha spectrum (on the average, around two

hundred cycles were necessary). By direct comparison of the

X-ray activities measured during this set of experiments

with the results obtained during the corresponding 30s

counting interval of the previous set of measurements, the

efficiency of the gas-jet system was obtained for these runs

where alpha-activities were recorded. As could be expected,

the relative efficiency of the various elements did not vary

between the second and third set of data (the average efficiencies were in most cases within 10% of each other).

Of course, this experiment relies on the assumption that the gas-jet system efficiencies measured could be extrapolated to the more neutron deficient products detected by the alpha measurements (that is that there is no mass effect between the various isotopes of the same element).

The evidence on this point is certainly indirect. No strong nuclear mass dependent effect is to be expected on the efficiency with which the nuclides attach to gas-molecule clusters, are then transported by the gas stream (with all the attendant focussing effect), and finally adhere to the catcher tape at the end of the system.

However a mass effect (through associated recoil momenta and ranges) is possible on the fraction of nuclides stopped by a given gas pressure in the target chamber. Thus experimental verification of some sort was desirable. In the absence of mass spectrometric measurements, the best that could be done was a measurement of the apparent half-life of the X-ray emitting species contributing to specific X-ray spectral lines, and using these half-lives to

estimate the most probable isotopic composition of the samples measured.

In order to verify the validity of the assumption that there was no mass effect, the following tests were performed.

First the decay curves obtained during the 5 minute counting interval, in which the thick catcher and the gas-jet transported specimen were measured, were compared. Fig.12 shows the relative ratios of the two decay data for several X-ray lines. It can be seen that, within available precision, the curves are flat. This indicates that the nuclide mixtures responsible for the two decay curves of which the ratios are plotted were undistinguishable, and that there was no discernible mass effect on the gas-jet transport efficiency.

The second test consisted in measuring the X-ray radioactivity of spallation products (from a gold target) collected at the end of the gas-jet transport system during 30 seconds for various flow-rates of ethylene. The decay of the various X-rays emitted was recorded immediately after the end of collection and followed for 12 minutes. The

Figure 12

Variation as a function of the decay time of the ratios of various X-Ray radioactivities collected with the gas-jet system, and caught on a thick catcher placed behind the target. The ratios displayed correspond to the following X-Ray: a) Os, b) Re, c) Ta, d) Hf, e) Lu
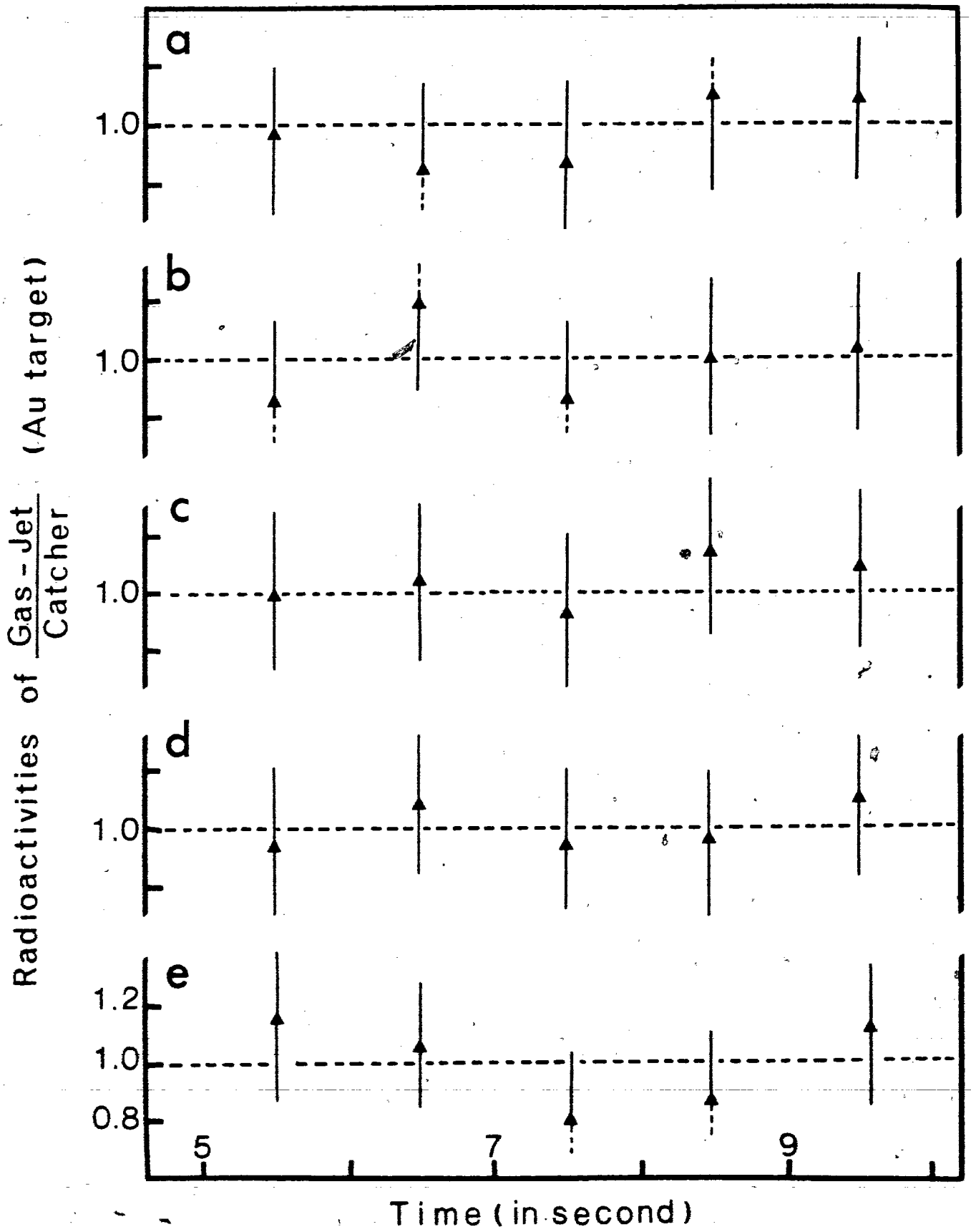
corresponding decay curves were analysed in the following way:

- First an average half-life was obtained for the mixture of activities detected near the end of the counting interval. This allowed an estimation of the mass of the heaviest isotopes for each element detected.

- Next an average half-life was obtained for the activities detected at the beginning of the counting period (that is immediately following the collection). In this way, an estimate could be made of the more neutron-deficient isotopes detected.

If a mass effect (such as could be introduced by a difference in recoil range inside the production chamber) had a significant effect on the gas-jet efficiency, this effect would be more pronounced at low pressure in the production chamber and one would expect that the relative yields of lightest and heaviest isotopes of same elements would show a systematic variation as a function of the pressure at which the production chamber was kept. The simplest fashion to control this pressure is by adjusting the flow-rate of gas. This was done and the results,

displayed in Fig.13, show the relative collection yields of various nuclides as a function of the flow rate (that is also as a function of the pressure in the production chamber). Certainly no variation can be observed on this figure, and if there is indeed a such effect, it is small and it is reasonable to neglect it.

2,2 - Results

A summary of the transport efficiencies obtained in this fashion for the various targets measured is presented in Table III. While for reasons not fully understood, the absolute efficiency for the same element varied from one target to another - generally the yield decreases with increasing Z of the target -, the relative yields follow a reproductible pattern. In order to check this point, and to have a survey of data from as many product elements as possible, the results from different targets were normalised (in such a way that corresponding product elements overlapped) and the result is displayed Fig.14. The normalised values for the various products -indicated at the bottom of the figure- are represented with different symbols according to the target from which they arose. As can be seen, the relative yields are not

Figure 13

Variation with the flow-rate of ethylene of the ratios

of activities of various nuclides of different masses

at the end of the gas-jet system.

The approximate masses were obtained by collecting the

samples for 30s and following the decay for 12min. In this

way average half-lives were obtained near the end of the

counting interval, and at its beginning. The approximate

masses of which the ratios are displayed are:

$Ta_{k\alpha_1}$ ~1min ($\sim^{168}W$)   ,   ~10min ($\sim^{172}W$)

$Pt_{k\alpha_1}$ <1min ($^{183-4}Au$) ,   ~8min ($\sim^{188}Au$)

curve a) : ratio of $\sim^{168}W/^{172}W$ (A ~ 6)

curve b) :   " $\sim^{183-4}Au/^{188}Au$ (A ~ 5)

curve c) :   " $\sim^{168}W/^{188}Au$ (A ~ 20)

Relative yields of collection

Flow rate of ethylene
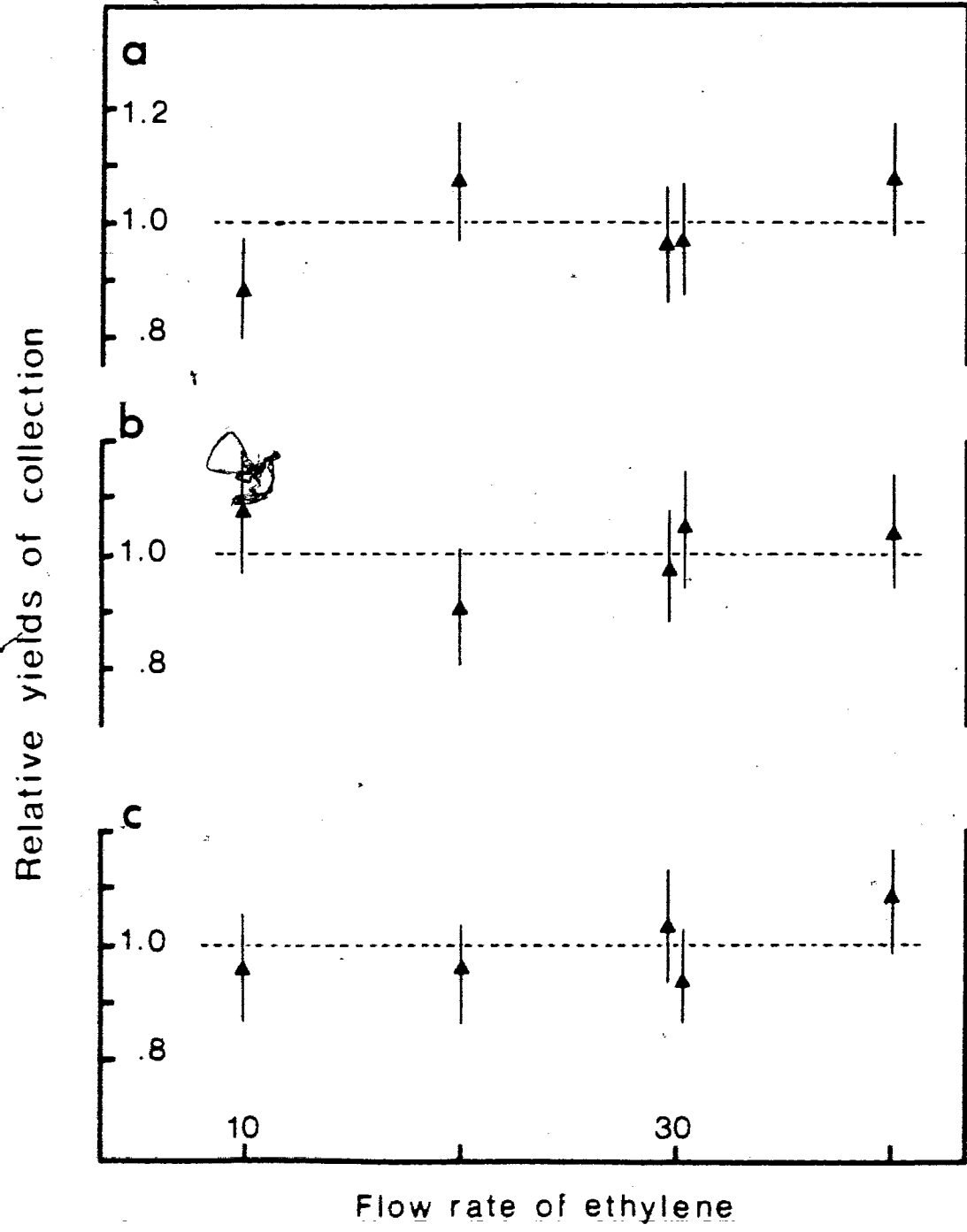
Table III

GAS-JET SYSTEM TRANSPORT EFFICIENCY (%)

PRODUCTS.	TARGETS				
	HO	TM	TA	RE	AU
Pm	17.				
Sm	20. ± 5.				
Eu					
Gd	17. ± 6.				
Tb	18. ± 1.	4.7 ± 0.3			
Dy	22. ± 1.	4.0 ± 1.3	8. ± 2.		
Ho	25. ± 2.	8. ± 1.	8.7 ± 1.0	14. ± 3.	
Er		3.5 ± 1.	6.6 ± 0.8	6.5 ± 0.5	
Tm		4.5 ± 1.	6.2 ± 0.15	7.2 ± 0.4	2.9 ± .1
Yb			6.7 ± 0.3	7.6 ± 0.4	2.5 ± .2
Lu			6. ± 0.5	8.3 ± 0.4	2.5 ± .4
Hf			6.7 ± 1.	9.8 ± 0.3	2.9 ± .15
Ta			5.1 ± 0.5	9.5 ± 1.0	3.6 ± .6
W				9.2 ± 0.4	2.27 ± .05
Re				5.4 ± 0.5	1.61 ± .02
Os					1.73 ± .09
Ir					1.9 ± .08
Pt					2.2 ± .2
Au					1.4 ± .2

Figure 14

·Relative collection efficiencies of elements ranging

from Gd to Au from various targets. The different targets

have been normalized as explained in the text.

The straight line represents a linear variation of the

efficiency with the 'Z' of the products.
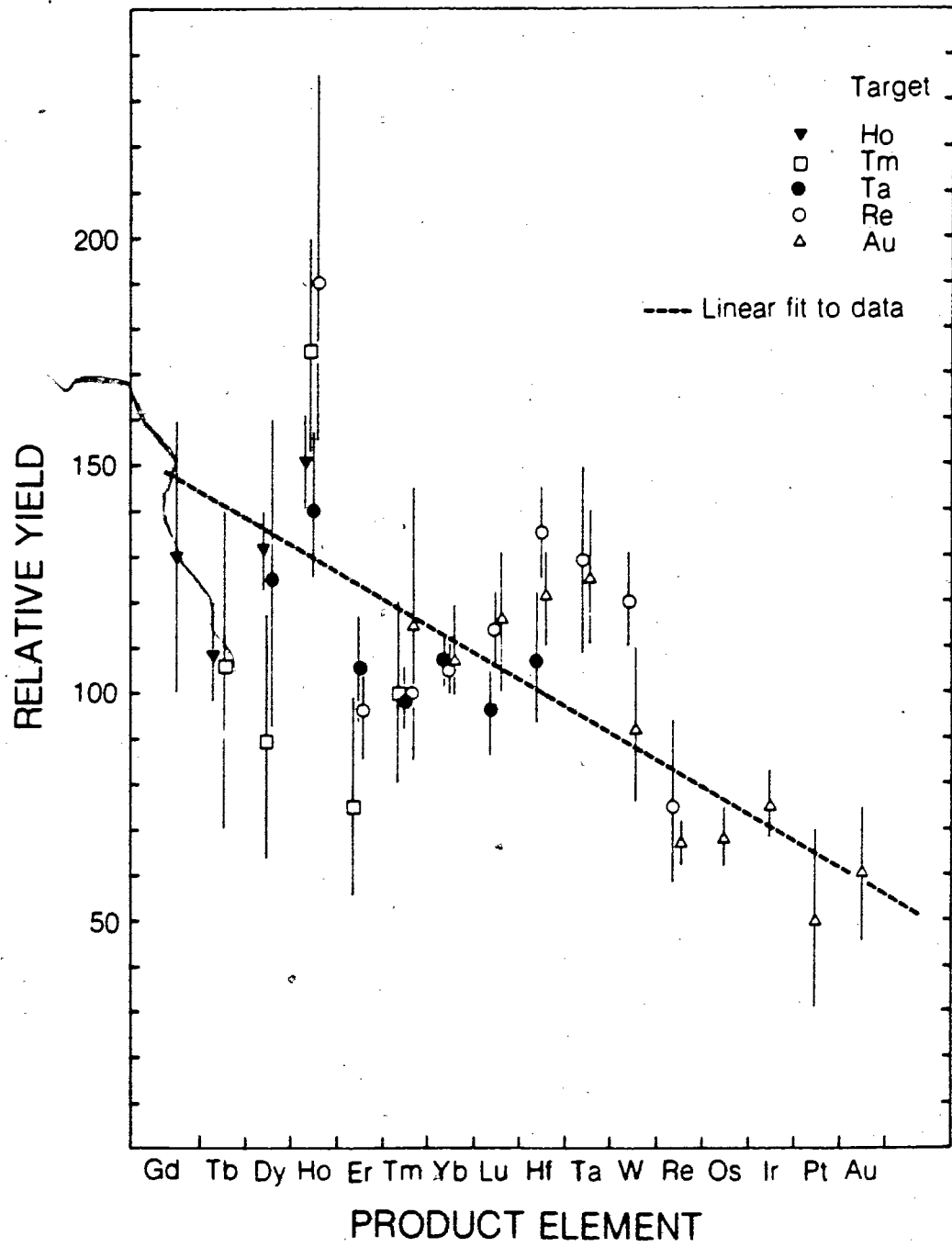
completely inconsistent (within statistics) with a constant
efficiency as a function of the Z of the product. However an
efficiency varying irregularly with Z seems more probable
considering the reproducibility of the pattern of relative
efficiencies from various targets. A third possibility,
namely a linear variation is displayed by the broken line.
Since there is no understanding as to why any of these three
possibilities might occur, the linear relation was used when
the efficiency of products was needed, but could not be
measured directly by the previously described set of
experiments (Of course the relative yields were then
corrected for the necessary normalisation factor).
Generally the divergence between the fitted curve and the
data points does not exceed 20% .

3) Transport time

If, as was initially intended, one considers the
time spent by the radioactive products in the production
chamber and subsequently in the capillary as being
equivalent to a delay (or cooling time), all one needs to
know is the average over-all time between production and
detection of the products, so that the corresponding
radioactive decay can be taken into consideration when

extracting production rates from radiation measurements taken for the various nuclides.

This information can be obtained through theoretical calculations, as the sum of the expected average transit time in the capillary and the average retention time in the production chamber. Such calculations are discussed in the Appendix I; however, there are several unknowns such as the extent of the focussing effect of the clusters towards the center of the capillary, and the effective volume of the production chamber. Since some of the activities measured are as short as 1.5 seconds, it was imperative to know transit times with a precision better than 0.5 second; as a result, there was need to determine these numbers experimentally, at least to check the calculated values.

To obtain this information, the beam of the cyclotron was modulated, with the beam on for 7 seconds and off for 6 seconds. This was achieved by the TRIUMF Operations group by chopping the 300-keV beam injected into the cyclotron. The gas-jet transport system was operated continuously, so that a stable gas-flow pattern could be established. The collection tape was kept moving at a constant velocity so that a constant fraction of the collected radioactivity was

recorded by the detection system. Thus the observed time variation of the collected activity was due only to the effect of the modulation of the cyclotron beam intensity, of the transit time in the gas-jet system, and of the later's variation about its mean value.

The results are shown Fig.15,16 for different ethylene flow rates and a beryllium target. The analysis of these data led to the formulation of the simple theory described in Appendix I-2 and, as a result, to a slightly different relation between the detected activities and the coresponding cross-sections than in a classical irradiation experiment. On the curves, the solid line corresponds to a fitting of the data according to the treatment described in Appendix I-2, with the following function:

$$A(t) = 0 \qquad\qquad : t < t_o + t_1$$

$$A(t) = \varepsilon N I \sigma \, \frac{\lambda \Lambda t_2}{\lambda + \Lambda} \, \exp{- \lambda(t_o+t_1)} [1 - \exp{-(\lambda+\Lambda)(t-t_o-t_1)}] \; : t > t_o + t_1$$

A(t) is the activity detected at the time t after the
    beginning of bombardment.

t_o is the transport time

t_1 is the time taken by the tape to bring the activity
    in front of the detector

Figure 15

Activity of ^{8}Be collected at the end of the gas-jet
system as a function of time, the cyclotron beam being
turned off and on as described in text. The ethylene gas
flow-rate was constant at 70 $cm^3.s^{-1}.atm^{-1}$.

Counts/channel vs. Time in sec. (.05 sec. per channel)
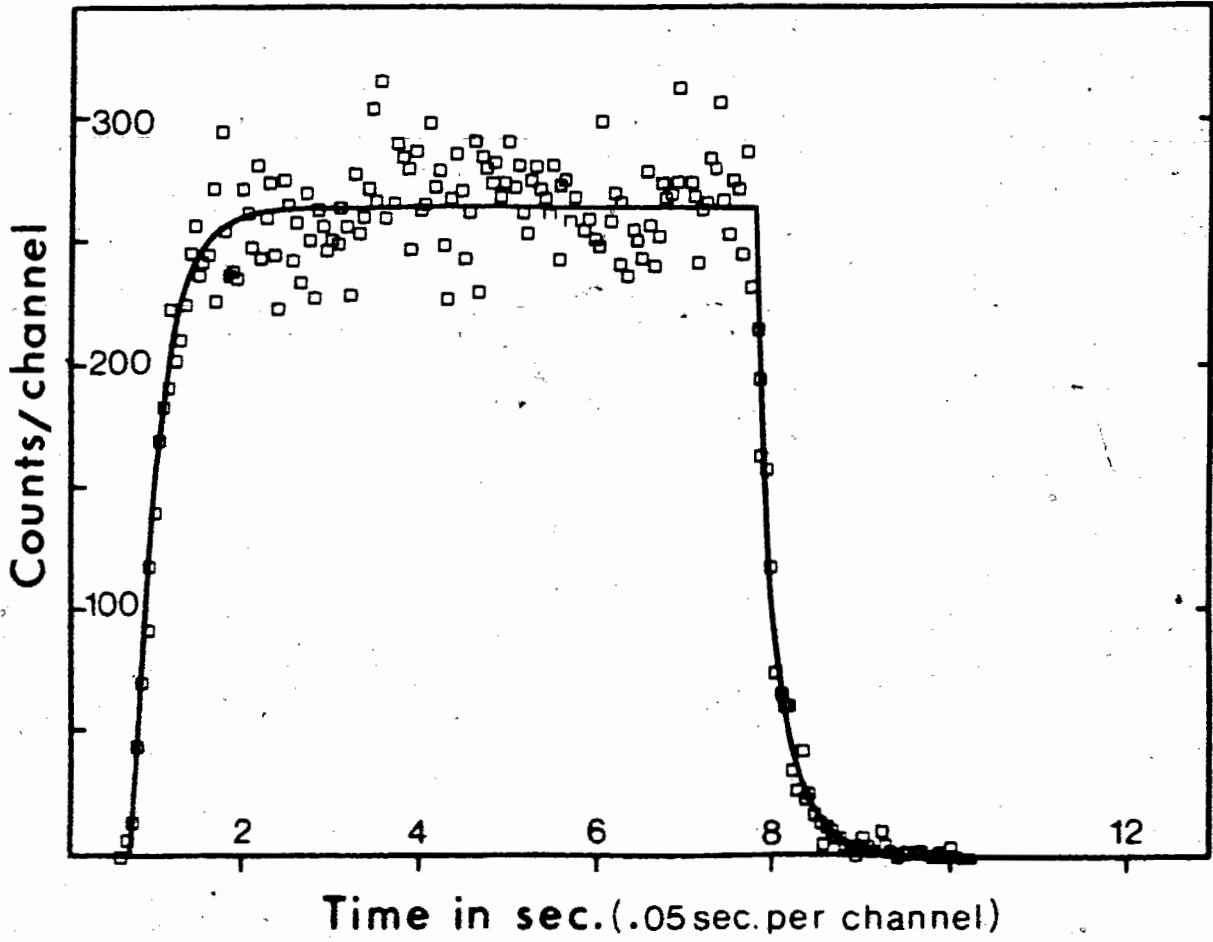
Figure 16

Activity of ^{8}Be collected at the end of the gas-jet system as a function of time, the cyclotron beam being turned off and on as described in text. The ethylene gas flow-rate was constant at 25 $cm^3.s^{-1}.atm^{-1}$.
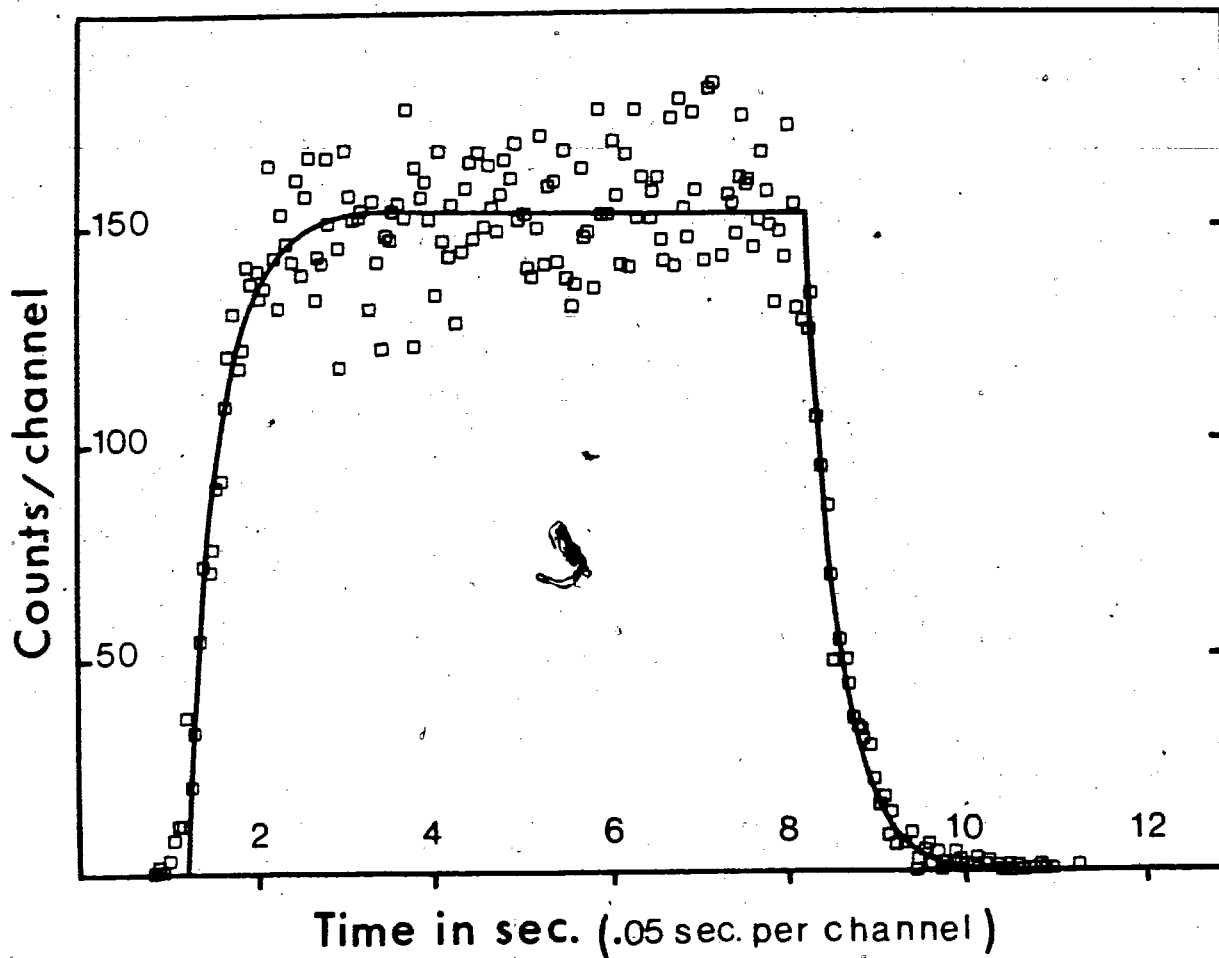
t_2 is the time during which the activity is in the field

   of the detector

ϵ is the gas-jet efficiency

N is the target thickness in atoms.cm^{-2}

σ is the production cross-section of the species measured

λ is the decay constant of the radioactive species measured

Λ is defined as ρ/V where ρ is the gas flow, and V the

   volume of the irradiation chamber

I is the intensity of the proton beam.

4) Beam monitoring

This was accomplished by means of a secondary emission monitor in which gold plated foils intercepted a fraction of the proton beam. The electrical current generated by collection and amplification of the secondary emitted electrons was proportional to the proton beam intensity. The calibration of this secondary emission beam monitor (S.E.M.) was performed by G.Mackenzie and J.Vincent (Mac.78) via comparison of the S.E.M. reading with the results obtained both with a Faraday cup, and the production of ^{22}Na in an aluminum foil. They found that for each microcoulomb of proton beam (at a bombarding energy of 480 MeV), a charge of .37 microcoulomb was generated in the S.E.M..

III - DATA ANALYSIS AND RESULTS

III-A - General considerations

The identification of the various activities measured was achieved by comparison of their emitted radiation energy (generally measured with an accuracy of the order of 5 keV) and half-lives with published values. Since the various radioactivities obtained vary in half-life from around one second to several minutes, various collection and counting times (as described previously) were selected to enhance the production and detection of the various nuclides investigated (i.e. ^{156}Tm of 1.5s half-life was measured with a 5-second collection time, followed by ten counting intervals of .5 second each).

Generally speaking, the following timing cycles were found adequate to permit measurement of half-lives of present interest:

collection time	5s	10s	30s	60s
total counting time	5s	30s	60s	300s

The collection time was limited to a maximum of one minute, due to the fact that when it much exceeded this value, the build-up of material from the gas stream onto the collector became thick enough that a degradation in energy resolution of the alpha peaks became noticeable.

The background in the α-spectrum due to the decay of ^{8}Li and ^{8}Be (nuclear-reaction products from the carbon in the ethylene gas) was kept to a minimum by using the lowest flow-rate of gas compatible with a high transport efficiency of the gas-jet (as discussed previously and indicated in Fig.7).

In order to verify the absence of contamination of the system by heavy elements, blank runs (with an aluminum target) were routinely performed. The results indicated, that if such contaminants were present in the system, they did not produce detectable amounts of alpha-emitting nuclides.

III-B - Analysis

Typical α-spectra (obtained from various targets) are presented in Fig.17-20 and the most intense α-activities are listed in Tables IV-X, together with their identification. It can be seen that in all cases, the measured peak energy has not been affected by deposit build-up at the end of the gas-jet system.

The data, once retrieved in the form of such spectra corresponding to decay of the radioactive species at successive delay times after the end of collection, were analysed with the computer code Gamanal (Gun.72). This program initially written for the analysis of gamma-ray spectra experienced some difficulties in reproducing exactly the shape of the low-energy tail of the alpha peaks. Nevertheless the effect was minimal on the accuracy with which spectrum peak areas could be extracted as can be judged from Fig.21. The Gamanal code was preferred over other available codes for analysis of the present data since it presented the advantage of consistency in peak location and in background determination.

The areas of the alpha peaks as a function of time

Figure 17

Typical α spectrum from a Ho target: collection and counting times were 5 seconds.
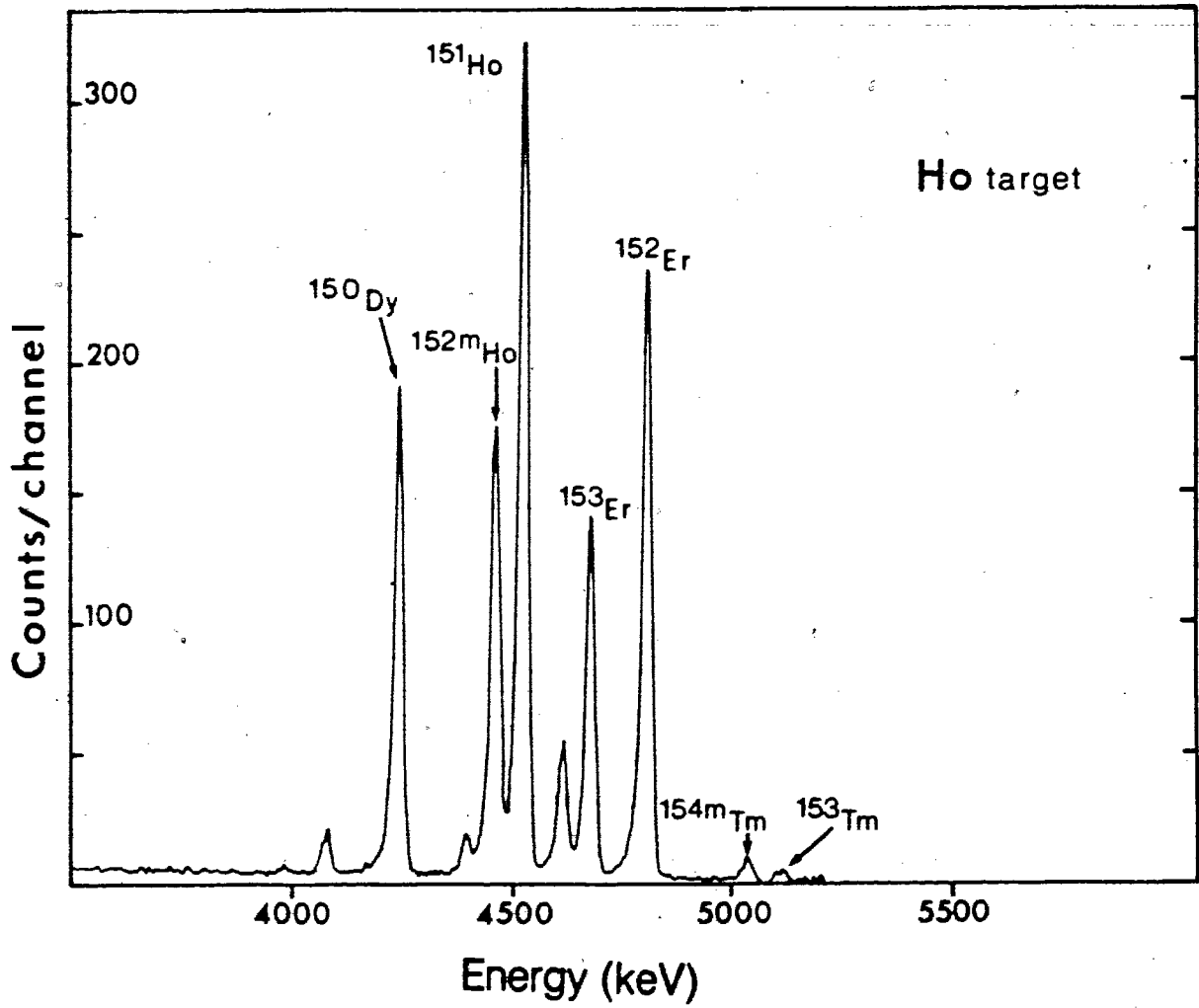
Figure 18

α spectrum from radioactive products collected from a

Re target. Collection time 10s. and counting time 30s.

Re Target
10s Collection

COUNTS / CHANNEL vs ENERGY IN KEV
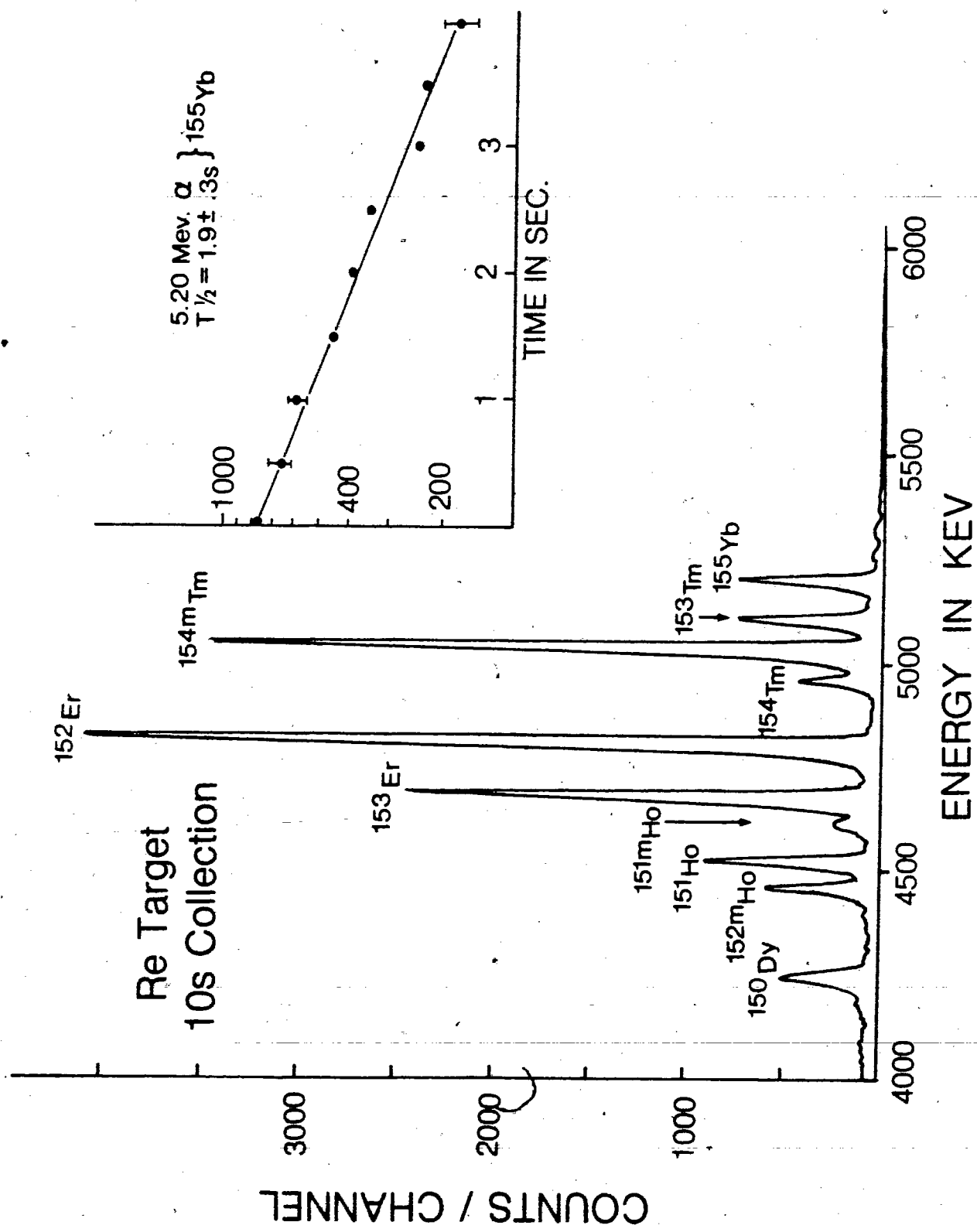
Figure 19

α spectrum from radioactive products collected from an Ir target. Collection time 10s and counting time 30s.
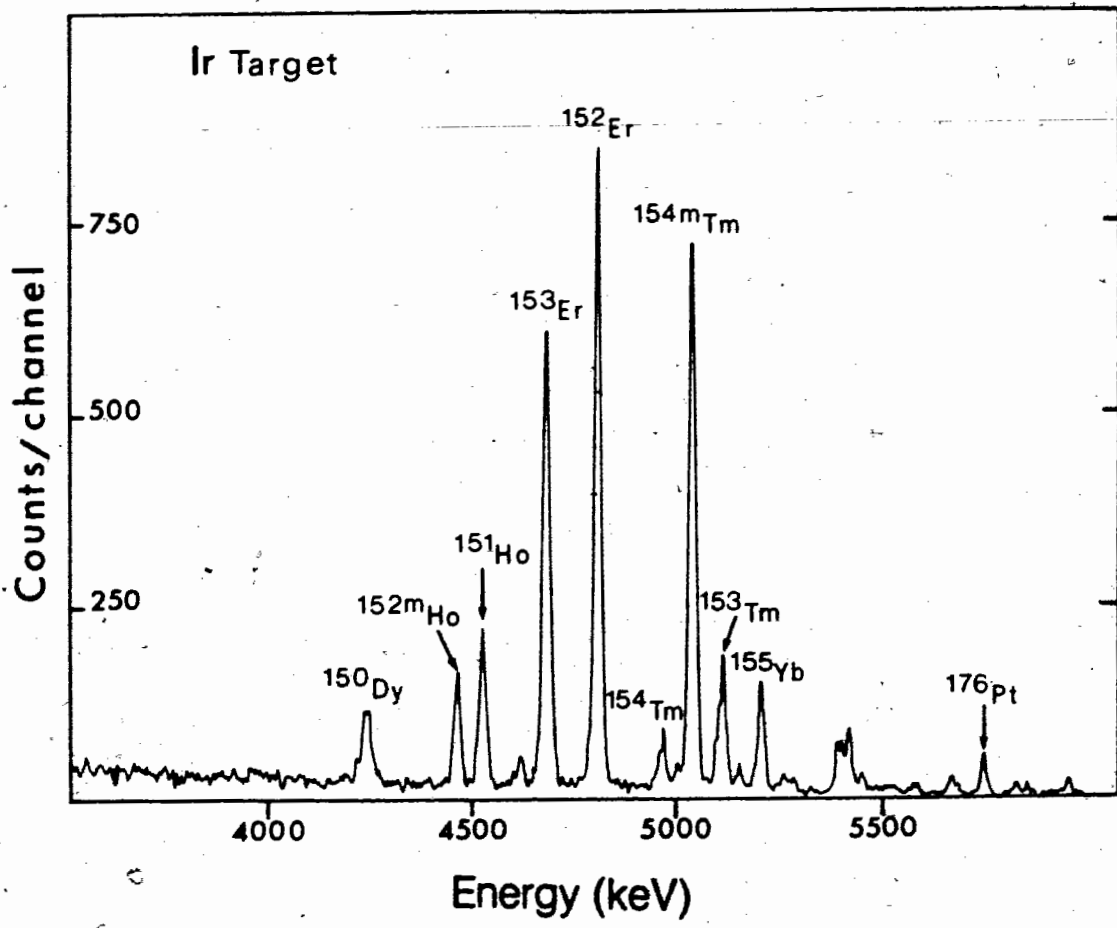
Figure 20

α spectrum from radioactive products collected from a
Au target. Collection and counting time 10s.
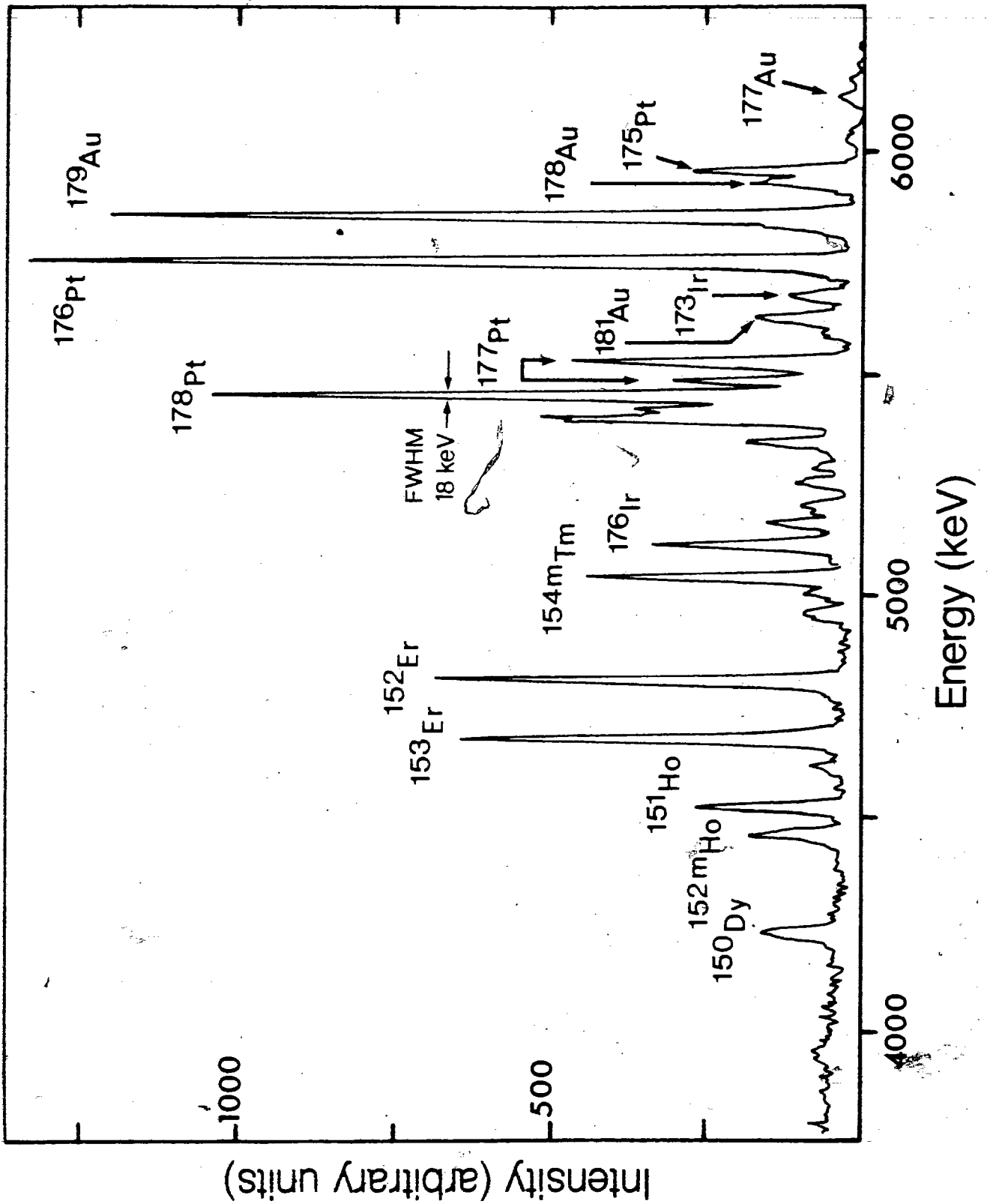
Table IV

Alpha-activities measured from a Ho target

Experimental data		Assignment*	Literature values	
E (MeV)	$T_{1/2}$(second)		E (MeV)	$T_{1/2}$(second)
5.104	1. ± 1.	b)^{153}Tm (85%)	5.103	1.6 ± 0.1
5.032	3.0 ± 0.3	b)^{154m}Tm(85%)	5.030	3.0 ± 0.1
4.801	9.5 ± 0.5	b)^{152}Er (86%)	4.799	9.8 ± 0.3
4.673	35.2 ± 0.8	b)^{153}Er (53%)	4.671	36. ± 1.
4.611	50.4 ± 1.	b)^{151m}Ho(13%)	4.607	47. ± 2.
parent	17. ± 4.	a)^{151}Er (0%)		23. ± 2.
4.518	33. ± 0.5	b)^{151}Ho (13%)	4.517	35.6 ± 0.4
4.456	49. ± 2.	b)^{152m}Ho(6.5%)	4.453	52.3 ± 0.5
4.388		b)^{152}Ho (12%)	4.387	142. ± 10.
4.234	435. ● 10.	b)^{150}Dy (34%)	4.232	430.2 ± 1.5
parent	23. ± 4.	d)^{150}Ho (0%)		~30.
4.070	>500.	b)^{151}Dy (5.5%)	4.067	1020. ± 15.
parent	30. ● 10.	b)^{151}Ho (13%)	4.517	35.6 ± 0.4

a) Gau.75, b) Bow.72, d) See.74

*) The numbers in parenthesis correspond to the
   alpha-branching ratios.

Table V

Alpha-activities measured from a Tm target

Experimental data		Assignment*	Literature values	
E (MeV)	$T_{1/2}$(second)		E (MeV)	$T_{1/2}$(second)
5.199	1.6 ± 0.2	c)^{155}Yb (90%)	5.202	1.65 ● 0.15
5.104	1.4 ± 0.05	b)^{153}Tm (85%)	5.103	1.6 ± 0.1
5.032	3.1 ± 0.06	b)^{154m}Tm(85%)	5.030	3.0 ± 0.1
4.957	7.5 ± 0.5	b)^{154}Tm (85%)	4.955	5. ± 1.
4.799	10. ± 0.2	b)^{152}Er (86%)	4.799	9.8 ± 0.3
4.673	36.6 ± 1.	b)^{153}Er (53%)	4.671	36. ● 1.
4.611 parent	~45. ~20	b)^{151m}Ho(13%) a)^{151}Er (0%)	4.607	47. ± 2. 23. ● 2.
4.518	36.3 ± 1.	b)^{151}Ho (13%)	4.517	35.6 ± 0.4
4.456	51.7 ± 0.5	b)^{152m}Ho(6.5%)	4.453	52.3 ± 0.5
4.388	150. ● 10.	b)^{152}Ho (12%)	4.395	142. ± 10.
4.233 parent	420. ± 15. 22. ± 3.	b)^{150}Dy (34%) d)^{150}Ho (0%)	4.232	430.2 ± 1.5 ~30.
4.172	>200.	b)^{154}Er (5.5%)	4.166	348. ± 10.
4.07 parent	>300. ~30. ± 10.	b)^{151}Dy (5.5%) b)^{151}Ho (13%)	4.067 4.517	1020. ± 15. 35.6 ± 0.4

a) Gau.75, b) Bow.72, c) Hag.77, d) See.74

*) The numbers in parenthesis correspond to the
   alpha-branching ratios.

Table VI

Alpha-activities measured from a Ta target

Experimental data		Assignment*	Literature values		
E (MeV)	$T_{1/2}$(second)		E (MeV)	$T_{1/2}$(second)	
5.199	1.8 ± 0.2	c)^{155}Yb (90%)	5.202	1.65	± 0.15
5.104	1.6 ± 0.1	b)^{153}Tm (85%)	5.103	1.6	± 0.1
5.032	3.17 ± 0.07	b)^{154m}Tm (85%)	5.030	3.0	± 0.1
4.957	8.3 ± 0.3	b)^{154}Tm (85%)	4.955	5.	± 1.
4.799	10.7 ± 0.2	b)^{152}Er (86%)	4.799	9.8	± 0.3
4.673	36.5 ± 0.5	b)^{153}Er (53%)	4.671	36.	± 1.
4.611	42. ± 3.	b)^{151m}Ho(13%)	4.607	47.	± 2.
parent	21. ± 4.	a)^{151}Er (0%)		23.	± 2.
4.518	35. ± 1.	b)^{151}Ho (13%)	4.517	35.6	± 0.4
4.456	49. ± 1.	b)^{152m}Ho(6.5%)	4.453	52.3	± 0.5

a) Gau.75, b) Bow.72, c) Hag.77, d) See.74

*) The numbers in parenthesis correspond to the
   alpha-branching ratios.

Table VII

Alpha-activities measured from a Re target

Experimental data		Assignment*	Literature values		
E (MeV)	$T_{1/2}$(second)		É (MeV)	$T_{1/2}$(second)	
5.199	2. ± 0.5	c)^{155}Yb (90%)	5.202	1.65	± 0.15
5.104	1.7 ± 0.2	b)^{153}Tm (85%)	5.103	1.6	± 0.1
5.032	3.15 ± 0.05	b)^{154m}Tm(85%)	5.030	3.0	± 0.1
4.957	5. ± 1.	b)^{154}Tm (85%)	4.955	5.	± 1.
4.799	10.5 ± 0.5	b)^{152}Er (86%)	4.799	9.8	± 0.3
4.673	36.8 ± 1.	b)^{153}Er (53%)	4.671	36.	± 1.
4.611 parent		b)^{151m}Ho(13%) a)^{151}Er (0%)	4.607	47. 23.	± 2. ± 2.
4.518	36. ± 1.5	b)^{151}Ho (13%)	4.517	35.6	± 0.4
4.456	45. ± 5.	b)^{152m}Ho(6.5%)	4.453	52.3	± 0.5
4.230 parent	25. ±	b)^{150}Dy (34%) d)^{150}Ho (0%)	4.232	430.2 ~30.	± 1.5

a) Gau.75, b) Bow.72, c) Hag.77, d) See.74

*) The numbers in parenthesis correspond to the
   alpha-branching ratios.

Table VIII

Alpha-activities measured from a Ir target

Experimental data			Assignment*	Literature values		
E (MeV)	T$_{1/2}$(second)			E (MeV)	T$_{1/2}$(second)	
5.957	~2.		a)^{175}Pt (55%)	5.960	2.52	± 0.08
5.750	5.	± 2.	a)^{176}Pt (42%)	5.750	6.33	± 0.15
5.670	2.	± 1.	a)^{173}Ir ?	5.665	3.	± 1.
5.44	35.	± 10.	a)^{178}Pt (7.2%)	5.44	19.	± 2.
5.41	9.5	± 2.				
5.39	4.	± 1.				
5.200 parent	2. ~5	± 0.5	c)^{155}Yb (90%)	5.202	1.65	± 0.15
5.104 parent	1.6 17.	± 0.1 ± 3.	b)^{153}Tm (85%)	5.103	1.6	± 0.1
5.032	3.3	± 0.2	b)^{154m}Tm(85%)	5.030	3.0	± 0.1
4.957	10.	± 3.	b)^{154}Tm (85%)	4.955	5.	± 1.
4.795	10.	± 1.	b)^{152}Er (86%)	4.799	9.8	± 0.3
4.673	37.	± 1.	b)^{153}Er (53%)	4.671	36.	± 1.
4.610 parent	~40 ~20		b)^{151m}Ho(13%) a)^{151}Er (0%)	4.607	47. 23.	± 2. ± 2.

a) Gau.75, b) Bow.72, c) Hag.77, d) See.74

*) The numbers in parenthesis correspond to the alpha-branching ratios.

Table IX

Alpha-activities measured from a Au target

Experimental data		Assignment*	Literature values		
E (MeV)	$T_{1/2}$(second)		E (MeV)	$T_{1/2}$(second)	
6.125	2.5 ± 0.5	a)^{177}Au (?%)	6.115	1.3	± 0.1
		a)^{180}Hg (?%)	6.118	2.9	± 0.3
5.955	2.0 ± 0.4	a)^{175}Pt (55%)	5.960	2.52	± 0.08
5.929	3. ± 1.	a)^{178}Au (?%)	5.92	2.6	± 0.5
		a)^{181}Hg (?%)	5.92	3.6	± 0.3
5.852	6.9 ± 0.3	a)^{179}Au (?%)	5.848	7.2	± 0.5
5.749	6.2 ± 0.2	a)^{176}Pt (42%)	5.750	6.33	± 0.15
5.672	2.0 ± 0.5	a)^{173}Ir (?%)	5.665	3.	± 1.
5.622		a)^{181}Au (?%)	5.623	11.5	± 1.
5.521	10. ± 2.	a)^{177}Pt (5.9%)	5.525	11.	± 2.
5.480	9. ± 1.5	a)^{177}Pt (3.1%)	5.485	11.	± 2.
5.449	22. ± 2.	a)^{178}Pt (7.2%)	5.44	19.	± 2.
5.394		a)^{175}Ir (?%)	5.393	4.5	± 1.
5.345 parent		a)^{183}Au (.5%)	5.343	50.	± 2.
		a)^{183}Hg (1.1%)		8.8	± 0.5
5.201		a)^{179}Pt (.27%)	5.20	33.	± 4.
5.161		a)^{179}Pt (.1%)	5.15	33.	± 4.
5.113 parent	~10.	a)^{176}Ir (?%)	5.118	8.	± 1.
		a)^{176}Pt (42%)	5.75	6.33	± 0.15
5.038	3.5 ± 0.2	b)^{154m}Tm(85%)	5.030	3.0	± 0.1
4.804	10.5 ± 1.	b)^{152}Er (86%)	4.799	9.8	± 0.3
4.676	35. ± 5.	b)^{153}Er (53%)	4.671	36.	± 1.
4.523	30. ± 5.	b)^{151}Ho (13%)	4.517	35.6	± 0.4
4.457	~40.	b)^{152m}Ho(6.5%)	4.453	52.3	± 0.5

a) Gau.75, b) Bow.72, c) Hag.77, d) See.74
*) The numbers in parenthesis correspond to the alpha-branching ratios.

Table X (part 1)

Alpha-activities measured from a Bi target

Experimental data			Assignment*	Literature values		
E (MeV)	$T_{1/2}$(second)			E (MeV)	$T_{1/2}$(second)	
6.702	1.8	± .4	a)$195m_{Po}$	6.698	2.	± 0.2
6.611	4.6	± .8	a)195_{Po}	6.608	4.5	± 0.5
6.567	5.0	± 1.5				
6.520	5.7	± 0.2	a)196_{Po} (95%)	6.517	5.5	± 0.5
6.478	3.6	± .1	a)$193m_{Bi}$	6.48	3.5	±
6.426	11.0	± 2.5				
6.380	25.7	± .5	a)$197m_{Po}$(85%)	6.378	26.	± 2.
6.361	75.	± 25.				
6.313	~12		a)191_{Bi} (40%)	6.32	13.	± 1.
			a)186_{Pb} (2.4%)	6.32	8.	± 2.
6.281	53.	± 5.	a)197_{Po} (90%)	6.280	56.	
6.228	150.	± 100.	a)202_{At} (9%)	6.227	183.	± 4.
6.180	97.	± 9.	a)198_{Po} (70%)	6.178	105.	± 3.
6.161	220.	± 70.				
6.109	120.	± 30.	a)$195m_{Bi}$(4%)	6.11	90.	± 5.
6.058	~100.		a)192_{Bi} (20%)	6.06	42.	
			a)$192m_{Po}$(28%)	6.059	252.	
5.971	26.5	± 1.0	a)188_{Pb} (3.3%)	5.98	24.5	± 1.5
5.908	65.	± 10.	a)193_{Bi} (60%)	5.90	64.	± 4.
5.864	520.	± 150.	a)200_{Po}(12.2%)	5.860	684.	± 10.
5.839	6.8	± 0.4	a)179_{Au}	5.848	7.2	± 0.5

Table X (continued)

Alpha-activities measured from a Bi target

| Experimental data | | Assignment* | Literature values | |
E (MeV)	$T_{1/2}$(second)		E (MeV)	$T_{1/2}$(second)
5.736	5.3 ± 1.0	b)^{176}Pt (42%)	5.743	6.33 ± 0.15
5.707	77. ± 30.	a)^{189}Pb (.2%)	5.73	51. ± 3.
5.625	81. ± 12.	a)^{194}Bi(<.2%)	5.61	108.
5.605	27. ± 10.			
5.574	56. ± 12.	a)^{190}Pb (.2%)	5.58	72. ± 6.
5.507	9.0 ± 1.5	b)^{177}Pt(5.9%)	5.510	11. ± 2.
5.466	12.5 ± 3.0	a)^{177}Pt (3.1%)	5.485	11. ± 2.
5.435	20. ± 2.	b)^{178}Pt (7.2%)	5.440	19. ± 2.
5.330	25. ± 7.	a)^{178}Pt (.2%)	5.31	21.0 ± 1.5
5.149	?	b)^{179}Pt(.27%)	5.156	33. ± 4.
4.662	36. ± 6.	b)^{153}Er (53%)	4.671	36. ± 1.
4.222	>300.	b)^{150}Dy (34%)	4.232	430.2 ± 1.5

a) Gau.75, b) Bow.72, c) Hag.77, d) See.74

*) The numbers in parenthesis correspond to the alpha-branching ratios.

Figure 21

GAMANAL fit of a typical triple peak.

The circles show the experimental data. The open squares correspond to the result of the fitting process. The broken line shows the background assumed in the fitting procedure. The segmented line connecting the open squares is there to guide the eyes only.

Nb. of counts per channel

Channel number
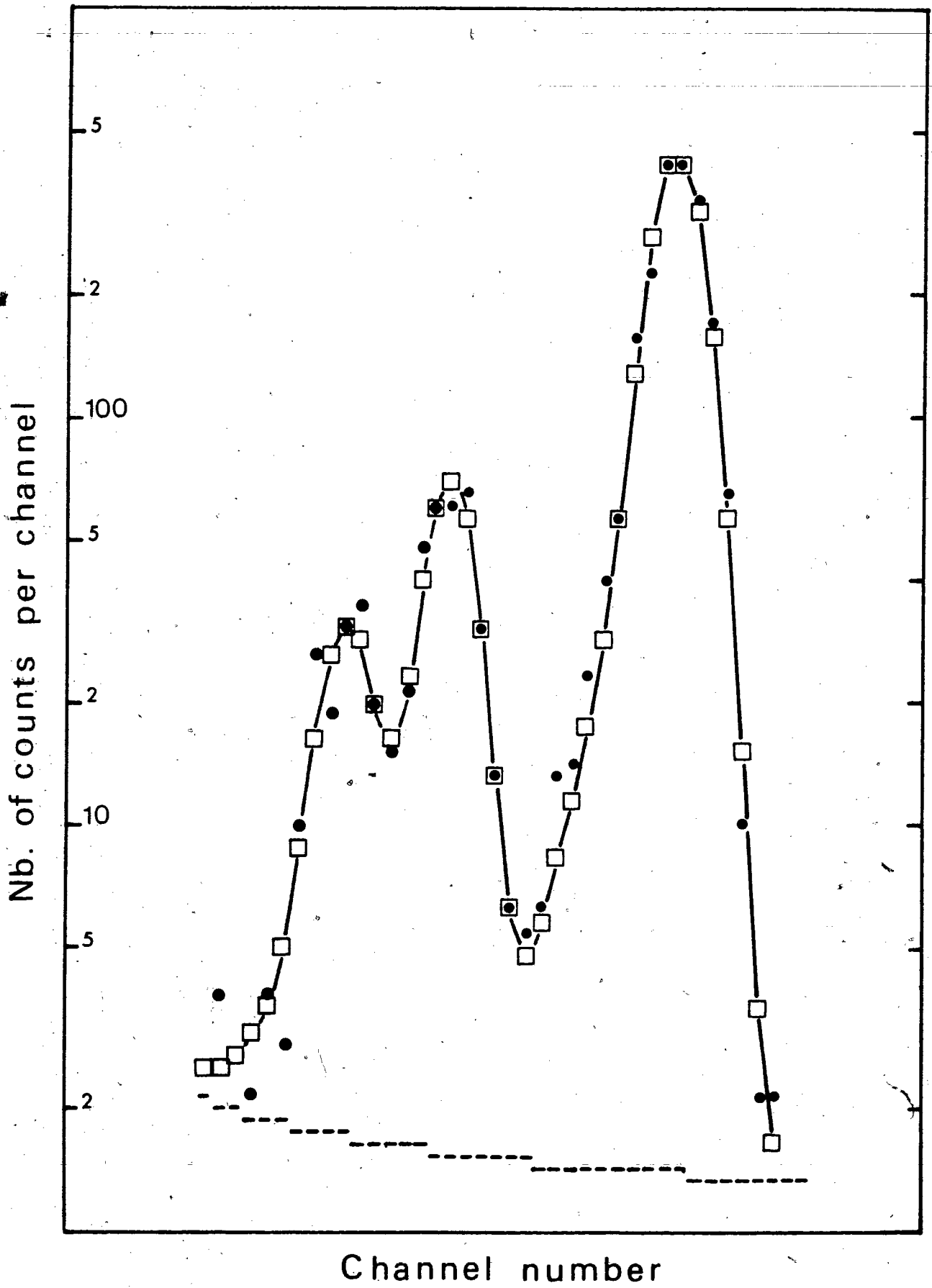
(corresponding to the decay of the various spallation products) were then analysed in terms of a sum of exponential decay terms by means of a least-square fitting procedure DECALS (written in Fortran IV by the author). This program uses the customary decay relationships, including parent-daughter relationships when needed. A list of the command cards can be found in the Appendix II.

The number of data points available on a decay curve was limited by one or both of the following reasons:
a) Sometimes it was necessary to group together spectra corresponding to several decay times in order to improve statistical precision.
b) When using the Nova 3 computer for data acquisition, the limited amount of memory space available for storage of the data in turn limited the number of decay points.

As a result the decay curves were generally restricted to between 10 and 20 points. This limitation could have been a cause for concern in the case of a complex mixture, were it not for the special simplifying circumstances of rapidly falling formation cross-sections for products with compositions more and more remote from stability. This in turn reduced the number of parent-daughter decay

relationships contributing to the decay data.

This may perhaps be most easily appreciated by reference to figure 24 and the typical case of ^{152}Er (measured in this work, for which N/Z=1.235) of which the possible precursors are ^{152}Tm (N/Z=1.203) and ^{156}Yb (N/Z=1.228).

The change in (N/Z) resulting from the beta decay of ^{152}Tm is relatively large - 0.032 - and the corresponding displacement along the yield curve of Figure 24 towards smaller N/Z values is accompanied by an expected drop in yield of a factor of ten. Thus in this case, contribution to the measured ^{152}Er α-activity due to the yield of ^{152}Tm is unimportant.

In the case of the α-decaying precusor ^{156}Yb, the change (N/Z) is only 0.007. Thus the expected yield difference between the measured ^{152}Er and the ^{156}Yb precursor is only ~40% and must be taken into account in interpreting the data. An additional factor may be noticed by empirical observation of the alpha decay systematics in the mass region considered. An alpha decaying precursor of a given measured alpha emitter in general has an

alpha-branching ratio lower than its daughter by a factor of about ten. Thus the importance of the precursor contribution is reduced thereby.

Cross-checking between the various cycling times allowed the presence or absence of a complex mixture of isotopes to be recognized, since in the case of a complex mixture one would obtain varying results as a function of the collection time. Such situation arose for example in the analysis of the 4.611 MeV alpha-line assigned to $151m$Ho . It was found to decay with a 50 $\pm$ 1 seconds half-life, in reasonable agreement with the literature value of 47 $\pm$ 2s. No buildup from 151Er was evident, but the relative production rates of this nuclide (from a Ho target) were found to be 46, 54, 64, 71 atoms.s^{-1} for the respective collection times 6, 12, 30, 60 seconds. The analysis of such variation led to an estimate of 19 $\pm$ 4s half-life for a parent, a value which agrees reasonably with the literature value of 23 $\pm$ 2s for 151Er. The production rates could then be obtained for both nuclides.

It is realised that on occasions, contributions from a parent and/or from an adjacent unresolved alpha line might have been unnoticed, or when suspected it was not possible to take it into account in a proper fashion. For example,

the alpha line assigned to ^{154}Tm exhibits as shown below slightly varying decay half-lives as a function of the target element (indicated in parenthesis): 7.05 $\pm$.5s (Tm), 8.3 $\pm$.3s (Ta), 9.0 $\pm$.5s (Re) which is indicative' of a more complex decay curve than the simple single component assumed.

Nevertheless, it is felt that such unaccounted for contributions were negligible, and that certainly any error introduced in this way would be small compared to errors from other sources, such as for example the efficiency of the gas-jet system, or the effective target thickness. As a result, it is believed that the cross-sections obtained in this work are in general accurate within a factor of two.

The peak areas were converted into cross-sections via the relation :

$$n_o = \frac{\omega \epsilon N I \sigma}{\lambda} \frac{\Lambda}{\lambda+\Lambda} \exp^{-\lambda(t_o+t_1)} (1-\exp^{-\lambda t_c})$$

n_o = number of atoms detected after the collection time: t_c

t_o = transit time of the clusters in the capillary

t_1 = time taken by the tape to bring the activity in front of the alpha detector

ϵ = gas-jet efficiency

ω = detector efficiency

N = effective target thickness

I = intensity of the proton beam

σ = production cross-section

λ = decay constant of the products measured

Λ = inverse of the turn-over time of the gas in the

   production chamber

IV - THEORETICAL REVIEW

It has been known for a long time (Loc.55, Ber.52) that emitted particle spectra from nuclear reactions induced by projectile energies in excess of 100 MeV exhibit the dual aspect of a rather isotropic evaporation-like component with a broad spectrum peaked at low energy, superimposed on which are high-energy particles strongly peaked in the forward direction. It was also observed (Cun.47) that a broad spectrum of products results from the interaction of medium energy protons with medium to heavy mass targets.

The interpretation of these phenomena was first proposed by Serber (Ser.47) in terms of a two step process. In a first short ($10^{-20}, 10^{-22}$ s. (Gad.73)) stage, usually referred to as the "prompt cascade", fast direct interaction between the projectile and individual nucleons takes place. Upon completion of this stage, the residual nucleus undergoes evaporation on a longer time scale ($10^{-15}, 10^{-19}$s.).

IV-A - Prompt cascade

When a high energy projectile strikes a target nucleus, it may hit one or several nucleons during its path through the nuclear matter. These struck nucleons may in turn, depending upon the amount of energy exchanged in the collision, escape from the nucleus, strike other nucleons or just contribute to the total excitation energy of the nucleus. When the bombarding energy exceeds about 300 MeV, pion production must also be considered and will have an appreciable effect on the propagation of the cascade.

This partition of projectile energy between few degrees of freedom progressing to more complicated configurations, until an equilibrium distribution of energy is attained, has been approached by several models that will be briefly considered next.

1 - Intranuclear cascade model.

This model dates back to 1947 when Serber (Ser.47) pointed out that for incident nucleon energies in excess of 100 MeV, the interactions could be treated as quasi free

scattering processes between nucleons (impulse approximation). Justification of this approximation may be found in (Por.68, Hud.68, Mil.59).

The propagation of the cascade of collisions between projectiles and nucleons and between nucleons has been computed by the Monte Carlo method. That is, instead of using analytical integration to calculate the end result of the cascade process,the result is sampled statistically cascade by cascade. A general description of the Monte Carlo method can be found in (Bus.66). At every point in the calculation where a decision must be made, the result is given by a random choice, weighted according to the probability distribution of the event in question. This model has evolved through many steps of increasing sophistication due to the work of M.L.Goldberger (Gol.48), G.Bernardini (Ber.52), N.Metropolis (Met.58), H.Bertini (Ber.63, Ber.78), K.Chen et al (Che.68, Che.71), G.D.Harp (Har.74).

For each scattering event, the position of collision inside the nucleus is chosen statistically and, the energies and direction of each particle are followed explicitly in three dimensional geometry until either all particles

involved in the cascades have been emitted or their energy
falls below some arbitrary minimum. Mean free-paths and
energy transfers in the assumed two-body scattering process
are based on experimental nucleon-nucleon scattering
cross-sections and angular distributions. Collisions in
which either of the partners is left with an energy lower
than the Fermi energy are forbidden according to the Pauli
principle. At bombarding energies above 350 MeV, pion
production and absorption play an important role as they
efficiently convert the kinetic energy of the incoming
particles into nuclear excitation.

Other information needed for the calculations includes:
- The density distribution of nucleons inside the nucleus
(uniform density, step function, or trapezoidal
approximation), with or without reflection and refraction at
the boundaries between regions with different nuclear
density.
- The type of nuclear potential (fixed or velocity
dependent) as well as its variation as the cascade develops.
- The effect of nucleon pair correlations.

At the present time, there are essentially two computer
codes that are widely used to reproduce the intranuclear

cascade: the code developed by Bertini at Oak Ridge

National Laboratory (usualy referred to as the ORNL code),

and the code developed first by Chen et al and lately by

G.D.Harp (Har.74) at Brookhaven National Laboratory and

Columbia University (referred to as the BNL code).

The ORNL code is simpler, in organisation as well as in

the model of the nucleus used for the calculations, than the

BNL code.

- a) Development of the cascade

The BNL code follows simultaneously the trajectories of

the various particles involved in each increment of time,

which increments are chosen small compared to the

nucleon-nucleon collision time.

The ORNL code on the other hand follows one particle

at a time, from a given collision. It is done in a clever

fashion, but nonetheless does not allow inclusion of the

effects of other collisions as the cascade proceeds.

- b) Nuclear properties of the models

Both codes assume the nucleus to be spherically

symmetric, consisting of a dense central core surrounded by

concentric regions of diminishing nuclear density. The

energy distribution of the bound nucleons within each region is assumed to be that of a zero-temperature Fermi distribution. The Pauli principle is taken into account as mentioned previously. The various interaction probabilities are computed on the basis of nucleon-nucleon experimental cross-sections and angular distributions.

The main differences lie in the dynamical properties of the two codes. The BNL code has the option of including (BNL-VPTO) or not including (BNL-STEPNO) reflection-refraction phenomena, effects of nucleon-pair correlations and an energy dependent nuclear potential. The ORNL code includes none of these items.

Comparisons (Bar.72, Ber.74) of the predictions of the two versions of the intranuclear cascade model with each other, and with experimental results indicate:

1) There is a general agreement between the two models even though the BNL-VPTO version includes a more detailed representation of a real reaction process than the ORNL version (the simpler version BNL-STEPNO leading to results similar to the ORNL code)

2) Both calculations underestimate the production of secondary nucleons at small and especially at large angles,

BNL-VPTO being slightly better for large angles than ORNL. On the other hand, the inclusion of reflection refraction effects leads to serious discrepancies between the production of low energy secondary particles as estimated by the BNL code and the corresponding experimental results.

On the basis of its general superiority in reproducing experimental data, the BNL code (in its ISOBAR version) has been used to calculate nuclide yields for comparison with the present experimental data. However no attempt has been made to explore the effect on the calculated yields of inclusion of reflection-refraction effects, or nucleon-nucleon correlations, as these details had been investigated by previous extensive comparisons with experiments (Che.71, Har.73, Har.74, Ber.74, Ber.78) and shown to impair validity of the calculation results.

Unfortunately, although the results are generally quite consistent with the experimental results, and detailed information such as angular distributions as well as energy spectra can be generated, the computer codes based on this model are time consuming due to the large number of computations performed. Nonetheless, the expenditures were considered worthwhile, and other calculation models

described below (which are less well adapted to the subject reaction regime) were not pursued.

2 - Phase space models.

To simplify cascade calculations, for lower energies and complex projectiles, and reduce the time involved, models have been developed in which the three dimensional system of coordinates is replaced by a phase space. It is then only necessary to follow the partition of energy between particles and holes in time, and not the directions and position of the nucleons in the nucleus. Of course, as a result one loses the ability to calculate angular distributions.

These models have in common with the intranuclear cascade model the assumption that energy transfers occur by binary interactions at all energies. They also are of Monte Carlo type.

2,1 - Harp-Miller-Berne model. (HMB)

In this model (Har.71), energy bins are first defined and the number of available single particle levels in each bin is computed using a Fermi gas model. Starting from the

initial configuration, the fractional occupancy of each bin

is followed as a function of time (in units of time short

with respect to the nucleon-nucleon collision time). This

is performed through a set of differential equations that

computes the probability of scattering in and out of each

bin and of emission from bins with energies above the

particle binding energy.

2,2 - Exciton model.

This model due to Griffin (Gri.66,Gri.67), assumes that

energy equilibration between target and projectile is

achieved by a succession of two-body interactions. In a

fashion similar to the single particle model, each state is

characterised by a number of excitons defined as the sum of

the number of excited particles (particles raised above the

Fermi energy by interaction with another nucleon) plus the

number of holes (levels left empty by the excited

particles). The transition rate from a state with n

excitons to one with $n' = n+2$ excitons is taken as

proportional to the density of exciton-states (for the ad

hoc excitation energy). This density of state for a system

of p particles and h holes (that is $n = p+h$ excitons) assuming

a constant single particle level density g at the excitation

E is expressed by the Ericson formula (Eri.60)

$$P_{ph}(E) = P_n(E) = \frac{g(gE)^{n-1}}{p!h!(n-1)!}$$

Since this function is a rapidly increasing function of n, the transitions to $n'=n$ or $n'=n-2$ are neglected.

The probability for emission of a particle -c- with an energy between e and e+de, leaving the nucleus at an excitation U, is given by :

$$W(e)de = \sum \frac{P_{n-1}(U) \, P_c(e)de}{P_n(E)}$$

More sophisticated formulas have later been developed (Bla.70, Obl.74, Gad.73), and lately (Wu .78) the formalism has been expanded to include the emission of complex particles.

2,3 - Geometry dependent hybrid model. (GDH)

The original version the "Hybrid model" was suggested by Blann (Bla.71); it combined the characteristics of the HMB and exciton models (hence its name). Excited particle populations during equilibration are calculated by use of partial state densities as in the exciton model, and intranuclear transition rates of the excited particles are determined from calculations of the mean free path of

nucleons in the nuclear matter. A later formulation the "Geometry Dependent Hybrid Model" includes effects of interactions in the diffuse nuclear surface (Bla.72a). Predictions of this model are in good agreement with the experimental data (Bla.75), for lower energy nuclear reactions.

IV-B - Evaporation stage

Upon completion of the fast intranuclear cascade, the kinetic energy deposited inside the nucleus is presumed more or less equilibrated among the nucleons, and the nucleus de-excites by the statistical emission of nucleons or light particles in competition with fission if energetically allowed.

The probability for evaporation of a particle from a nucleus was derived more than 40 years ago by Weisskopf (Wei.37) using the principle of detailed balance. The probability per unit of time for the emission of a particle -x- with kinetic energy between e and e+de is :

$$P_x(e)de = \frac{2s_x+1}{\pi^2 h^3} e\, m_x\, \sigma\, (p'(E-B_x-e)/p(E))$$

s_x, m_x, B_x, e are the spin, mass, binding energy and kinetic energy of the emitted particle. E is the total excitation energy of the nucleus. p' and p are the level densities of the final and initial nuclides respectively and σ is the inverse reaction cross-section. Among the numerous evaporation calculations performed with this formalism are those due to Dostrovsky et al (Dos.59). Inclusion of

angular momentum effects leads to a similar equation describing the transition of a particle from an initial state "i" to a final state "f" (Tho.64, Rud.69).

$$P(E_i, J_i; E_f, J_f) = \frac{2s_x + 1}{\pi^2 h^3} \; e \; \mu \; \sigma(e, J_i, J_f) \; \frac{p(E_f, J_f)}{p(E_i, J_i)}$$

μ is the reduced mass of the particle

S is the so-called "channel spin" (S=1+s) in which 1 is the angular momentum.

J is the spin of the target nucleus.

e is the energy of the emitted particle

Many calculations for low excitation systems have been based on formulations similar to this. These include SFUMAP (Rud.68), FISMAP (Blo.75), ALICE (Bla.73), and JULIAN (Hil.78), each of which adopted different calculation schemes and approximations.

The various parameters involved in this formula will be briefly considered.

- - Cross-section for inverse reaction: σ

Detailed treatment can be found in (Pre.63, Por.68, Hud.68). A common formulation is :

$$\sigma(e, J_i, J_f) = \frac{\pi \, \lambda^2 \, (2J_c + 1)}{(2s+1)(2J_f + 1)} \; \sum_{S = |J_f - s|}^{J_f + s} \; \sum_{1 = |J_c - S|}^{J_c + S} T_1(e)$$

λ is the reduced DeBroglie wavelength of the system, the subscript -c- refers to the compound nucleus (that is the initial state in the evaporation process). The transmission coefficients T_1 are computed using the optical model. Sometimes (Bla.72,Bla.73) the s-wave approximation is used i.e. the angular momentum carried away by the evaporated particles is neglected.

- Nuclear level density.

A review of the various models used for calculation of nuclear level density can be found in (Hui.72a).

The density of nuclear levels depends strongly on the excitation energy -E- and on the mass -A- of the nucleus. The simplest model : the "equidistant model" (Bet.36, Lan.66, Kan.68), applies to a system composed of two kinds of particles, a total state density which is approximately given by :

$$p(E) = \frac{\sqrt{\pi}}{12} E^{-5/4} a^{-1/4} \exp(2\sqrt{aE})$$

where - a - the so called level density parameter is given by

$$a = \pi^2 g / 6$$

and -g- is the single particle level density. This model

predicts -a- to be $\sim A/10$ MeV^{-1}. Because of its simplicity, this model is widely used in data analysis (Hui.72b).

Similar equations may be obtained using a Fermi gas model. With simplifications the introduction of angular momentum effects leads to the relation (Seg.77) :

$$p(A,E,J,\pi) = \frac{2J+1}{24} \; a^{1/2} \; (\frac{h^2}{2})^{3/2} \; (E-E_r)^{-2} \cdot \exp(2\sqrt{a(E-E_r)})$$

E_r: the rotational energy is given by the relation :

$$E_r = J(J+1)(h^2/2\mathcal{J})$$

Moments of inertia $--$ are often expressed in terms of the value for a rigid sphere : $\mathcal{J} = (2/5) mAR^2$. The level density parameter "a" in the case of a Fermi gas model is given by :

$$a = 2(\frac{\pi}{3})^{4/3} \; \frac{mr_o^2}{h^2} \; A$$

where r_o is the radius parameter and m the mass of the particles considered . Generally a value of $A/8$ MeV^{-1} is accepted as reasonable (Hui.72a). More sophisticated formulas have been derived, with different expressions of the level density parameter for neutrons and protons, in the case of nuclides far from stability.

IV-C - Semi-empirical calculations

An alternative approach to the theoretical treatments described above is a semi-empirical correlation of experimental data. Rudstam (Rud.66) has pioneered this route, and published recipes for prediction of unknown spallation yields via interpolation and extrapolation from measured values.

Silberberg and Tsao (Sil.73) carried this process further and used the foregoing theoretical models as a firmer basis for such extrapolations, particularly to yields of nuclides further from stable composition. Present calculations via the Silberberg and Tsao code are described more fully in Section V.

V - COMPARISON OF EXPERIMENTAL DATA
AND CALCULATED VALUES

The yields of alpha emitting nuclides produced by spallation from various targets which were measured in the present work are presented in Tables XI-XV and plotted in Fig.22-26 as a function of the N/Z of the products considered, together with the values predicted via two computing procedures labelled as SILBERBERG-TSAO and ISOBAR-EVA. The computer programs involved are briefly described in Appendix II as well as other codes which were considered but not employed as explained in the Appendix.

Table XI

Measured and experimental Yields of products
from a Ho target (in mb)

Product	Reaction*	Exp. cross-section	Calculated cross-sect. ISOBAR+EVA	Silberberg and Tsao
$154m_{Tm}$	(p,π^-12n)	1.5×10^{-2}	$7. \times 10^{-3}$	
153_{Tm}	(p,π^-13n)	4.6×10^{-3}	$4. \times 10^{-3}$	
153_{Er}	$(p,13n)$	2.8×10^{-1}	6.37×10^{-1}	
152_{Er}	$(p,14n)$	1.3×10^{-1}	5.6×10^{-1}	
151_{Er}	$(p,15n)$	2.4×10^{-1}	1.3×10^{-1}	
$152m_{Ho}$	$(p,p13n)$	3.32	3.31	7.9×10^{-1}
152_{Ho}		$<1. \times 10^{-1}$		
$151m_{Ho}$	$(p,p14n)$	3.32×10^{-1}	1.75	2.7×10^{-1}
151_{Ho}		1.50		
150_{Ho}	$(p,p15n)$	9.6×10^{-1}	8.5×10^{-1}	6.25×10^{-2}
151_{Dy}	$(p,2p13n)$	5.7	6.84	1.64
150_{Dy}	$(p,2p12n)$	4.34	6.08	3.6×10^{-1}

*) not reaction mechanism

Table XII

Measured and experimental Yields of products
from a Tm target (in mb)

Product	Reaction*	Exp. cross-section	Calculated cross-sect. ISOBAR+EVA	Silberberg and Tsao
155_{Yb}	(p,15n)	1.9×10^{-2}	$2. \times 10^{-2}$	
153_{Tm}	(p,p16n)	1.2×10^{-1}	2.2×10^{-1}	7.3×10^{-3}
$154m_{Tm}$	(p,p15n)	3.1×10^{-1}	4.7×10^{-1}	2.6×10^{-2}
154_{Tm}		3.8×10^{-2}		
152_{Er}	(p,2p16n)	1.14	2.51	6.2×10^{-2}
153_{Er}	(p,2p15n)	2.47	3.61	1.6×10^{-1}
151_{Er}	(p,2p17n)	1.67	6.78×10^{-1}	1.1×10^{-2}
$151m_{Ho}$	(p,3p16n)	7.1×10^{-1}	3.69	2.7×10^{-1}
151_{Ho}		2.75		
$152m_{Ho}$	(p,3p15n)	6.16	6.22	7.5×10^{-1}
152_{Ho}				
150_{Ho}	(p,3p17n)	1.96	2.20	6.5×10^{-2}
150_{Dy}	(p,4p16n)	5.7	7.83	1.5

*) not reaction mechanism

Table XIII

Measured and experimental Yields of products
from a Ta target (in mb)

Product	Reaction*	Exp. cross-section	Calculated cross-sect. ISOBAR+EVA	Silberberg and Tsao
^{155}Yb	(p,4p23n)	4.2×10^{-2}	4.8×10^{-2}	4.3×10^{-4}
^{153}Tm	(p,5p24n)	7.5×10^{-2}	2.40×10^{-2}	8.4×10^{-4}
^{154m}Tm	(p,5p23n)	3.0×10^{-1}	3.61×10^{-1}	$3. \times 10^{-3}$
^{154}Tm		2.95×10^{-2}		
^{153}Er	(p,6p23n)	1.25	1.37	2.0×10^{-2}
^{152}Er	(p,6p24n)	5.05×10^{-1}	1.25	7.3×10^{-3}
^{151}Er	(p,6p25n)	5.8×10^{-1}	$1. \times 10^{-1}$	1.3×10^{-3}
^{151m}Ho	(p,7p24n)	3.03×10^{-1}	1.06	3.3×10^{-2}
^{151}Ho		1.72		
^{152m}Ho	(p,7p23n)	2.72	1.83	9.4×10^{-2}

*) not reaction mechanism

Table XIV

Measured and experimental Yields of products from a Re target (in mb)

Product	Reaction*	Exp. cross-section	Calculated cross-sect. ISOBAR+EVA	Silberberg and Tsao
^{155}Yb	(p,6p27n)	2.15×10^{-2}		2.77×10^{-4}
^{154m}Tm ^{154}Tm	(p,7p27n)	7.4×10^{-2} 6.1×10^{-3}	1.3×10^{-1}	1.88×10^{-3}
^{153}Tm	(p,7p28n)	2.42×10^{-2}	$2. \times 10^{-2}$	5.29×10^{-4}
^{153}Er	(p,8p27n)	3.14×10^{-1}	1.9×10^{-1}	1.18×10^{-2}
^{152}Er	(p,8p28n)	1.19×10^{-1}	2.7×10^{-1}	4.48×10^{-3}
^{151}Er	(p,8p29n)	1.46×10^{-1}	$2. \times 10^{-2}$	7.9×10^{-4}
^{152m}Ho	(p,9p27n)	6.8×10^{-1}	3.4×10^{-1}	5.31×10^{-2}
^{151m}Ho ^{151}Ho	(p,9p28n)	3.66×10^{-2} 4.6×10^{-1}	1.7×10^{-1}	1.94×10^{-2}
^{150}Ho	(p,9p29n)	1.6×10^{-1}	$4. \times 10^{-2}$	4.6×10^{-3}
^{150}Dy	(p,10p28n)	3.5×10^{-1}	1.1×10^{-1}	1.05×10^{-1}

*) not reaction mechanism

Table XV

Measured and experimental Yields of products from a Au target (in mb)

Product	Reaction*	Exp. cross-section	Calculated cross-sect. ISOBAR+EVA	Silberberg and Tsao
^{183}Hg	(p,15n)	3.22×10^{-1}	$8. \times 10^{-2}$	
^{183}Au	(p, p14n)	1.64	1.5	2.9×10^{-1}
^{175}Pt	(p,2p21n)	2.17×10^{-2}	8.0×10^{-2}	1.64×10^{-4}
^{176}Pt	(p,2p20n)	1.09×10^{-1}	2.5×10^{-1}	9.94×10^{-4}
^{177}Pt	(p,2p19n)	2.4×10^{-1}	$5.0 \quad 10.1$	2.93×10^{-3}
^{178}Pt	(p,2p18n)	7.5×10^{-1}	1.75	1.56×10^{-2}
^{154m}Tm	(p,dA=44)	5.0×10^{-3}		4.1×10^{-4}
^{152}Er	(p,dA=46)	8.5×10^{-3}		9.7×10^{-4}
^{153}Er	(p,dA=45)	3.15×10^{-2}		2.6×10^{-3}
^{151}Ho	(p,dA=47)	3.5×10^{-2}		4.2×10^{-3}
^{152m}Ho	(p,dA=46)	6.0×10^{-2}		1.1×10^{-2}

*) not reaction mechanism

Figure 22

Yields of alpha emitting spallation products from a Ho
target as a function of their N/Z; comparison with
cross-sections predicted from calculations described in
the text.

Ho
target

- ● Exp. data
- ▲ ISOBAR+EVA
- ◆ Silberberg-Tsao

Cross-section (μbarns)

N/Z of products

1.23   1.25   1.27

Figure 23

Yields of alpha emitting spallation products from a Tm target as a function of their N/Z; comparison with cross-sections predicted from calculations described in the text.
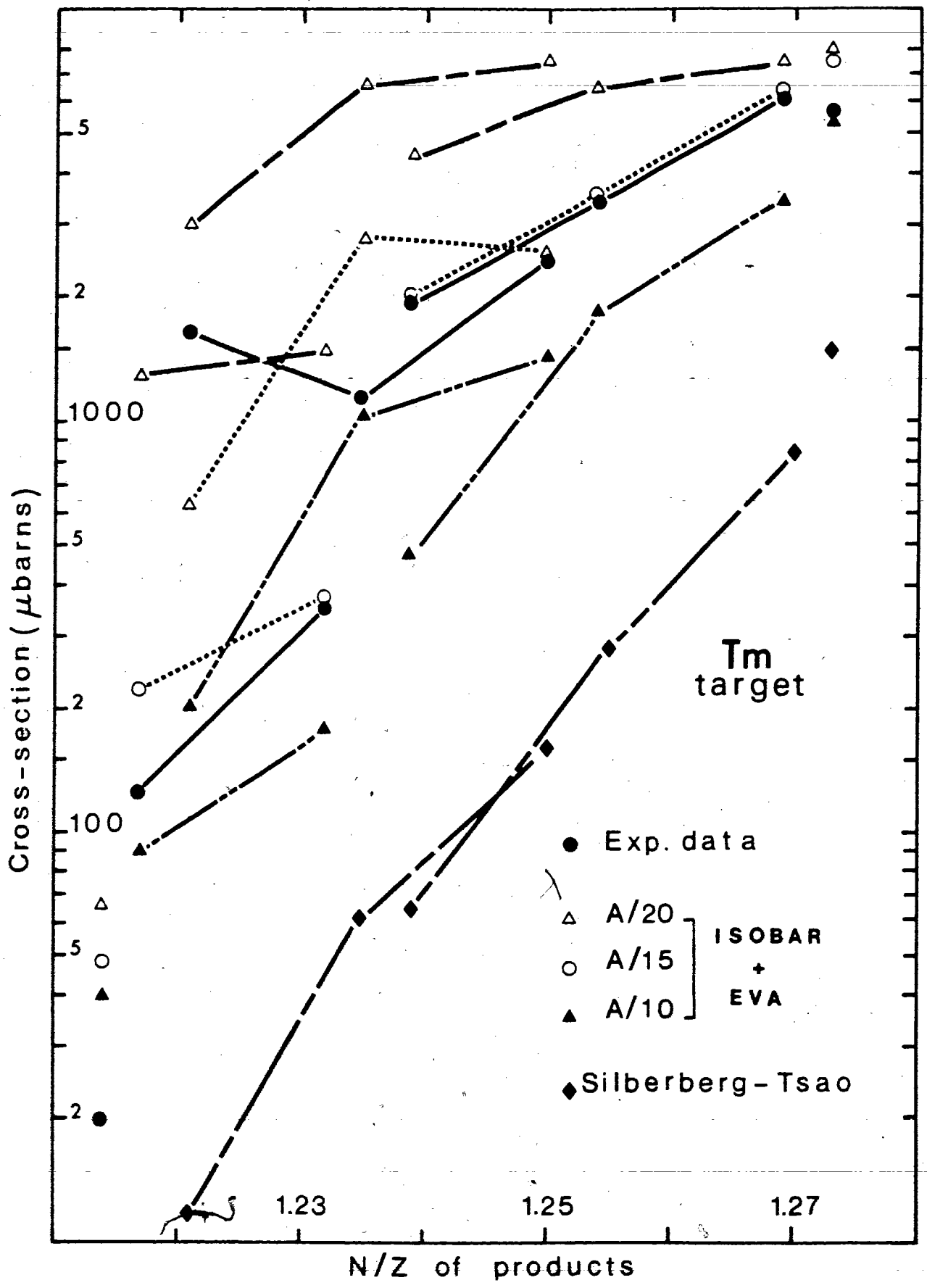
Figure 24

Yields of alpha emitting spallation products from a Ta
target as a function of their N/Z; comparison with
cross-sections predicted from calculations described in
the text.
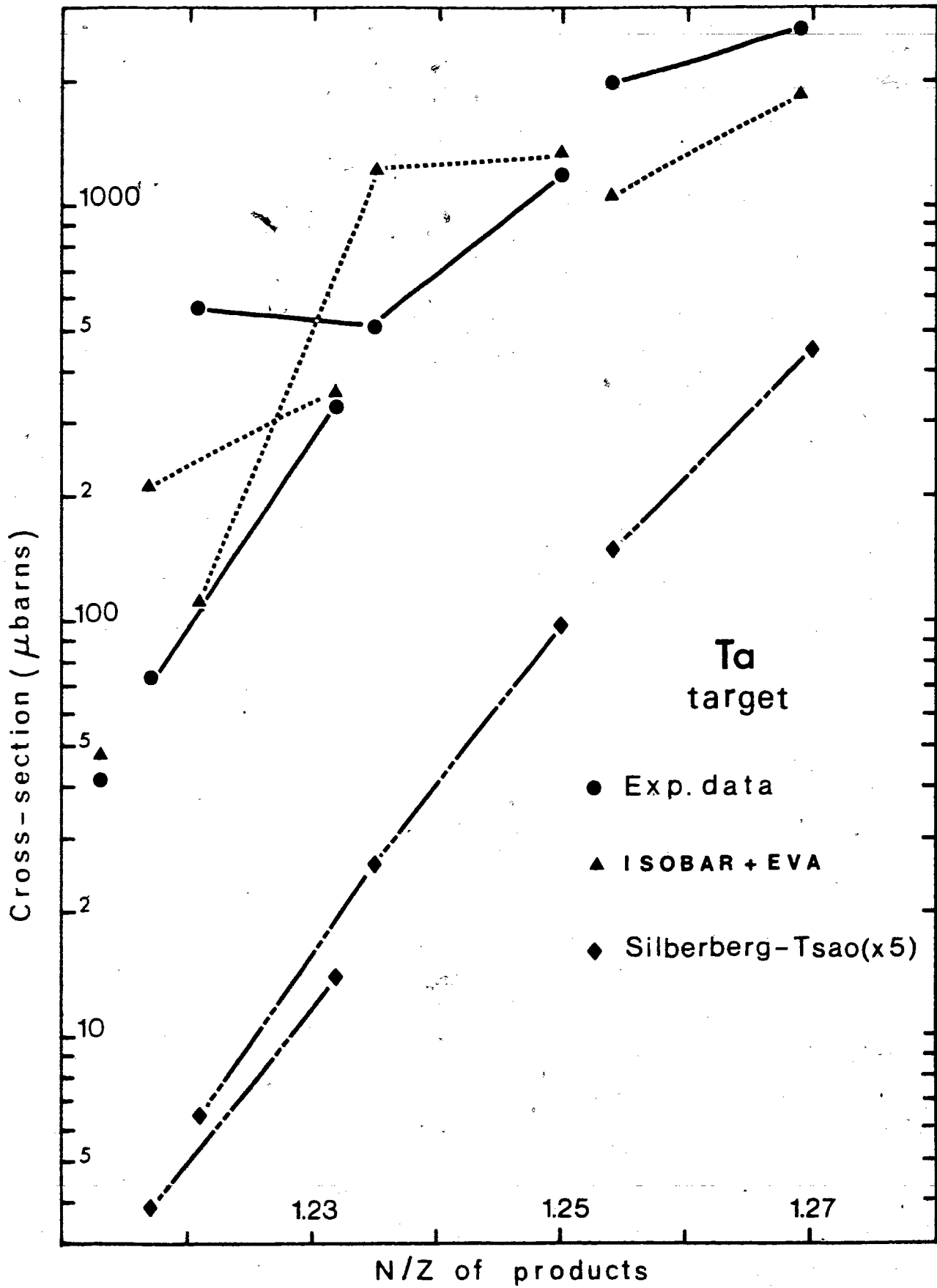
Figure 25

Yields of alpha emitting spallation products from a Re target as a function of their N/Z; comparison with cross-sections predicted from calculations described in the text.
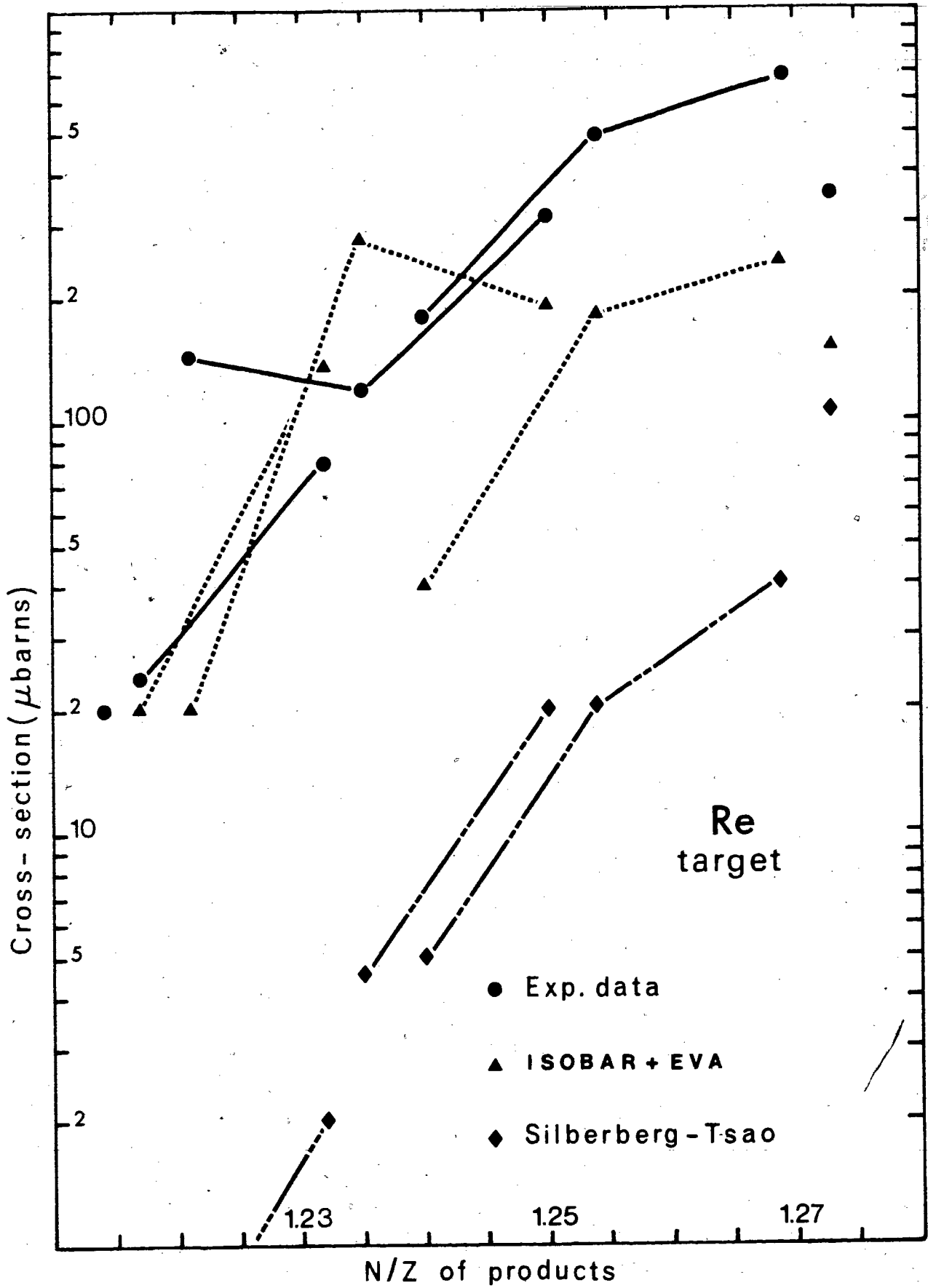
Figure 26

Yields of alpha emitting spallation products from a Au target as a function of their N/Z; comparison with cross-sections predicted from calculations described in the text.
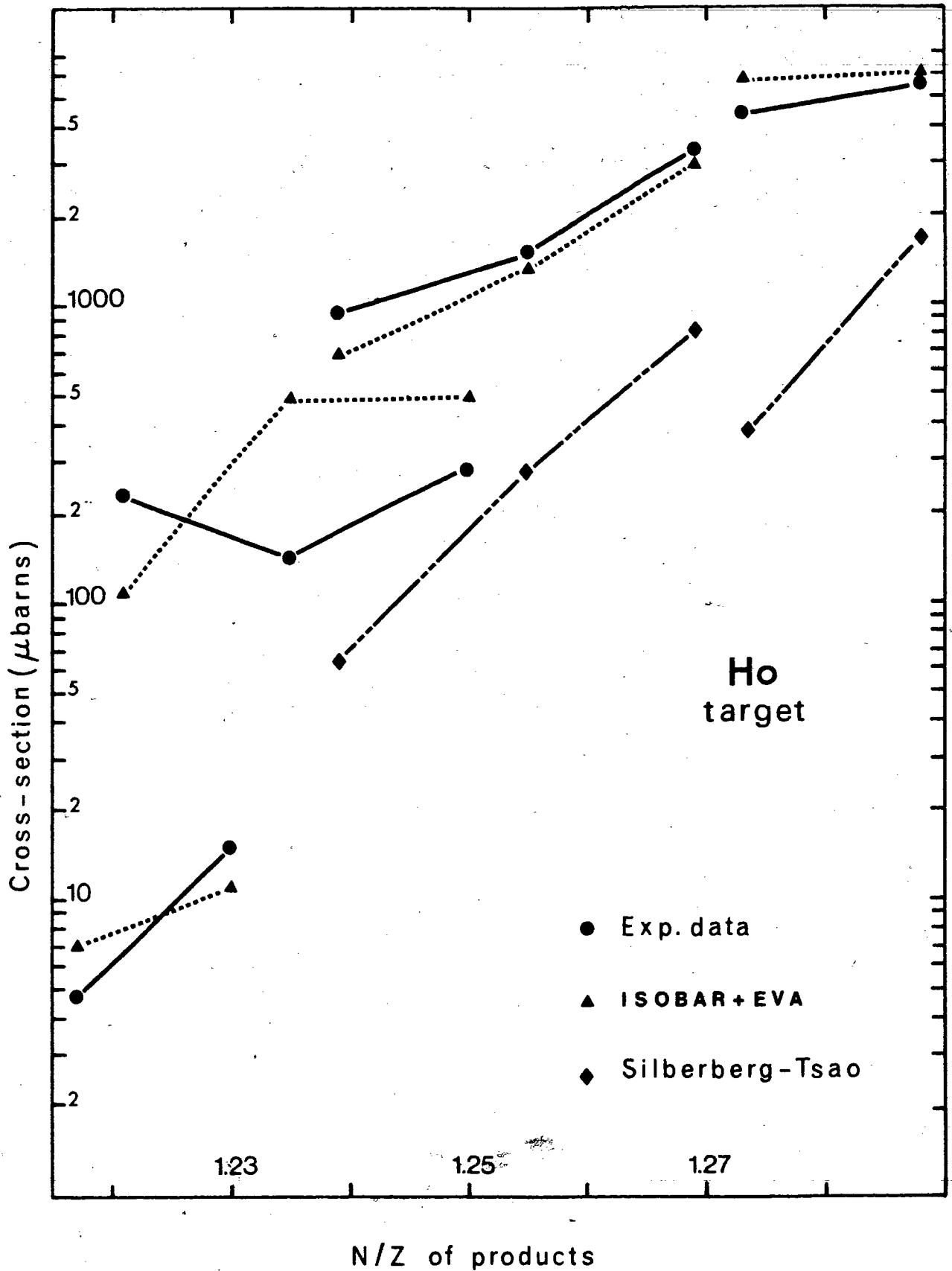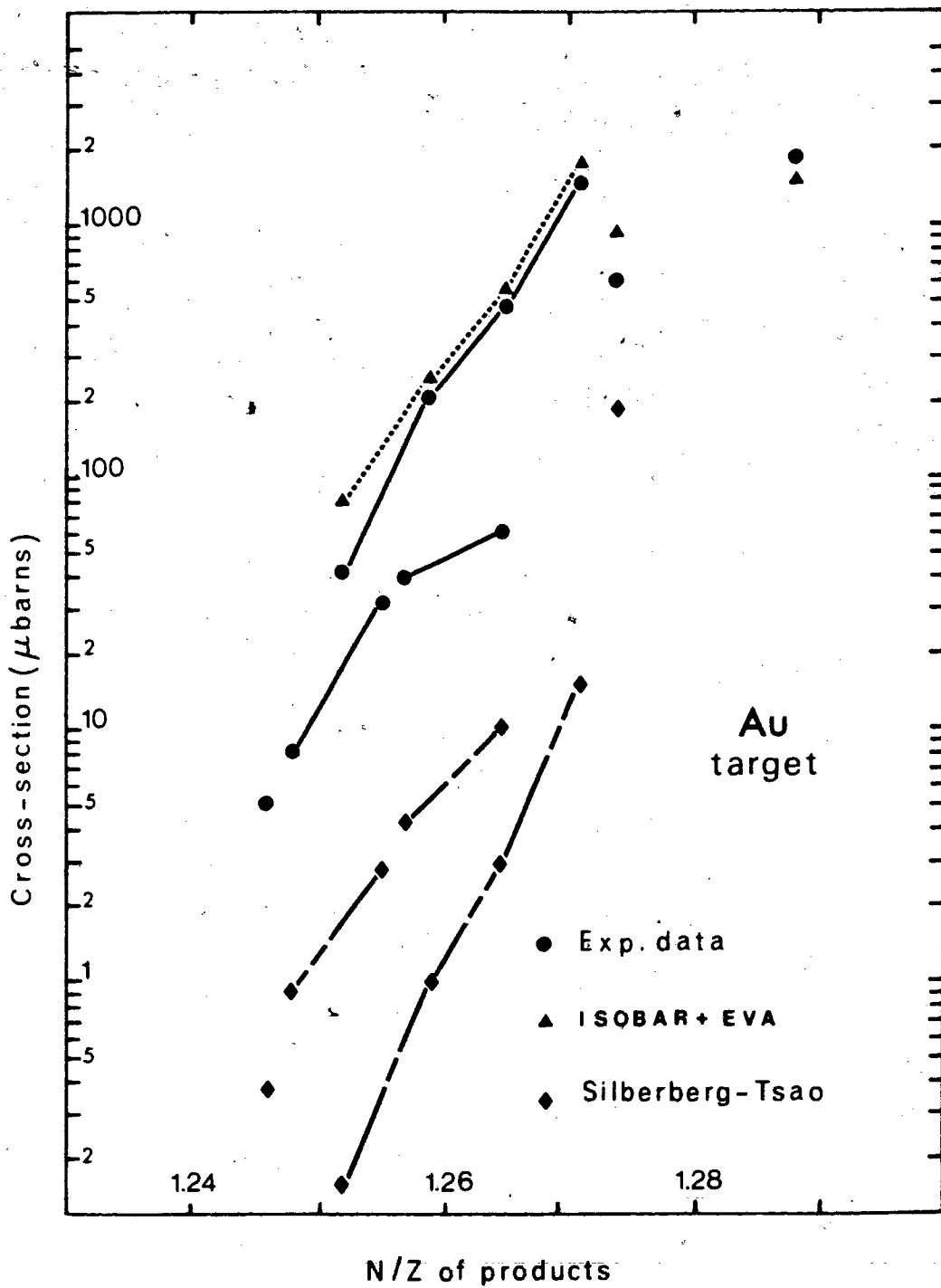
V-A - SILBERBERG-TSAO

This program (Sil.73) based on the semi-empirical formalism of Rudstam (Rud.66), was used as a first check of the experimental results because it was known to give good results for yield trends of products of composition close to stability with various bombarding energies and target elements. It presented the added advantage of being simple and fast.

Generally speaking it can be observed that there is little agreement between the experimental data and the predictions from the SILBERBERG-TSAO code, the disagreement increasing with the difference in mass between the product nuclides and the target element. This may perhaps be understood by the fact that, since there was no information on the absolute yields of very neutron-deficient spallation products in the mass region considered, the parameters used in the calculations had been derived for nuclides near stability (Sil.73). Furthermore, the cross-sections measured in this work correspond to products in a region of rapidly changing yield from one isotope or element to the adjacent one, and as a result small errors in extrapolation may lead to large discrepancies with the experimental data.

V-B - ISOBAR-EVA

These calculations were performed according to the formalism of the two step process described above.

First, the computer code ISOBAR (see sect.IV) (the higher energy version (Har.74) of VEGAS (Che.71))was used to calculate an average of 3000 intranuclear cascades (non tranparencies) per target bombarded at 500 MeV, the results of which served as input for the evaporation stage calculated by the program EVA (essentially the Monte Carlo calculation according to Dostrovsky et al (Dos.59).

Since the computations involved in the latter evaporation step were faster (by a factor of 30) than those involved in the preceding intranuclear cascade step, each cascade product was used as an input to 10 evaporation calculations in order to obtain better statistical significance in the calculation of cross-sections smaller than one millibarn. Of course in some instances distortion might thereby have been introduced if, upon completion of the cascade calculation, the results included too few nuclides possessing the necessary composition to lead to the

production of the nuclides measured. This problem would be compounded if the excitation energy of the cascade products was (due to poor statistics) much higher or lower than the average given by more extended calculations, thus greatly affecting the probability of evaporating large numbers of nucleons. In the case of the holmium target, concern over this possibility led to 6000 intranuclear cascades (non transparencies) being calculated in order to obtain a better statistical precision in the calculation of residual nuclides that would lead to the production of ^{153}Tm and ^{154}Tm.

It was initially intended to compute the evaporation stage with the computer code JULIAN since it presented many improvements over EVA, notably the influence of the angular momentum taken into account. Unfortunately, this program was reported (Hil.78, Gin.78) not to be in a running condition, in any of the laboratories involved in its development, such that it could be satisfactorily applied to this study. As a consequence, the simpler EVA was used, under the assumption that the width of the cascade product distributions in charge, mass, energy and angular momentum would reduce the dependence of the evaporation calculation

results on the sophistication of the calculation techniques, and, that in effect the experimental data obtained in this work represent a test of the ability of the ISOBAR code to predict the probability of events with relatively high (>150MeV) deposited energy with a 500 MeV proton projectile on medium mass nuclides.

The agreement between results from these calculations and experimental results is generally acceptable, and sometimes, maybe fortuitously, very good. There are nevertheless several points to notice:

1) General trends

Generally, the further away from the target composition is that of the nuclides for which cross-sections are measured, the less acceptable is the agreement between the experimental and calculated values. The latter are systematically lower than the experimental data, as can be seen in Fig.27 which displays the experimental and predicted yields of ^{151}Ho as a function of its mass difference from various targets.

A level density parameter of A/15 was chosen for the lowest Z targets in agreement with previous studies (Sah.72,

Figure 27

Experimental and predicted yields of ^{151}Ho from various targets. Circles show the experimental data (with the solid line to guide the eye). Triangles and the broken line show the result of calculations via ISOBAR plus EVA.

Yield of ^{151}Ho

Cross-section(μbarns)

5

2

1000

5

2

100

5

2

● Exp. data

▲ ISOBAR + EVA

15　　20　　30　　40

ΔA between targets and ^{151}Ho
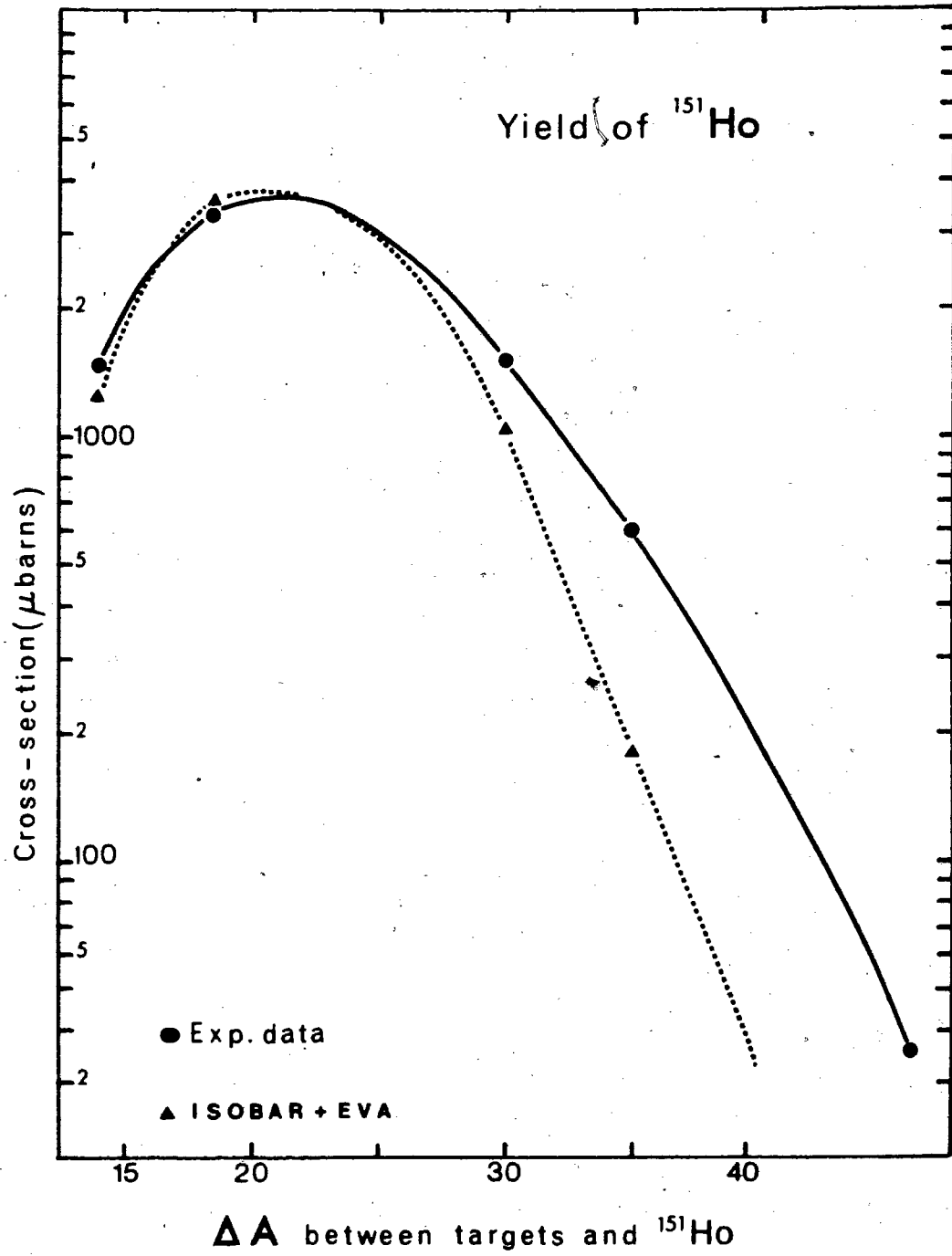
Dos.59). It can be observed from Fig.23, that this value

gave the best agreement with the experimental results.

In the case of the gold target only a level density

parameter of A/20 brought reasonable accord between

calculations and measured cross-sections of Pt, Hg and Au

activities.

The difference in the value of "a" used in the

calculations from the accepted values ~ A/8, A/10

(ChapterIV) is not too surprising; the adjustment of the

value of "a" in a given calculation in effect compensates

for the neglect of angular momentum effects on the nuclear

evaporation. Thus, shifts in the angular momentum

distribution among the prompt cascades products due to

changes in target masses, might need to be compensated by

changes in the effective a-value used in the calculations of

the subsequent evaporation.

The remaining inability to reproduce the yield of

nuclides of composition remote from that of the target is

difficult to explain precisely. The failure of the EVA

program to take into account the angular momentum of the

evaporating nuclides is more severe here and the

calculations of the inverse cross-sections are performed in a semi-empirical fashion which may not be adequate for very neutron-deficient nuclides. Nevertheless, it is likely that to a large extent the underestimation of the production of spallation products remote in composition from the target is a result of the underestimation by the ISOBAR code of the frequency of production of nuclides with high excitation energy in the intranuclear cascade.

2) Reactions $Ho(p,\pi^-xn)^{153,154}Tm$

The contribution to the experimental results from reactions induced by secondary particles can generally be neglected due to the large excitation energy needed to evaporate 15 to 40 nucleons. The only exception might be the production of $^{153-154}Tm$ from a Ho target. The production of these isotopes via the direct reaction $Ho(p,\pi^-xn)$ is estimated to be so small that the alternative production by secondary emitted alphas through the reaction $Ho(\alpha,xn)$ must be investigated. An estimate of the latter process can be obtained by the following considerations.

a) The energy corresponding to maximum of the excitation function for the $Ho(\alpha,15n)$ reaction was estimated by

extrapolation from the results of Djaloeis (Dja.75)
Fig.28-b, and the corresponding cross-section obtained in
the same way (Fig.28-a). The respective results thus
obtained corresponded to a maximum cross-section of 110 mb
for an alpha energy of 200 MeV.

b) The differential cross-section data of Korteling and
co-workers (Gre.78) for Ag + 500 MeV protons was used to
estimate the probability of production in the Ho target of
alpha-particles of energies between 150 and 250 MeV needed
to induce the α,15n reaction. The data were integrated over
angles to the beam direction between 0. and 90. degrees,
assuming that the 20 degrees value was an upper limit to the
average value in this angular region, to give a
alpha-production cross-section of 3 mb.

Combined with a target thickness of 100 mg.cm^{-2}, this
yields an overall cross-section of the order of 1x10^{-4}mb
for the production of ^{154}Tm. This number is lower by a
factor ~50 than the measured data. Thus it seems likely
that this process does not contribute significantly to the
production of ^{153}Tm, ^{154}Tm.

It is interesting to note that the predicted yields for
the extreme process (p,π^-xn) are in very good agreement

Figure 28

Characteristics of (α,xn) reactions :

- a) Variation of the α energy corresponding to the
maximum of the (α,xn) cross-section as a function
of -x-.

- b) Variation of the maximum of the yields of the
(α,xn) reactions as a function of -x-.
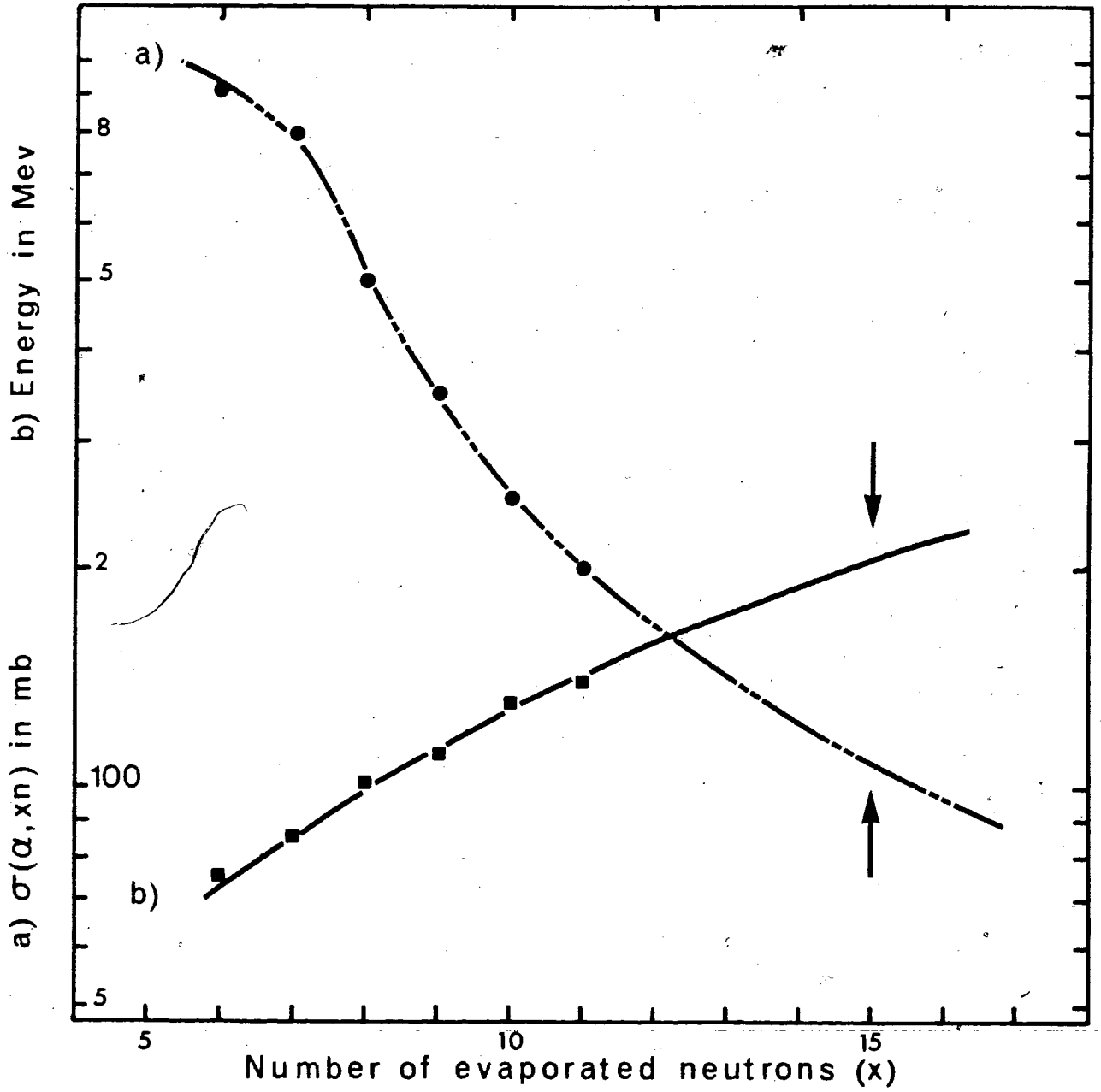
with the experimental results.

3) Reactions ^{197}Au(p,..)Dy,Tm,Ho

While the discrepancies mentioned above do not for most nuclides studied exceed a factor five, the situation is completely different in the case of these products. The predicted yields are too low to be generated by the computations, but by extrapolation one obtains values of the order of $10^{-2}\mu$b. This is lower than the experimental data [1] by two order of magnitudes, and although the arguments developed previously might also apply in this case, other effects may also be responsible.

Studies (Hey.72) of the production yield of ^{149}Tb from a gold target bombarded with protons of 200-450 MeV indicated that it was most likely the residual nucleus left after fragment emission (A ~ 20-50) followed by evaporation. Similarly Chu et al (Chu.77) concluded that the production of nuclides with masses ranging from 40 to 50, from various targets, could not be explained in term of either fission or spallation alone. The emission of such fragments is now well established (Gre.79, Wes.78) and the cross-sections (for example ~200 μb for the production of Sodium from a

Silver target) are large enough to be a contributing factor to the production of the subject nuclides as residues of such emissions.

VI - CONCLUSION

Cross-sections for the production of very neutron deficient products, resulting from the interaction of 480 MeV protons with various targets, have been obtained for the first time in the mass region studied.

The nuclides of which the yield has been measured are produced in the majority of cases by the so-called 'spallation' process; however it was also possible to measure cross-sections involving unusual and not yet well known processes such as: pion production and fragmentation.

The results compared with the semi-empirical code due to Silberberg and Tsao show little agreement; however they generally agree with the more fundamental calculations of the Isobar code, when the combination of parameter values previously employed by others was adopted.

The data obtained point to several areas of potentially very interesting research: the study of the gas-jet system, the improvement of the codes used to predict the yields of 'spallation' products, the study of the unusual processes observed in this study.

1) - The gas-jet transport system.

Further studies of the gas-jet recoil transport system
would present the immediate interest of reducing the
experimental error. This would involve the study of:

a - The effective target thickness, in order to determine
to what extent the assumptions made are valid, and to
improve the quality of the data obtained. It would be
highly desirable for example to measure effective target
thicknesses of products closer to the nuclides for which the
cross-sections have been measured.

b - The gas-jet efficiency. Presently, nobody can claim to
have a complete understanding of the gas-jet system.
Further studies are needed in order to improve the
confidence in the measured efficiencies, and to be certain
that these efficiencies are controlled. It would be most
useful to improve the gas-jet yield, in order to decrease
the influence of this factor on the statistical uncertainty
of the data. (Recent experiments give credence to the
seemingly erratic variation of the efficiency as a function
of the "Z" of the products; they also indicate that one
might be able to control this variation)

Further experiments to understand the mechanism of the

gas-jet system would be highly desirable in their own right, rather than just as a tool to measure cross-sections; if, as recent experiments (only in preliminary stage) indicate, this seemingly erratic variation of the efficiency of the gas-jet system as a function of the "Z" of the products is real, and if as they also indicate, it is possible to influence and control these efficiencies, this would be a powerful addition to the gas-jet technique and might solve the main problem associated with it, namely the identification of unknown species. Identification is presently possible only with the use of expensive apparatus, and at the cost of a severe reduction in the efficiency of collection. A systematic study of this variation across the periodic table would also certainly provide new information on the mechanism responsible for the selective attachment of the recoiling nuclei on to gas molecule clusters.

2) - Improvement of predictions

The data obtained can be used as a base to generate new parameters in the code of Silberberg and Tsao. They also indicate that the neglect by ISOBAR of the fragmentation process is not a serious problem in most cases, but however may lead to gross underestimation of the yields of rare products.

3) - Study of nuclear reactions

In addition to the interest in improving and extending the existing results, there are two types of reactions wich would be particularly interesting to study:

a - The $(p, \pi^- xn)$ reactions which are easily observed with the existing system are of considerable current interest. Total product formation cross-sections represent complementary data to pion energies and angular distributions obtained in "physics" experiments. For example, a complete measurement at one bombarding energy and from one target of all the $(p, \pi^- xn)$ reactions would perhaps permit extraction of the nuclear excitation energy spectrum associated with pion emission, for comparison with theory.

2 - The production of the lighter spallation products from the Au target. For example, both an excitation function measurement and a study of the forward to backward recoil intensity ratio of these products (which would not be too difficult with the gas jet system) would help in the understanding of the production mechanism for these nuclides. Forward to backward recoil intensity ratios in particular provide a means of assessing (through the work of Sugarman and others) the momentum deposited by the projectile in interactions leading to such products.

APPENDIX   I

(All symbols are defined on pages 146-147)

1 - A few mathematical expressions leading to the
evaluation of a steady state flow through a pipe of
constant cross-sectional area.

The following is a brief review of gas dynamics. It is
useful to understand the behaviour of the gas through the
gas-jet system, and to allow the user to choose the right
experimental conditions. It is extracted from standard
textbooks on gas dynamics such as for example: Sha.53,
Mis.58, Mcl.63.

The gas-flow is assumed to be such that there is no
work, and no heat transfer to or from the walls of the
tubing (adiabatic flow).

Furthermore, the gas-flow is assumed to be laminar. In
this case, the viscosity will govern the flow pattern, with
the velocity of the gas being zero against the walls, and at
a maximum along the axis of the tubing. The velocity
distribution for such a flow is given by :

$$v_r = v_o \left(1 - \frac{r^2}{R^2}\right) \qquad (1)$$

In such a flow, all particles are moving in the same direction. As the velocity increases, inertial forces become so large that instability results and, except near the walls, the velocity along the radius of the tube is nearly uniform. This flow is called turbulent. Fig.29 displays the velocity profiles corresponding to the two types of flow.

The consideration of these two profiles will make clear the need for a laminar flow. If a cluster is travelling with the gas, the gas velocity on one side being greater than on the other, it will be imparted a rotating motion. This will, in a fashion similar to a spinning base-ball or tennis ball, curve the trajectory of the clusters towards the region of higher velocity. This can be explained simply by the following qualitative arguments. The spinning motion of the clusters is such (Fig.29) that there is a greater friction between the clusters and the gas on their side further away from the center of the capillary (point A) than on the opposite side (point B). This friction results in a local slowing down of the gas in -A-, and, according to

Figure 29

Schematic representation of gas-flow velocity profiles (turbulent and laminar) across the diameter of the gas-jet capillary tube. The spinning balls represent clusters carried by a laminar flow. Points A and B refer to discussion in the text.
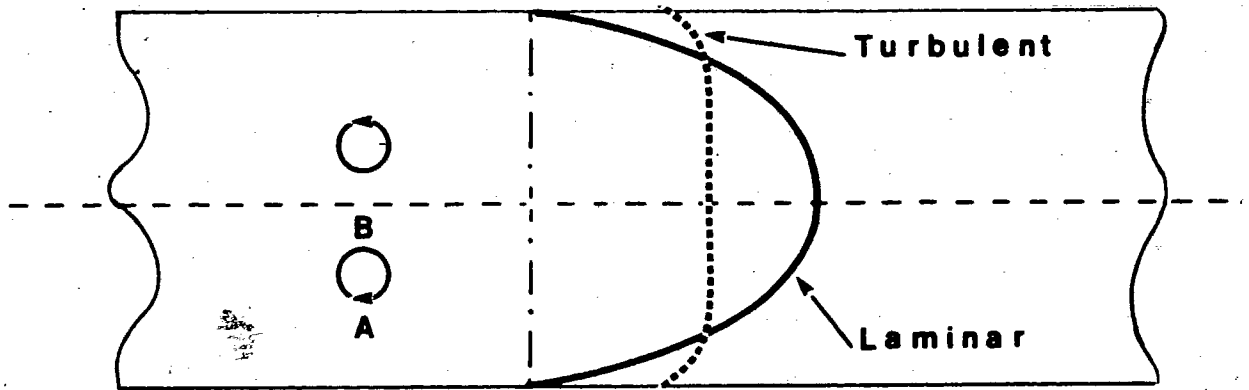
Bernoulli's law, there will be an increase in pressure at this point and creation of a force directed towards the center of the capillary.

This force proportional to the aerosol cross-section, and to the square of the difference in gas velocities is given by (Wol.76):

$$F \sim m^{4/3} v_o^2 r_c^2 \rho \tag{2}$$

Turbulent flow cannot lead to any focussing effect towards the center of the tubing, since the velocity gradient along the radius is zero, except in a narrow region near the walls.

Furthermore the turbulences may carry the recoils in the vicinity of the capillary walls onto which they then are likely to adhere or disintegrate; also a passage from laminar to turbulent flow will result in an increase of the friction coefficient, which will decrease the gas velocity. Laminar flow will be maintained if the Reynold's number:

$$R_e = \frac{\rho \, vD}{\mu} \tag{3}$$

is kept below 2000.

In the case of an adiabatic flow along a pipe of constant cross-sectional area, with no exchange of heat or work, the

steady-flow energy equation:

$$h_o = h + \frac{v^2}{2} \quad \text{leads to} \quad dh + \frac{d(v^2)}{2} = 0$$

or, since A the cross-sectional area of the tubing is constant, and the mass flow-rate $w/A = \rho v = $ cst:

$$dh - (w/A)^2 \frac{d\rho}{\rho^3} = 0 \tag{4}$$

This equation describes a family of curves called Fanno lines; the shape of these curves can be obtained by integration of the equation (1), which gives:

$$h = h_o - \frac{(w/A)^2}{2} \left(\frac{1}{\rho^2} - \frac{1}{\rho_o^2} \right) \tag{5}$$

These curves are displayed Fig.30.

An interesting situation to consider corresponds to an entropy maximum, that is: $dS = 0$. From the thermodynamic relationship:

$$dh = TdS + \frac{dP}{\rho} \quad , \text{ relation (1) becomes :}$$

$$TdS + dP - (w/A)^2 \frac{d\rho}{\rho^2} = 0 \tag{6}$$

Since $dS = 0$, one obtains:

$$\left(\frac{dP}{d\rho}\right)S = (w/A)^2 \frac{1}{\rho^2} = 0 \qquad\qquad (7)$$

Taking into account

$$\left(\frac{dP}{d\rho}\right) = gR_g T = a^2 \quad \text{and} \quad \frac{(w/A)^2}{\rho^2} = v^2 \, ,$$

one obtains $v=a$ that is the velocity of the gas reaches

sonic speed.

It has been demonstrated that for a maximum entropy,

the gas is flowing at sonic speed (that is the Mach number

$M=1$); however in the case of an adiabatic flow, the second

law of thermodynamics implies that the entropy must increase

(irreversible process). From this it follows that, either

at subsonic or supersonic velocities, there is a tendency to

reach the conditions of sonic velocity. On a Fanno line,

for $h_o > h > h_m$ (Fig.30) the flow is subsonic; as the

entropy increases the Mach number tends to the limit value

of 1, since further increase in " M " would imply a decrease

in entropy, which is forbidden by the second law of

thermodynamics.

Further, in the case of an adiabatic flow with constant

conditions, a subsonic flow can never become supersonic, nor

can a supersonic flow become subsonic.

Figure 30

Typical Fanno lines for gases. For details see text.
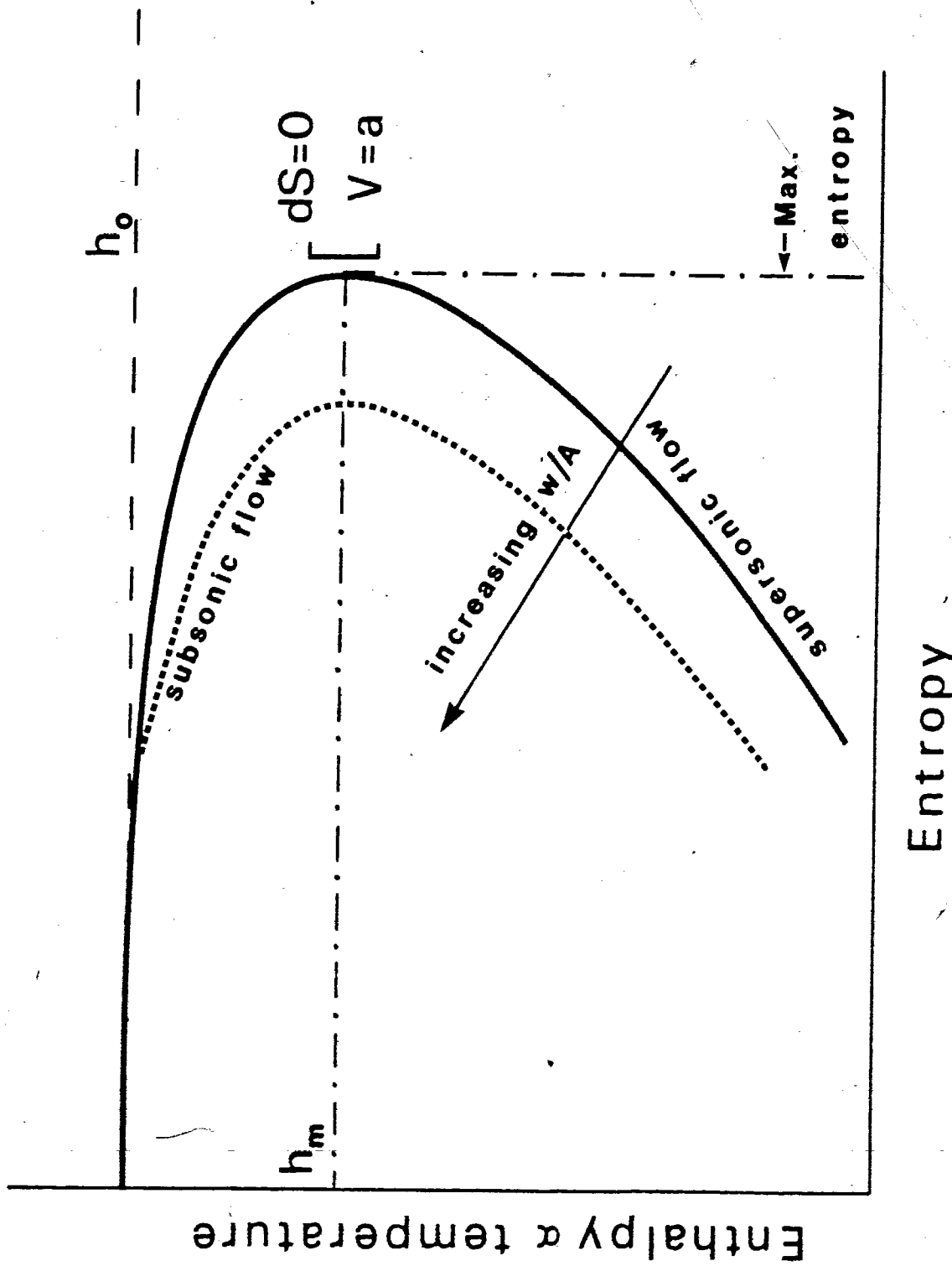
- Fanno relations for perfect gases.

From the following equations:

$$T = T_o(1 + \frac{g-1}{2} M^2)^{-1} \qquad \text{(adiabatic flow)}$$

w/A = cst. (along a Fanno line)

$$\frac{dP}{P} + \frac{dM}{M} + \frac{1}{2}\frac{dT}{T} = 0 \qquad \text{(equation of continuity)}$$

The following relations can be derived. They allow the determination of a state on a Fanno line, knowing another state on the same Fanno line.

Entropy change
$$\frac{dS}{R_g} = \frac{dM}{M} - \frac{g+1}{2(g-1)} \times \frac{d(1+[(g-1)/2]M^2)}{1+[(g-1)/2]M^2} \qquad (8)$$

Density change
$$\frac{\rho}{\rho_1} = \frac{M_1}{M} (\frac{1+[(g-1)/2]M^2}{1+[(g-1)/2]M_1^2})^{1/2} \qquad (9)$$

Pressure change
$$\frac{P}{P_1} = \frac{M_1}{M} (\frac{1+[(g-1)/2]M_1^2}{1+[(g-1)/2]M^2})^{1/2} \qquad (10)$$

A very convenient reference state , in the case of the gas-jet system, is the state on the Fanno line where the

Mach number = 1. This will allow development of the
relations between the gas characteristics (temperature,
pressure and density) at the inlet (T,P,ρ) of the tubing and
at the exit (T^*,P^*,ρ^*) of the tubing, assuming that at this
point (as is usually desirable) the gas has reached sonic
velocity.

$$\frac{T}{T^*} = \frac{g+1}{2} \left(1+ \frac{g-1}{2} M \right)^{-1} \qquad (11)$$

$$\frac{\rho}{\rho^*} = \frac{1}{M} \left(\frac{g+1}{2}\right)^{1/2} \left(1+ \frac{g-1}{2} M^2 \right)^{-1/2} \qquad (12)$$

$$\frac{P}{P^*} = \frac{1}{M} \left(\frac{g+1}{2}\right)^{1/2} \left(1+ \frac{g-1}{2} M^2 \right)^{-1/2} \qquad (13)$$

In the above set of equations, M is the mach number at the
inlet of the capillary. The last equation (13) is
particularly interesting, since it gives a mean of checking
whether or not sonic speed has been reached at the exit of
the capillary tubing.

- Effect of energy loss

So far the problems related to any kind of energy loss have been neglected. By considering the Fanno lines of Fig.30, it may be noticed that they tend to be tangent to the $h=h_o$ line. This is due to the fact that at low velocities the entropy may increase as a result of friction, while the enthalpy remains almost constant. Assuming there is no obstacle in the way of the gas, and that the tubing is essentially straight, the main source of energy loss is the friction between the gas and the walls of the tubing. In this case, the momentum equation :

$$\frac{dP}{P} + \frac{g}{2} dM^2 + \frac{g}{2} M^2 \frac{dT}{T} + \frac{g}{2} M^2 f \frac{dx}{D} = 0 \qquad (14)$$

leads to the relation:

$$f \frac{x-x_1}{D} = \frac{1}{g}(\frac{1}{M_1^2} - \frac{1}{M^2}) + \frac{g+1}{2g} \text{Log} \frac{M_1^2}{M^2}(\frac{1+[(g-1)/2]M^2}{1+[(g-1)/2]M_1^2})$$
$$(15)$$

Thus for a given mass flow , the maximum length which allows sonic speed at the exit is given by the relation:

$$f \frac{L}{D} = \frac{1}{g} (\frac{1}{M_1^2} - 1) + \frac{g+1}{2g} \text{Log} (\frac{[1+(g-1)/2] M_1^2}{1+[(g-1)/2] M_1^2})$$
$$(16)$$

If the length L of the tubing is made longer than L for this specific w/A value, the entropy cannot go beyond the maximum value; however, adding more length adds more friction, and thus results in an entropy change. It may be seen from Fig.30 that an increase in "S" shifts to a new Fanno line with a smaller flow rate. Since the Mach number at the exit is one, the extra length will decrease the Mach number at all points upstream. Fig.31 displays the results of such calculations giving " fL/D " (Dau.73) versus "M_1" for three gases ethylene, nitrogen, helium.

By combining equations (13) and (16) a relation can be obtained between P*/P (minimum pressure ratio needed to reach sonic speed at the end of the capillary) and " fL/D ". The result is displayed Fig.32.

2 - Transport time

The transport time of the radioactive species between the moment of production and the moment of collection, can be decomposed into two times, first the time spent in the production chamber, second the transit time in the capillary. An estimate of these times can be obtained from simple equations. The average time spent in the

Figure 31

Variation on fL/D with the mach number at the exit
of the gas-jet capillary tube, for the gases helium,
nitrogen and ethylene.
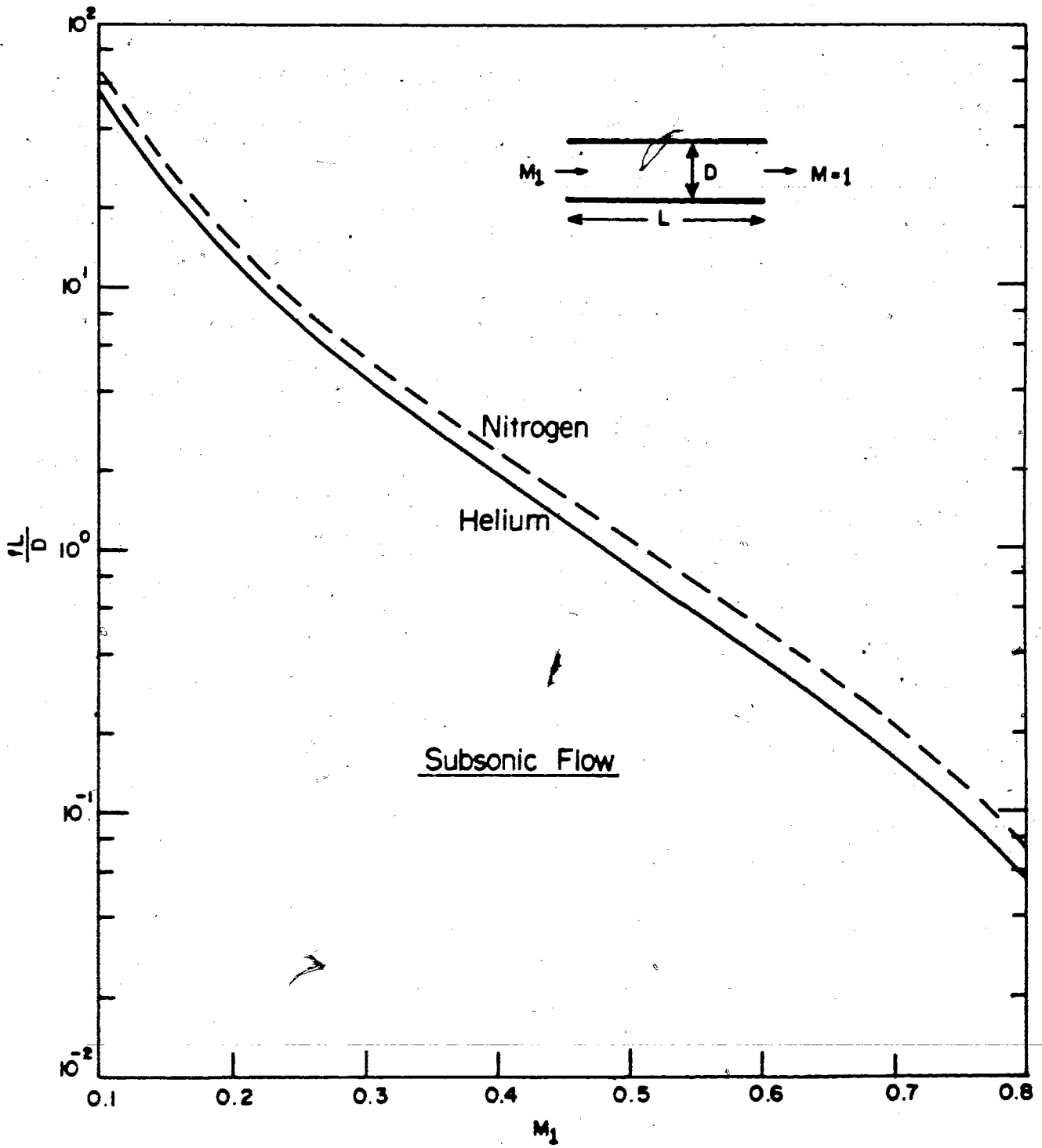
Figure 32

Variation of fL/D as a function of P*/P, assuming

sonic speed of the gas a the exit of the capillary.

For details and symbol definition see text.
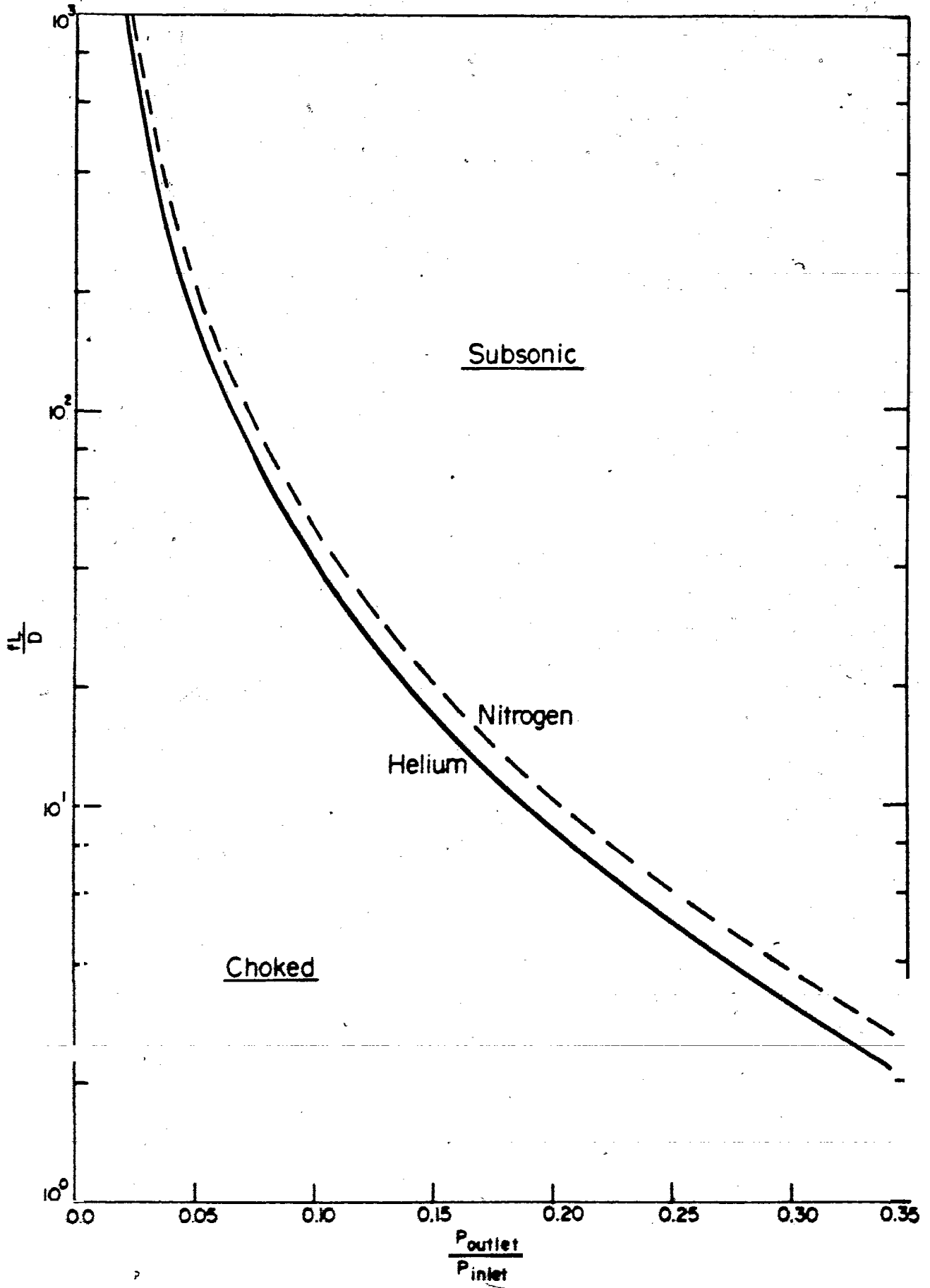
chamber can be approximated as the "turnover" time that is :

V/φ   where V = volume of the chamber

φ = gas flow rate

This is an approximation only since the gas does not sweep the entire volume of the chamber with the same speed (a more fundamental error is introduced by the fact that not all clusters will spend the same amount of time in the chamber). The expression of the time spent in the capillary is complex and, as a result, various approximations have been used (Dau.73, Wei.75). A simple equation is obtained if the gas speed reaches sonic velocity at the exit of the gas jet (Mach number -M- equal 1)

$$t_o = \frac{L}{a} \left(\frac{2+M_1}{3 \, M_1} \right)$$

In this equation M_1 is the Mach number of the gas at the entrance of the capillary, and "a" is the speed of sound in the gas.

Nevertheless since the half-lives of the radioactivities measured extended to values as short as 1.5 second, it was important to know the transit time with a precision better than .5 second (value which would be the lowest limit of confidence if one used the above assumptions). As a result, the experiment described previously (section II-C) was

carried out. Its interpretation led to the formulation of the following theory

1) The gas inside the chamber was assumed to be mixed in a time short enough compare to the "turnover time", so that the spatial distribution of activity inside the chamber could be considered constant throughout the chamber.

2) The gas was assumed to move with a single flow rate; (this is equivalent to assuming that the clusters are entirely focalised along the axis of the tubing).

We then can define the variation of the number of recoils " n " (total number) inside the chamber as :

dn/dt= production rate - decay rate - exit rate

- the production rate = $\epsilon N I \sigma$

- the decay rate = λn

- the exit rate = $n \phi /V$

we obtain

$$\frac{dn}{dt} = \epsilon N I \sigma - n \left(\lambda + \frac{\phi}{V} \right)$$

it can be seen that ϕ/V is equivalent to a decay constant and we call it "Λ" the exit constant

$$dn/dt = \epsilon N I \sigma - (\lambda + \Lambda)n \qquad (1)$$

the solution of such a differential equation is very simply:

$$n = \frac{\varepsilon NI\sigma}{\lambda+\Lambda} (1-\exp^{-(\lambda+\Lambda)t}) \qquad (2)$$

The exit rate $= \Lambda n = \frac{\varepsilon NI\sigma\Lambda}{\lambda+\Lambda}(1-\exp^{-(\lambda+\Lambda)t})$ (3)

and consequently the collection rate (after a transit time t_0 through the capillary) is given by:

$$C(t) = \varepsilon NI\sigma \frac{\Lambda}{\lambda+\Lambda} \exp^{-\lambda t_0}(1-\exp^{-(\lambda+\Lambda)(t-t_0)}) \qquad (4)$$

After a further delay time — t_1 — (time taken by the tape to transport the radioactivity in front of the detector, and assuming that the tape spends a time t_2 , short compared to the half-lives of the nuclides measured, in the field of view of the detector) the counting rate of the alpha detector becomes:

$$a(t) = \varepsilon NI\sigma \frac{\lambda\Lambda t_2}{\lambda+\Lambda} \exp^{-\lambda(t_0+t_1)}(1-\exp^{-(\lambda+\Lambda)(t-t_0)}) \qquad (5)$$

This expression can be of further interest. If one consider the case of a regular gas-jet collection-counting running mode. Since in this case the beam is almost never turned off, the equation (4) simplifies, and becomes:

$$C(t) = \varepsilon NI\sigma \ \frac{\Lambda}{\lambda + \Lambda} \ \exp^{-\lambda(t_0 + t_1)} \tag{6}$$

It can be seen that this equation is similar to a regular production of radioactivity with a usual bombarding experiment with the exception of the term $\Lambda/\lambda + \Lambda$ which takes into account the decay of the products in the production chamber. This leads to a slight modification of the usual equations governing the buildup of radioactivity. For example, the number of atoms n_0 collected after a collection time t_c would be (In the case of a simple decay):

$$n_0 = \frac{\varepsilon NI\sigma}{\lambda} \ \frac{\Lambda}{\lambda + \Lambda} \ \exp^{-\lambda(t_0 + t_1)} (1 - \exp^{-\lambda t_c}) \tag{7}$$

Obviously the initial assumptions may not always be entirely valid, and especially at low flow rate, there cannot be an instantaneous uniform spacial distribution of recoils in the chamber. However this will have an effect only during a very short periods of time (~.1 s) at the beginning of the irradiation, as can be observed Fig.14-15, and as a result is negligible. In order to test the second assumption, the results were analysed assuming no focussing during transportation and the correct velocity distribution across the radius of the capillary (equation (1)-Appendix I-1). It

was then impossible to reproduce the experimental results,
proving that indeed the focussing effect is quite
pronounced.

List of symbols

v = average gas velocity

v_o = maximum velocity (along the axis of the capillary)

v_r = velocity at a radius r

M = Mach number (speed of gas in units of sound velocity)

M_1 = Mach number at the inlet of the capillary

a = velocity of the sound in the gas

t_o = time taken by the clusters to travel through the capillary

r = distance of the aerosol from the capillary axis

R = radius of the capillary

D = the diameter of the tubing

A = cross-sectional area of the capillary

L = length of the capillary

V = volume of the production chamber

m = aerosol mass

r_c = radius of the clusters

μ = viscosity of the gas

P = pressure of the gas (P_o refers to the stagnation state)

T = temperature of the gas (T_o "   "   ")

ρ = density of the gas ($_o$ "   "   ")

h = enthalpy   (h_o "   "   ")

S = enthropy   (S_o "   "   ")

w = mass flow rate of gas

ϕ = volume flow rate of gas

$g = C_p/C_v$

R_g = gas constant

R_e = Reynold's number

N = number of atoms per cm^2 of effective target thickness

σ = production cross-section

I = beam intensity

λ = decay constant of the recoils under study

$\Lambda = \phi/V$ (exit constant)

ϵ = gas jet efficiency

ω = efficiency of the alpha detector

APPENDIX II

COMPUTER PROGRAMS

The following is a list of the computer programs most often used, or of significance for the interpretation of the results.

1 - DATA ACQUISITION

A) FOLDAP

This is not properly speaking a program but a modification of the FOCAL interpreter. Programs written in FOCAL are not translated into machine language to be stored in the computer, but are stored one character at a time as typed on the printer (or read from Dectape). During the program execution the FOCAL compiler interprets and executes each line as it is called for execution. A description of the FOCAL language can be found in (Foc.70), and a complete description of the functions added to it in FOLDAP can be obtained from R.G.Korteling (Chemistry department S.F.U). Such a description is not warranted here, and only their scope will be described. There are six types of functions

- a) Functions which allow the user to retrieve and/or modify the contents of absolute or indexed core locations.

- b) Arithmetic conversion. They allow the user to convert a number from decimal to octal, or binary (and vice versa). This is especially useful for example when one wishes to examine a storage location bit by bit.

- c) Camac functions. They allow reading and writing from and to a Camac crate, thus interfacing the program with the various systems used. For example this has allowed control of the gas-jet system.

- d) Functional panel control. These functions are related to the previous ones but instead of interacting with the Camac crate they do so with a control panel and thus allow the user to control (stop,start,branch) the program during execution.

- e) Tape-file control. These functions control the storage and retrieval of data files on tape (Dectape or Magtape)

- f) The last type of function controls the data acquisition, and on line analysis of the incoming events as required.

   A complete listing of a program used would be of little

value; however, to give the reader a feeling for the type of language, an exerpt of the part dealing with the gas jet is given in Fig.33.

B) DUMB

This is the second data acquisition program used. As mentioned previously, it was written for the NOVA 3 computer. Its general features are not unlike a (very) simplified version of FOLDAP. A listing of one of the programs used is given in Fig.34. Such a program is very impressive by its conciseness (each letter is a command, with the preceeding number(s) being its argument). Since it is DUMB's destiny to be retired shortly, it would be of little interest to give a detailed explanation of the command and only a broad description of each line is thus given in the Fig.34.

2 - DATA ANALYSIS

A) GAMANAL

A detailed description of the initial version can be found in (Gun.72). The one used at S.F.U was an adaptation to the S.F.U computer of a version obtained from the C.E.R.N. Following is a listing of the most important

Figure 33

Partial listing of a FOLDAP program

```
20.40T "",#;I (-FCP$(4))20.4;S OP=1;S A=0;D 16;S D=FBIT(-1,FCVT(7)+23,0,FPOW(14));S CI=-1

20.41 I (10-SCN) 20.42;S SCN=10

20.42 S D=FINT();D 44;T " WAITING FOR SIGNAL ",!

20.44 S N=FTIM(-1);S CI=CI+1;S K=1;S D=FSTP(-1);S D=FCOR(-1,FCVT(9),0);S J=FPOW(33);S M=0;F I=1,8;D 20.7

20.45 S D=FXCR(2,C,CI) ;I (D-J) 20.46,20.46;S W=1;D 20.6;D 46;G 20.61

20.46 S D=FXCR(0,C,CI)-1;I (J-D) 20.5;S D=FOLD();I (FABS(FPSH()-1)) 46.12,20.5;I (FPSH()-2) 20.47,46.05,20.47

20.47T "",#;I (CI)46.12,20.46;S M=FTIM(-1);I (M-N-RT)20.46;S W=2;D 20.6;D 46;G 20.61

20.50 S D=FXCR(9,C,CI);S D=FBEG();S D=FSTP(-1);S M=-(FTIM(-1)+1+9*TI);S D=FBEG();S D=FBIT(-1,FCVT(8),0,65536)

20.51I (FOLD()) 3.3,20.51;S D=FCOR(-1,FCVT(9),0);S K=K+1;I (8-K) 20.52,20.51,20.51

20.52 S D=FOLD();S D=FCOR(-1,FCVT(12)+16,-1);S D=FOLD();S D=FBIT(-1,FCVT(7)+23,0,65536);S D=FOLD()

20.54S D=FCOR(-1,FCVT(9),0);S D=FOLD();S D=FBIT(-1,FCVT(8),0,65536);S D=FOLD();S D=FCOR(-1,FCVT(12)+8,M+FTIM(-1))

20.56 I (FOLD()) 46.12,20.56;I (SCN-K) 20.44,20.44;S K=K+1;S D=FOLD();S M=M-TI;G 20.52

20.60 T "WARN HPD #",%Z2,W,!

20.61 T "",#;F I=0,200;S D=FOLD()

20.62 G 20.61

20.70 S M=M+TI;S D=FCOR(-1,FCVT(12)+I,-M);S D=FCOR(-1,FCVT(12)+8+I,-1);S D=FBIT(-1,FCVT(7)+15+I,0,65536)
```

Figure 34

Listing of a DUMB program

Figure 34

0QS0,13KZ26,22X2,22X2,1K,22+X2,2K,22+X2,3K,22+Y2,4K,22+X1G

1QS0A0<0,21X0,3&1=2G3GT0<4G2G0,21X0,2&2=9C

2Q25,22X24,22X2,1K,22+X0<20<E>2,1K,22+X0,2&2=26,22X

3Q0<0,21X0,1&1=0<1U16,21X100<E>0,21X0,1&0=0<0,21X0,1&1=100<E>

4Q2<3G>24,22X5W26,22X3G5G

5Q0AB8GE1KAB8GE2KAB8GE3KAB8GE4KAB1WE5KAB1WE6KAB1WE7KAB1WE6G

6Q8KAB2WE9KAB2WE10KAB4WE11KAB4WE

7Q1K,2KF,3KF,4KF,5KF,6KF,7KF,8KF,9KF,10KF,11KF,12KF,13KFC

8Q272<0,100Z>

9QE26,22XT1K,13KI0,2K,22+YV0,22XV

command cards operational at S.F.U.

EFFIN : input of efficiency calibration

ENCALIB : energy calibration will be calculated from next

spectrum using a set of known energies

(following cards)

ENPARAMS : used to enter energy calibration coefficients,

when known

PROCESS : this card and following convey information as to

what analysis is to be performed, and start the

program.

OPTIONS : input of the various print-out options.

OPERATORS: input of the criteria for peak finding and

fitting procedures.

SHAPEIN : input of the peak-shape parameters when known.

SHAPEAKS : the following cards contain information about

the peaks to be used for peak-shape parameters

determination.

STOP : end of analysis.

The main charateristics of this program are as follow:

- 1) Background determination. It is performed globally for

the entire spectrum by a combination of successive

interpolations (using a step function) between data points

on either sides of detected peaks, and smoothing of the new spectra thus generated.

- 2) Peak determination and fitting. The peak detection is performed through a combination of first and second derivative methods (consideration being also given to the difference between the data point and the computed background). The peak fitting procedure uses a function which corresponds to a basic gaussian shape plus an asymmetry term (on the low energy side of the peak).

As mentioned earlier it was found to give reliable answers, even though the shape of the alpha-peaks proved to be difficult to fit with the existing function.

B) DECALS (DEcay Curve Analysis by Least Square fit)

This program performed the analysis of the decay curves of the various activities measured. It uses a regular iterative least square fitting procedure with a modified Gaus-Jordan method. In its present version, it can accomodate up to 200 data points and 5 half-lives plus a background. Following is a list of the command cards with their description; (if the command field is left blank the previous command is assumed by default).

DATA (what 1-4):   one card for each data point

       what 1= number of counts

       what 2= starting time of counting of this data point

           (relative to the end of irradiation and/or

           collection),default being end of previous

           counting time interval.

       what 3= length of counting interval (if zero, default

           value is same as previous length)

       what 4= type of weight given to this data point:

           = 0   statistical weight - data

           = 1   unity

           = 2   statistical weight - 2xdata

           > 2   this number is the weight of this data

BGD (what 1-2):   background information

       what 1= estimate of background per unit of time

       what 2=   0: left floating

            >0: fixed to estimate

LAMBDA XX (what 1-5).(one card per component)

       XX = blank: regular radioactive component

       XX = P0   : parent isotope not measured itself

       XX = P1   : parent isotope itself being measured

       XX = D   : daughter isotope of previously entered parent

what 1-2= used only if guess of $T_{1/2}$ is done by the
computer. They correspond to data points
used for guess by the program of $T_{1/2}$

Default values are guessed by the program.

what 3= $T_{1/2}$. Default, estimate done by the program

what 4= N_o ''   ''   ''   ''

what 5= 0 $T_{1/2}$ and N_o are both floating

1 $T_{1/2}$ is fixed , N_o variable

2 $T_{1/2}$ variable, N_o fixed

3 $T_{1/2}$ and N_o are both fixed

DELTA follows LAMBDA (if what 5 of LAMBDA) >0

what 4, what 6= error on $T_{1/2}$ and/or N_o fixed

COLLECT (what 1)

what 1= irradiation (or collection time) used by
program to calculate production rates (if
not entered or what 1=0 no production rate
calculated).

GO (what 1-4) start fitting procedure.

what 1= type of recovery from diverging matrix

what 2= diagnostic printout level

what 3= criterium for end of fit

what 4= maximum number of iterations - default=50

TITLE The next card is a title card

RESET (what 1)

        what 1= 0 everything is reset

            = 1 the data are reset, the lambda of previous

               fit are entered as initial estimates

            = 2 the data are kept and will be fitted with

               new estimates

PLOT x (what 1-5)

        x= P = output on Calcomp plotter

        x= G = graph on printer

        x= B = both plot and graph

        what 1= starting time for plotting (default=start of

            counting)

        what 2= end time of plotting (def.=end of counting)

        what 3= control size of graph

        what 4-5= control X,Y size of plot

STOP exit from program

3 - CALCULATIONS OF THEORETICAL YIELDS

A) SILBERBERG - TSAO

      This program was written in FORTRAN IV by

W.Wiesehahn according to the relations developed by

R.Silberberg and C.H.Tsao (The following is just a brief

outline of their work and more detailed information may be
found in (Sil.73)). Depending upon the target material, the
bombarding energy, and the products of which the yields are
computed, three types of interaction are considered .

     1) Fission

     2) Stripping reaction : production of nuclides
       close to the target mass

     3) Spallation process

Since the cross-sections measured in this study correspond
to the production of these nuclides for which one would
expect the spallation process to be predominant, the
calculations leading to these cross-sections are the only
ones that will now be considered.

The evaluation of the yield of spallation-products is
performed using a modified form of the Rudstam's formula
(Rud.66).

The original and modified equations are in essence
similar, the difference being that in order to reproduce the
experimental data over a wide range of energy, (Ep >100 MeV)
and most of the periodic table, Silberberg and Tsao have
developed different expressions for the parameters as a
function of the bombarding energy, the target mass and the

product mass. Normalisation factors have as well been introduced.

B) ISOBAR

This program (Har.74) is a high energy version of VEGAS (Che.71), and was obtained from Z.Fraenkel. It computes the intranuclear cascade as described previously (section IV), and stores on magnetic tape the results cascade by cascade. This information may then afterwards be used as an input to an evaporation code. The computations performed follow essentially the description given in part IV-A of the intranuclear cascade.

Various options were available, and the choice of model used was as follow.

- a) The nucleus was divided into 8 regions of decreasing density (step model) with no refraction nor reflection (although this is theoretically unsatisfactory, the experimental results have generally been better reproduced in this way (Che.71))

- b) The total density was reduced after each collision

- c) The pion potential was constant with a value of 0 MeV

- d) There was no distance restriction

- e) The isobar nucleon exchange scattering was not allowed

C) EVA

This code -provided by Z.Fraenkel - has been utilised to compute the evaporation process, and compare the results with the experimental data.

The characteristics of the excited nucleus after completion of the intranuclear cascade are read from tape (as computed by the ISOBAR program described previously) . The evaporation is then computed by Monte Carlo calculations according to the formalism developed by I.Dostrovsky et al (Dos.59).

The program utilises the Weisskopf formula for the probability of emission of a particle j with a kinetic energy between E and E+dE :

$$P_j(E)dE = G_j \sigma E [W(_f)/ W(_i)] dE$$

Where $G_j = g_j m_j / \pi^2 h^2$, with g_j and m_j the number of spin states and the mass of the particle j, respectively.

σ : the cross-sections for the inverse reaction , are calculated using empirical equations .

W : the level density is given by the formula :

$$W(E) = C \exp\{2[a(E-d)]^{1/2}\}$$

The value of -C- is not specified, since only ratios of level densities enter the Weisskopf formula. The energy dependence of C is small compared to the exponential term, and as a result is neglected, as is the A dependence (assuming that over the narrow range of mass involved in a single evaporation step, its variation is negligible). An odd-even effect is nevertheless taken into consideration , in the following way:

$C_{even-even} = 4xC_{odd-odd}$

$C_{even-odd} = C_{odd-even} = 2xC_{even-even}$

d - is a pairing and shell effect correction term.

D) ALICE

This program computes the cross-sections for the formation of products obtained by evaporation of a compound nucleus (as decribed section IV-B). It has been developed and written by M.Blan and F.Plasil. Detailed information may be found in (Bla.72b, Bla.73).

Using provided information (target, projectile, bombardment energy) the properties of a compound nucleus are calculated (the Q of formation is computed using the Myers-Swiatecki mass formula, and the cross-section using a parabolic model (Tho.59)). This compound nucleus then

de-excites through evaporation of particles and/or fission.
Several options are available for the various calculations
involved as described below. - The Myers-Swiatecki mass
formula is used to compute the -Q- of formation of the
compound nucleus as well as particle binding energies (with
or without shell and pairing corrections) - The inverse
reaction cross-sections are obtained using the optical
model. - The effect of the angular momentum can be taken
into consideration in several ways : either standard
Weisskopf-Ewing calculations can be performed or the s wave
approximation can be used, with the rotational energy
calculated on the basis of the rotating drop model or
assuming for the compound nucleus a rigid rotor moment of
inertia. - Alternatively, the user may enter its own
experimental values if so desired.

This program is fast , but the compound nucleus
assumption limits its use in the case of a bombarding energy
of 480 MeV protons. Furthermore, since it is not of
Monte-Carlo type the number of products which can reasonably
be computed is limited (the normal values are A=10, Z=5).

This is why although this program was in running
condition at S.F.U. it was not retained for comparison with

the experimental data.

E) SFUMAP-FISMAP

a) SFUMAP - This code (Rud.69) is essentially similar to FISMAP (described below), the main difference being that only particle evaporation is considered. The description of FISMAP thus applies to SFUMAP with the omission of the fission process.

b) FISMAP - (Blo.75) An initial compound nucleus is first calculated (or read in) as an E-J matrix. In its present version, this matrix is dimensionned as 100x50 with a maximum energy of 200 MeV, and a maximum angular momentum of 100h. In principle nothing prevents these numbers from being increased if needed . The various probabilities of de-excitation (fission, particle emission) from each nuclear state (element of the E-J matrix) are calculated and normalised to the matrix population. The E-J matrices of the daughters thus generated are in turn examined, and the process repeated until either fission or particle emission is no longer possible from any state of any residual nucleus.

As in ALICE, such information as inverse reaction

cross-sections, fission barrier, and level density parameter can be either internally computed or entered by the user .

Both codes are readily available at S.F.U.. They present several advantages over the EVA code, notably the consideration of angular momentum effects and the calculations of "exact" cross-sections. These calculations are not of the Monte Carlo type and thus even very low cross-section values will still be calculated. Nevertheless the extension of the calculations to nuclides far from the target increases by a large amount both the time and computer's memory size needed by the program, to an extent which would render its use impossible.

LIST OF REFERENCES

Ale.68   J.M.Alexander in Nuclear Chemistry Vol.1 edit. by
          L.Yaffe; Academic Press, New York (1968) p.273

All.59   J.S.Allen, R.L.Burman, W.B.Herrmannsfeldt,
          P.Stahelin, and T.H.Braid Phys. Rev. 116: 134 (1959)

Azh.59   L.S.Azhgirey, I.K.Vzorov, V.P.Zrelov, M.G.
          Mescheryakov, B.S.Neganov, R.M.Ryndin and
          A.F.Shabudin Nucl. Phys. 13: 258 (1959)

Bar.72   V.S.Barashenkov, H.W.Bertini, K.Chen, G.Friedlander,
          G.D.Harp, A.S.Iljinov, J.M.Miller and V.D.Toneev
          Nucl. Phys. A187: 531 (1972)

Ber.52   G.Bernardini, E.T.Booth and S.J.Lindenbaum Phys.
          Rev. 88: 1017 (1952)

Ber.63   H.W.Bertini Phys. Rev. 131: 1801 (1963)

Ber.73   F.E.Bertrand, and R.W.Peelle Phys. Rev. C8: 1045
          (1973)

Ber.74   H.W.Bertini, G.D.Harp and F.E.Bertrand Phys. Rev.
          C10: 2472 (1974)

Ber.78   H.W.Bertini, A.H.Culkowski, O.W.Hermann, N.B.Gove
          and M.P.Guthrie Phys. Rev. C17: 1382 (1978)

Bet.36   H.A.Bethe Phys. Rev. 50: 332 (1936)

Bey.67   Y.Le Beyec and M.Lefort Nucl. Phys. A99: 131 (1967)

Bis.76   G.Bischoff, G.Cootte, H.Dautet, J.K.P.Lee,
          W.Wiesehahn, J.M.D'Auria, B.D.Pate – Proceeding 3rd
          inter. conf. on nuclei far from stability (Cargese) –
          CERN 76-13 (1976)

Bla.70   M.Blann and F.M.Lanzafame Nucl. Phys. A142: 559
          (1970)

Bla.71   M.Blann Phys. Rev. Lett. 27: 337 (1971)

Bla.72a M.Blann Phys. Rev. Lett. 28: 757 (1972)

Bla.72b M.Blann and F.Plasil Phys. Rev. Lett. 29: 303 (1972)

Bla.73   M.Blann and F.Plasil "Alice: a nuclear evaporation
         code" V.S.A.E.C Report 100 - 3494 - 10 (1973)
         unpublished

Bla.75   M.Blann Ann. Rev. of Nucl. Sc. Vol.25: 123 (1975)

Bla.76   M.Blann, R.R.Doering, A.Galonsky, D.M.Patterson and
         F.E.Serr Nucl. Phys. A257: 15 (1976)

Blo.75   H.Blok PhD Thesis, Simon Fraser University (1975)

Bow.72   J.D.Bowman, E.K.Hyde and R.E.Eppley L.B.L Nuc. Chem.
         Ann. Report N LBL 1666 (1972)

Bus.66   N.P.Buslenko, D.I.Golenko, Yu.A.Shreider, I.M.Sobol
         and V.G.Sragovich in The Monte Carlo Method edit. by
         Yu.A.Shreider, transl. from russian by G.J.Tee
         Pergamon Press (1966)

Cab.75   C.Cabot, C.Deprun, H.Gauvin, Y.Le Beyec and M.Lefort
         IPNO - RC - 75 - 02 (1975)

Cat.50   H.A.Cataldi, H.G.Drickamer J. Chem. Phys. 18: 650
         (1950)

Che.68   K.Chen, Z.Fraenkel, G.Friedlander, J.R.Grover,
         J.M.Miller and Y.Shimamoto Phys. Rev. 166: 949
         (1968)

Che.71   K.Chen, G.Friedlander, G.D.Harp and J.M.Miller Phys.
         Rev. C4: 2234 (1971)

Chu.77   Y.Y.Chu, G.Friedlander and L.Husain Phys. Rev. C15:
         352 (1977)

Coc.72   D.R.F.Cochran, P.N.Dean, P.A.M.Gram, E.A.Knapp,
         E.R.Martin, D.E.Nagle, R.B.Perkins, W.J.Shlaer,
         H.A.Thiessen and E.D.Theriot Phys. Rev. D6: 3085
         (1972)

Cum.68 J.B.Cumming Ann. Rev. of Nucl. Sc. Vol.13: 261 (1968)

Cun.47 B.B.Cunningham, H.H.Hopkins, M.Lindner,D.R.Miller,
        P.R.O´Connor,I.Perlman,G.T.Seaborg, and R.C.Thompson
        Phys. Rev. 72: 739 (1947)

Dau.73 H.Dautet, S.Gujrathi, W.J.Wiesehahn, J.M.D´Auria and
        B.D.Pate Nucl. Inst. and Meth. 107: 49 (1973)

Dja.75 A.Djaloeis, P.Jahn, H.J.Probst and C.Mayer-Boricke
        Nucl. Phys. A250: 149 (1975)

Dos.59, I.Dostrovsky, Z.Fraenkel and G.Friedlander Phys.
        Rev. 116: 683 (1959)

Eri.60 T.Ericson Adv. Phys. 9: 425 (1960)

Eri.75 M.Eriksson and G.G.Jonsson Nucl. Phys. A242: 507
        (1975)

Fri.55 G.Friedlander, J.Hudis and R.L.Wolfgang Phys. Rev.
        99: 263 (1955)

Fri.62 A.M.Friedman and W.C.Mohr Nucl. Inst. and Meth. 17:
        78 (1962)

Gad.73 E.Gadioli, E.Gadioli Erba and P.G.Sona Nucl. Phys.
        A217: 589 (1973)

Gar.73 C.K.Garrett and A.L.Turkevich Phys. Rev. C8: 594
        (1973)

Gau.75 H.Gauvin, Y. Le Beyec, J.Livet and J.L.Reyss Ann.
        Phys. 9: 241 (1975)

Gin.78 J.Ginocchio private communication 1978

Gol.48 M.L.Goldberger Phys. Rev. 74: 1269 (1948)

Gra.78 B.Grammaticos Phys. Rev. C17: 1244 (1978)

Gre.78 R.E.L.Green and R.G.Korteling Phys. Rev. C18: 311
        (1978)

Gre.79   R.E.L.Green private communication (1979)

Gri.66   J.J.Griffin Phys. Rev. Lett. 17: 478 (1966)

Gri.67   J.J.Griffin Phys. Lett. 24B: 5 (1967)

Gun.72   R.Gunnink and J.B.Niday Computerized analysis by
         gamma-ray spectrometry Vol.1 - UCRL - 51061 Vol.1
         (1972)

Hag.77   E.Hagberg, P.G.Hansen, J.C.Hardy, P.Hornshoj,
         B.Jonson, S.Mattsson and P.Tidemand-Petersson
         Nucl. Phys. A293: 1 (1977)

Har.60   B.G.Harvey Ann. Rev. of Nucl. Sc. Vol.10: 235
         (1960)

Har.71   G.D.Harp and J.M.Miller Phys. Rev. C3: 1847 (1971)

Har.73   G.D.Harp, K.Chen, G.Friedlander, Z.Fraenkel and
         J.M.Miller Phys. Rev. C8: 581 (1973)

Har.74   G.D.Harp Phys. Rev. C10: 2387 (1974)

Hey.72   H.R.Heydegger and A.Van Ginneken Nucl. Phys. A196:
         156 (1972)

Hil.78   M.Hillmann private communication 1978

Hud.68   J.Hudis in Nuclear Chemistry Vol.1 edit. by
         L.Yaffe; Academic Press, New York (1968) p.169

Hui.72a J.R.Huizenga and L.G.Moretto Ann. Rev. of Nucl. Sc.
         Vol.22: 427 (1972)

Hui.72b J.R.Huizenga Statistical properties of nuclei,
         ed. J.B.Garg New York: Plenum

Jun.71a H.Jungclas, R.D.Macfarlane and Y.Fares Phys. Rev.
         Lett. 27: 556 (1971)

Jun.71b H.Jungclas, R.D.Macfarlane and Y.Fares Radio. Chem.
         Acta 16: 141 (1971)

Kan.66   I.Kanestrom Nucl. Phys. 83: 380 (1966)

Kan.68   I.Kanestrom Nucl. Phys. A109: 625 (1968)

Kau.78   S.B.Kaufman, E.P.Steinberg and M.W.Weisfield Phys.
          Rev.   C18: 1349 (1978)

Kos.75   K.L.Kosanke, M.D.Edmiston, R.A.Warner,
          Wm.C.McHarris, M.F.Slaughter and W.H.Kelly Nucl.
          Inst. and Meth. 125: 253 (1975)

Lag.76   M.Lagarde-Simonoff, S.Regnier, H.Sauvageon and
          G.N.Simonoff Nucl. Phys. A260: 369 (1976)

Lan.66   D.W.Lang Nucl. Phys. 77: 545 (1966)

Loc.55   W.O.Lock, P.V.March and R.McKeague Proc. Roy. Soc.
          A231: 368 (1955)

Lux.78   C.R.Lux, and N.T.Porile Phys. Rev. C18: 148 (1978)

Mac.78   G.Mackenzie and J.Vincent private communication (1978)

Mcf.62   R.D.Macfarlane Phys. Rev. 126: 274 (1962)

Mcf.63   R.D.Macfarlane and R.D.Griffioen Nucl. Inst. and
          Meth. 24: 461 (1963)

Mcf.74   R.D.Macfarlane and Wm.C.Mc.Harris in Nuclear Spectroscopy
          and Reactions -part A- edit. by J.Cerny;
          Academic Press, New York (1974)

Mcl.63   E.B.McLeod "Introduction to fluid dynamics"
          Pergamon Press Oxford, New York (1963)

Met.58   N.Metropolis, R.Bivins, M.Storm, J.M.Miller,
          G.Friedlander and A.Turkevich Phys. Rev. 110: 204
          (1958)

Mil.59   J.M.Miller and J.Hudis Ann. Rev. of Nucl. Sc.
          Vol.9: 159 (1959)

Mis.58   R.Von Mises "Mathematical theory of compressible
          fluid flow" completed by H.Geiringer and
          G.S.S.Ludford Academic Press Inc. New York (1958)

Nei.72 B.Neidhart and K.Bachmann J. Inorg. Nucl. Chem. 34: 423 (1972)

Nit.70 J.M.Nitschke - Proceeding 1st Inter. conf. on the properties of Nuclei far from the region of beta stability. (Leysin) - CERN 70-30 (1970)

Nuc.73 Atomic Data and Nucl. Data Tables 12: 479 (1973)

Obl.74 P.Oblozinsky, I.Ribansky and E.Betak Nucl. Phys. A226: 347 (1974)

Pie.63 W.R.Pierson and N.Sugarman Phys. Rev. 130: 2417 (1963)

Por.68 N.T.Porile in Nuclear Chemistry Vol.1 edit. by L.Yaffe; Academic Press, New York (1968) p.57

Pre.63 M.A.Preston Physics of the nucleus Addison-Wesley publishing company, Inc. (1963)

Rud.66 G.Rudstam Z. Naturforschg. 21A: 1027 (1966)

Rud.68 F.H.Ruddy PhD Thesis, Simon Fraser University (1968)

Rud.69 F.H.Ruddy, B.D.Pate and E.W.Vogt Nucl. Phys. A127: 323 (1969)

Sah.72 G.B.Saha and L.Yaffe Nucl. Phys. A188: 409 (1972)

Sch.76 O.Scheidemann and N.T.Porile Phys. Rev. C14: 1534 (1976)

See.74 W.Seelmann-Eggebert, G.Pfennig and H.Munzel Chart of the Nuclides (1974)

Seg.77 E.Segre Nuclei and particles 2nd. ed. W.A.Benjamin, Inc. Advanced Book Program, Reading, Massachusetts (1977)

Ser.47 R.Serber Phys. Rev. 72: 1114 (1947)

Sha.53 A.H.Shapiro "The dynamics and thermodynamics of compressible fluid flow" Ronald Press Co. New York Vol.1 (1953), Vol.2 (1954)

Sil.73 R.Silberberg and C.H.Tsao "Partial cross-sections in high energy nuclear reactions" Astrophys. Jour. Suppl. ser 25: 315 (1973)

Sug.56   N.Sugarman, M.Campos and K.Wielgoz Phys. Rev. 101: 388 (1956)

Tho.59   T.D.Thomas Phys. Rev. 116: 703 (1959)

Tho.64   T.D.Thomas Nucl. Phys. 53: 558 (1964)

Tra.75   N.Trautamn, P.O.Aronsson, T.Bjornstad, N.Kraffrell, E.Kvale, M.Skarestad, G.Skarnemark and E.Stender Inorg. and Nucl. Chem Letters 11: 729 (1975)

Wei.37   V.Weisskopf Phys. Rev. 52: 295 (1937)

Wei.75   C.Weiffenbach, S.C.Gujrathi, J.K.P.Lee and A.Houdayer Nucl. Inst. and Meth. 125: 245 (1975)

Wes.78   G.D.Westfall, R.G.Sextro, A.M.Poskanzer, A.M.Zebelman, G.W.Butler and E.K.Hyde Phys. Rev. C17: 1368 (1978)

Wie.73a   W.J.Wiesehahn, H.Dautet, J.M.D'Auria and B.D.Pate Nucl. Inst. and Meth. 109: 613 (1973)

Wie.73b   W.J.Wiesehahn, J.M.D'Auria, H.Dautet and B.D.Pate Can. Journ. of Phys. 51: 2347 (1973)

Wie.74   W.J.Wiesehahn, J.M.D'Auria and J.C.Irwin Nucl. Inst. and Meth. 114: 401 (1974)

Wie.75   W.J.Wiesehahn, G.Bischoff and J.M.D'Auria Nucl. Inst. and Meth. 129: 187 (1975)

Wil.74   H.G.Wilhelm, H.Jungclas, H.Wollnik, D.F.Snider, R.Brandt, and K.H.Lust Nucl. Inst. and Meth. 115: 419 (1974)

Win.78   L.Winsberg   Nucl. Inst. and Meth. 150: 465 (1978)

Wol.75   H.Wollnik, H.G.Wilhelm, G.Robig and H.Jungclas Nucl. Inst. and Meth. 127: 539 (1975)

Wol.76   H.Wollnik Nucl. Inst. and Meth. 139: 311 (1976)

Wu .78   J.R.Wu and C.C.Chang Phys. Rev. C17: 1540 (1978)